Dissertation zur Erlangung des Doktorgrades
der Fakultät für Chemie und Pharmazie
der Ludwig-Maximilians-Universität München

Involvement of latent TGF-β binding protein 1 in CADASIL-relevant Notch3 aggregation

Jessica Janina Kast

aus Heilbronn

2014

Erklärung

Diese Dissertation wurde im Sinne von § 7 der Promotionsordnung vom 28. November 2011 von Herrn PD Dr. rer. nat. Christof Haffner betreut und von Herrn Prof. Dr. rer. nat. Martin Biel von der Fakultät für Chemie und Pharmazie vertreten.

Eidesstattliche Versicherung

Diese Dissertation wurde eigenständig und ohne unerlaubte Hilfe erarbeitet.

München, den

(Jessica Kast)

Dissertation eingereicht am 23. 10. 2014

1. Gutachter: Prof. Dr. rer. nat. Martin Biel

2. Gutachter: PD Dr. rer. nat. Christof Haffner

Mündliche Prüfung am 08.12.2014

Abstract

CADASIL (cerebral autosomal dominant arteriopathy with subcortical infarcts and leukoencephalopathy) represents the most prevalent hereditary form of cerebral small vessel disease (SVD) resulting in early-onset stroke and vascular dementia. It is caused by stereotyped missense mutations in the transmembrane receptor Notch3, which alter the number of cysteine residues in the extracellular domain (ECD). This leads to the abnormal multimerization and extracellular deposition of mutant Notch3-ECD at the plasma membrane of smooth muscle cells in small blood vessels. Notch3-ECD-containing aggregates are the earliest manifestation of the disease and excess Notch3-ECD is believed to recruit functionally important extracellular matrix proteins resulting in brain vessel dysfunction.

Biochemical and histological approaches on *post-mortem* brain tissue from CADASIL patients and control subjects as well as *in vitro* assays were used to study the consequences of Notch3-ECD deposition on the ECM components thrombospondin-2, fibrillin-1 and fibronectin and members of the latent transforming growth factor-β (TGF-β) binding protein (LTBP) family. It is demonstrated that the structural matrix components fibrillin-1 and fibronectin are enriched and contribute to the prominent thickening of CADASIL vessel walls without co-localizing with Notch3-ECD deposits, likely as a result of fibrotic adaptation secondary to aggregate formation. For LTBP-1, a key regulator of the TGF-β signaling pathway, an accumulation as well as a striking co-localization with Notch3-ECD deposits is shown suggesting specific recruitment into aggregates. Furthermore, increased levels of the TGF-β pro-domain (also known as latency-associated peptide, LAP) were found implying dysregulation of the TGF-β pathway in CADASIL development. Finally, a direct interaction of LTBP-1 with Notch3-ECD is demonstrated and evidence for a co-aggregation with mutant Notch3 *in vitro* is provided. Conclusively, I propose LTBP-1 as a novel component of Notch3 deposits with a role in CADASIL pathogenesis.

Zusammenfassung

CADASIL (cerebral autosomal dominant arteriopathy with subcortical infarcts and leukoencephalopathy) ist die häufigste monogen vererbte Ursache zerebraler Mikroangiopathien, die zu juvenilem Schlaganfall und Demenz führen. CADASIL wird verursacht durch Mutationen im Notch3 Transmembranrezeptor, wobei die Anzahl der Cysteinreste der extrazellulären Domäne (Notch3-ECD) verändert wird. Dadurch kommt es zu einer Multimerisierung und Ablagerung von Notch3-ECD an der Plasmamembran von glatten Gefäßmuskelzellen in kleineren Arterien. Diese Aggregate gelten als die frühste pathologische Veränderung bei CADASIL und sind verantwortlich für die Rekrutierung funktionell wichtiger Proteine.

In der vorliegenden Arbeit wurden biochemische und histologische Methoden an Hirngewebe von CADASIL-Patienten beziehungsweise von Kontrollen angewandt sowie *in vitro* Analysen angefertigt, um die Auswirkungen der Notch3-ECD Akkumulation auf die extrazellulären Matrixproteine Thrombospondin-2, Fibrillin-1, Fibronectin und Vertreter der latent transforming growth factor-β (TGF-β) binding protein (LTBP)-Familie zu untersuchen. Dabei konnte gezeigt werden, dass die strukturgebenden Matrixproteine Fibrillin-1 und Fibronectin in den verdickten Gefäßen bei CADASIL-Patienten angereichert sind, jedoch nicht mit Notch3-ECD überlagern. Vermutlich handelt es sich dabei um eine fibrotische Anpassung sekundär zu den Notch3-ECD-Aggregaten. Für LTBP-1, welches den TGF-β Signalweg reguliert, wurde sowohl eine Anreicherung als auch eine Ko-lokalisation mit Notch3-ECD gefunden. Dies deutet auf eine spezifische Rekrutierung in die Notch3-ECD Aggregate hin. Darüber hinaus wurde auch eine vermehrte Anreicherung der TGF-β Pro-Domäne LAP (latency-associated peptide) gefunden, was auf eine Involvierung des TGF-β Signalweges bei CADASIL hindeutet. Abschließend zeigen *in vitro*-Versuche, dass LTBP-1 mit Notch3-ECD direkt interagiert und dadurch auch ko-aggregieren kann. Damit lässt sich festhalten, dass LTBP-1 als neuartige Notch3-ECD-Aggregatkomponente identifiziert wurde, welche vermutlich maßgebend zu der Pathogenese von CADASIL beiträgt.

Table of contents

1 Introduction

Stroke is the third leading cause of death worldwide only outnumbered by coronary heart disease and cancer (Warlow et al., 2003). Moreover, it represents the most common cause for long-term neurological disability entailing a high cost expenditure estimated around annual 64 billion Euros in Europe (Olesen et al., 2012).

In about 20 % of the cases, strokes are hemorrhagic resulting from vessel wall rupture, which causes the extravasation of blood. Eighty percent of cases, however, are ischemic (Figure 1) as a consequence of vessel occlusion leading to a restriction of blood supply and a depletion of oxygen and nutrients in the tissue surrounding the site of the insult. The main causes underlying ischemic stroke are large-artery atherosclerosis, cardioembolism and cerebral small vessel disease (SVD, Figure 1) (Warlow et al., 2003). Although SVD accounts for only ~20 % of acute strokes (Figure 1) and its immediate effects on short-term disability and survival are less severe compared to other stroke subtypes, it represents the major cause for long-term disability and vascular dementia, the second most common form of dementia after Alzheimer's disease (Warlow et al., 2003). Moreover, recent studies identified SVD as the most prevalent neurological disorder in aging populations and it represents a considerable health care problem posing an increasing burden on our society (Pantoni, 2010). Thus, the exploration of the molecular causes of SVD is of high importance.

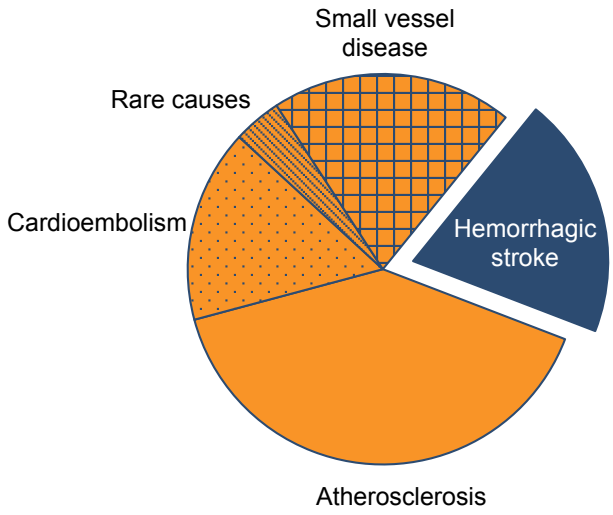

Figure 1: Frequency of hemorrhagic (blue) and ischemic (orange) stroke in industrialized countries. Ischemic stroke is further subdivided in several subtypes according to underlying causes.

Since this thesis focuses on cerebral SVD, an introduction into the brain vascular network is given in the following section.

1.1 Cerebral vasculature

The brain is the organ with the highest energy demand consuming roughly 20 % of the cardiac output (Wardlaw et al., 2013a). Due to its low storage capacities, this demand can only be satisfied by a constant blood supply provided by a complex brain vascular system.

1.1.1 Brain vascular network

Large arteries supply the brain with blood and they reach its base to form a circuit, the so-called circle of Willis, which separates into the three main intracranial arteries: the middle, anterior and posterior artery (1-10 mm diameter). At the brain surface, each artery branches into a wide-ranging network of small resistance arteries (0.1-1 mm diameter) and arterioles (20-100 μm diameter), which then submerge deeply into the brain as perforating arterioles (20-50 μm diameter) terminating in the white matter (Figure 2) (Pantoni and Garcia, 1997). This represents a unique ”outside in” vascularization pattern from the brain surface into the parenchyma, whereas other major organs are usually vascularized from the ”inside out” (Iadecola, 2013).

The basal ganglia, representing deep grey matter, are supplied by a second less extensive system of shorter arterial perforators, which originate directly from the circle of Willis and its proximal branches, the middle and posterior cerebral artery (Figure 2) (Pantoni and Garcia, 1997).

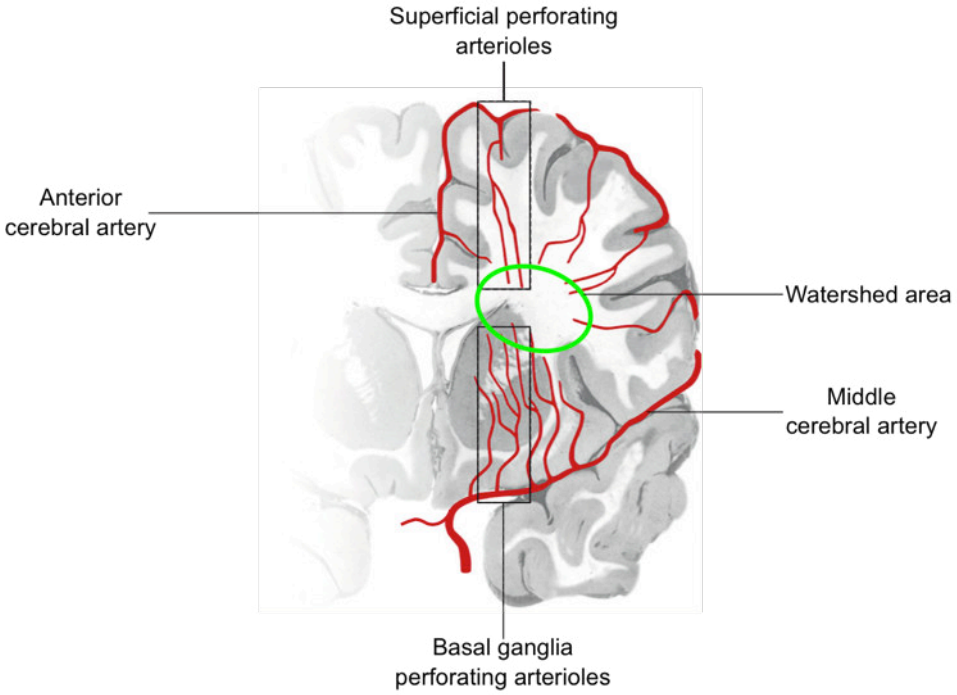

Figure 2: Schematic overview of the brain vascular system. The white matter is supplied by superficial perforating arterioles arising from the middle and anterior cerebral arteries. The basal ganglia, representing deep grey matter, are supplied by perforating arterioles diverging directly from the circle of Willis and its proximal branches. The two systems of perforating arterioles terminate in the watershed area (green circle) (adapted from Wardlaw et al., 2013a).

In SVD, perforating arterioles of the white and deep grey matter are affected, while the cortex is relatively spared (Viswanathan et al., 2006). In the deepest area of the brain, the so-called watershed area, the vascular network is terminating and does not overlap. Since a systemic or focal blood flow deficit cannot be compensated by collateral branches, this region is especially vulnerable to injuries (Iadecola, 2013).

1.1.2 Structure of cerebral blood vessels

Histological analyses over the last decades have shown that SVD is associated with changes in arterial morphology affecting one or more of the three principal layers: the tunica intima, the tunica media and the tunica adventitia (Figure 3).

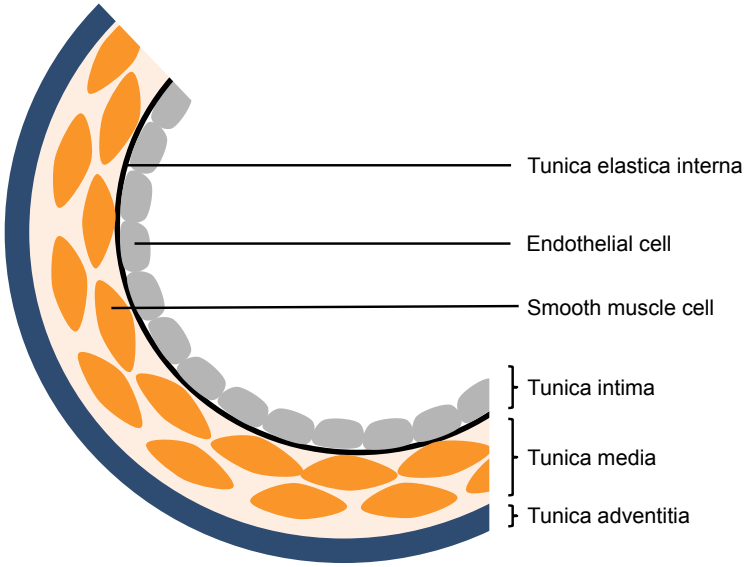

Figure 3: Structure of an arterial vessel. The tunica intima, the innermost layer, consists of a single layer of endothelial cells and the tunica elastic interna. The tunica media is build up by circumferentially arranged vascular smooth muscle cells. The external layer, the tunica adventitia, is composed of mainly fibroblasts and extracellular matrix.

The tunica intima consists of a single layer of endothelial cells that are connected by tight junctions sealing the vessel lumen to restrict the exchange of metabolites. The basement membrane, a thin layer of support tissue mainly composed of collagen type IV, proteoglycan, hyaluronan, fibrillin and fibronectin, underlies the endothelial cells. Next, the tunica elastica interna, which primarily contains elastin produced by endothelial cells, separates the tunica intima from the tunica media. Small fenestrations in the tunica elastica interna allow communications between the endothelium and vascular smooth muscle cells (vSMCs).

The tunica media is composed of several layers of circumferentially arranged vSMCs surrounded by organized layers of elastic fibers and interlamellar matrix (collagens and microfibrils) to increase the elasticity and strength of the vessel wall. VSMC are highly specialized cells, which can contract and relax to control the vessel lumen diameter and thereby blood flow. Capillaries lack the tunica media completely and are built up by an endothelial layer, basement membrane and discontinuous pericyte cell layer.

The tunica adventitia is an assembly of loose connective tissue consisting of mainly collagen type I, III and VI, fibrillin-1 and fibronectin produced by fibroblasts. This architectural framework not only integrates the vessels into the surrounding tissue but also maintains its mechanical and elastic properties and retains cytokines and growth factors.

Additionally, other cells e.g. of the inflammatory type (macrophages and lymphocytes) can be present.

1.2 Cerebral small vessel disease

1.2.1 Sporadic form

The term cerebral small vessel disease (SVD) describes a group of pathological conditions with various etiologies that affect the structure and function of perforating cerebral arterioles and capillaries, but also venules damaging the cerebral white and deep grey matter (Pantoni, 2010). SVD mostly develops unnoticed for many years before becoming clinically evident in form of sudden-onset stroke symptoms and/or global neurological dysfunction including substantial cognitive, psychiatric and physical disabilities (Wardlaw et al., 2013a). Since small vessels are difficult to image and investigate *in vivo* and clinical manifestations are diverse, the diagnosis of SVD remains a challenge (Wardlaw et al., 2001).

Despite a number of clinical studies, the pathogenesis of SVD is largely unknown precluding the development of new treatment options. Pathological data are mainly available from end-stage SVD complicating the identification of the earliest disease-causing events. A central aspect is hypoperfusion and ischemia mediated by narrowed arteries and a characteristic loss of vSMCs, which impairs adaptive responses of the vessel wall to changes in cerebral blood flow. However, little is known how this might cause the neurological and cognitive symptoms (Wardlaw et al., 2013a). Moreover, pathological processes are influenced by various genetic and environmental risk factors such as advanced age, hypertension, smoking, diabetes mellitus, hyperlipidemia and atrial fibrillation (Iadecola, 2013) making it difficult to determine clear cause-and-effect correlations. This problem of "mixed pathologies" can be at least partly circumvented by analyzing monogenic SVD forms with a defined etiology, which due to their early onset show pathologies largely independent of age effects (Dichgans, 2007). They are thus considered valuable model diseases to uncover biological pathways promoting vascular changes and to provide causal links between risk factors and dementia.

1.2.2 Monogenic forms of cerebral small vessel disease

Several monogenic causes of SVD forms have been identified so far (Table 1). Among them cerebral autosomal recessive arteriopathy with subcortical infarcts and leukoencephalopathy (CARASIL), retinal vasculopathy with cerebral leukodystrophy (RVCL) and COL4A1-related SVD are very rare conditions. Far more patients suffer from

cerebral autosomal dominant arteriopathy with subcortical infarcts and leukoencephalopathy (CADASIL), the most common monogenic cause of SVD and vascular cognitive impairment (Joutel et al., 1996, Chabriat et al., 2009). It thus represents the most widely studied inherited SVD and abundant clinical data are available, making CADASIL a valuable model condition to study pathological processes involved in SVD development.

Table 1: Overview of hereditary forms of small vessel disease.

Disorder (Mode of inheritance)	**Genetic identity**	**Characteristic clinical features**
CADASIL (Dominant)	*NOTCH3*	Migraine, subcortical infracts, dementia, mood disorder
CARASIL (Recessive)	*HTRA1*	Subcortical infarcts, dementia, spondylosis, alopecia
RVCL (Dominant)	*TREX1*	Retinopathy, nephropathy, migraine, ischemic strokes, dementia
COL4A1-related SVD (Dominant)	*COL4A1*	Infantile hemiparesis, intracerebral hemorrhage, microbleeds, intracranial aneurysms

CADASIL: Cerebral autosomal dominant arteriopathy with subcortical infarcts and leukoencephalopathy; CARASIL: Cerebral autosomal recessive arteriopathy with subcortical infarcts and leukoencephalopathy, RVCL: retinal vasculopathy with cerebral leukodystrophy; Htra1: High temperature requirement A1; COL4A1: Collagen type IVα1; SVD: Small vessel disease (Joutel et al., 1996, Hara et al., 2009, Kuo et al., 2012, Richards et al., 2007).

1.3 CADASIL

Starting in the 1970s, a number of case reports described a hereditary cerebral disorder with multiple early-onset infarcts and progressive dementia in European families (Sourander and Walinder, 1977, Stevens et al., 1977, Sonninen and Savontaus, 1987, Davous et al., 1991, Tournier-Lasserve et al., 1991, Mas et al., 1992). In 1993, the acronym CADASIL (cerebral autosomal dominant arteriopathy with subcortical infarcts and leukoencephalopathy) was coined highlighting the main characteristics of this disease (Tournier-Lasserve et al., 1993). Since then, more than 500 families worldwide have been reported. A small study from Scotland estimated the prevalence at 4.15 cases per 100 000 in Scotland (Razvi et al., 2005), however, the overall prevalence is unknown (Chabriat et al., 2009).

1.3.1 Clinical features

The clinical manifestations of CADASIL include a variety of neurological and neuropsychological aspects (Figure 4), however, four principle symptoms are considered central to the disease: migraine with aura, recurrent subcortical infarcts, mood disturbances (e.g. apathy) and cognitive impairment (Chabriat et al., 2009). The first ischemic attack occurs on average with ~51 years (Opherk et al., 2004). As the disease progresses, cognitive decline develops but may also precede the first symptomatic ischemic episodes (Amberla et al., 2004). Initially, executive and organizing functions are affected and patients present with poor concentration and general mental and psychomotor slowing and at later disease stages, cognitive impairment ultimately results in vascular dementia (Dichgans, 2009). Already by the age of 65 years, roughly 80% of the patients are demented (Kalimo et al., 2002).

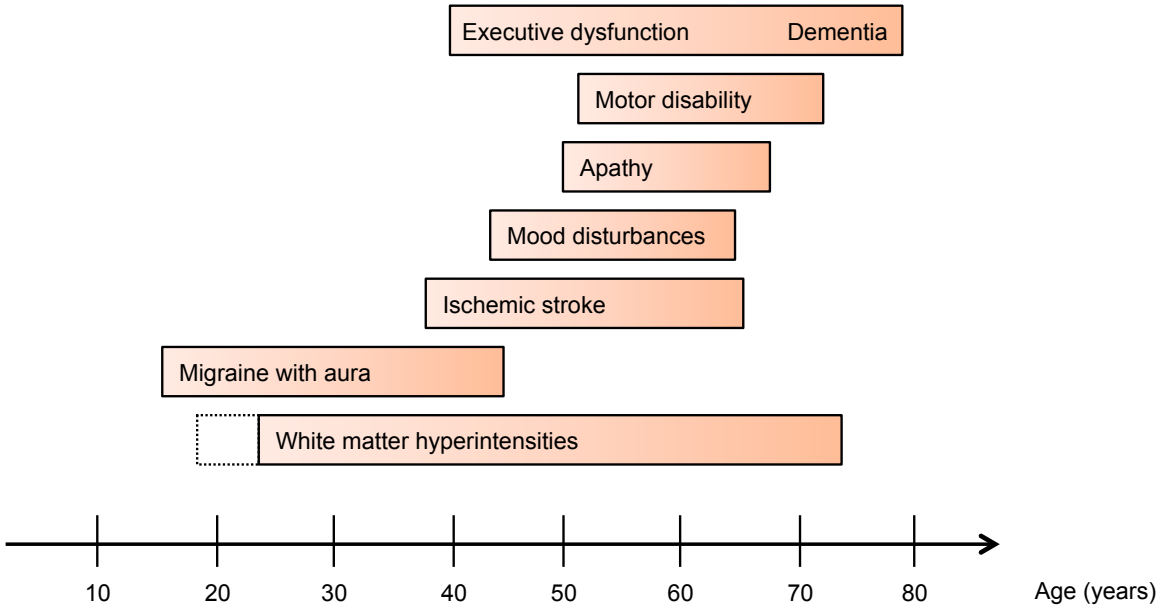

Figure 4: Overview of the main clinical manifestations of CADASIL. The exact appearance of the first white matter abnormalities are unknown and thus represented with a dotted line (adapted from Chabriat et al., 2009).

The disease progresses slowly and its aggravation is associated with recurrent strokes. Within a mean of 23 years after the first symptoms have occurred, CADASIL complications leads to death (Dichgans et al., 1998). To date, no CADASIL treatment is available except for the amelioration of migraine symptoms (Forteza et al., 2001).

CADASIL patients show considerable alterations on cranial magnetic resonance imaging (MRI), a routine neuroimaging tool widely used in clinical practice (Wardlaw et al., 2013b).

Symptomatic but also asymptomatic patients display characteristic white matter hyperintensities (Figure 5) and their extent broadly correlates with the severity of the clinical status (Chabriat et al., 1998, Dichgans et al., 1998, Kalimo et al., 2002). White matter hyperintensities, thought to arise from axonal demyelination, increase during the course of the disease and their absence almost excludes this diagnosis (Chabriat et al., 1998). Additionally, lacunes, fluid-filled cavities of past infarcts (Figure 5), and brain atrophy as a result from neuronal loss are frequently observed (Dichgans et al., 1999, Peters et al., 2006, Duering et al., 2012, Duering et al., 2013).

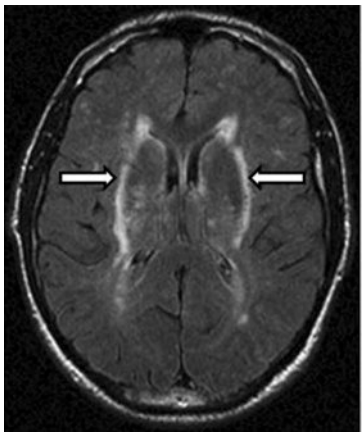

Figure 5: MRI scans of CADASIL patients showing characteristic white matter hyperintensities (arrows) (Opherk et al., 2009b).

Based on the clinical features, a number of affected families were collected in the 1990s to search for the underlying gene defect.

1.3.2 Genetics

In 1993, Tournier-Lasserve and coworkers performed genetic linkage analysis in two unrelated French families and mapped the CADASIL-causing locus to chromosome 19 (Tournier-Lasserve et al., 1993). The subsequent investigation of 13 additional families allowed a further refinement of the genetic interval (Ducros et al., 1996) and finally the identification of the critical gene, *NOTCH3*, on chromosome 19p13 (Joutel et al., 1996).

NOTCH3 encompasses 33 exons and encodes a single-pass type I transmembrane receptor of 2321 amino acids. It belongs to an evolutionary conserved family involved in cell-cell-mediated signaling playing essential roles in the development of multicellular organisms (Artavanis-Tsakonas et al., 1999). In addition, Notch receptors exert functions in adult animals including humans, which is reflected by their involvement in several clinical conditions (Penton et al., 2012). They all show the same domain organization with a large

extracellular domain (ECD) comprising 34 epidermal growth factor (EGF)-like repeats and three notch/lin-12 repeats, a transmembrane domain and an intracellular domain (Notch-ICD) consisting of seven ankyrin repeats and a PEST motif (Figure 6). Notch proteins are synthesized as ~280kDa proteins which undergo three successive proteolytic cleavages (S1-3) (Figure 6, black arrows).

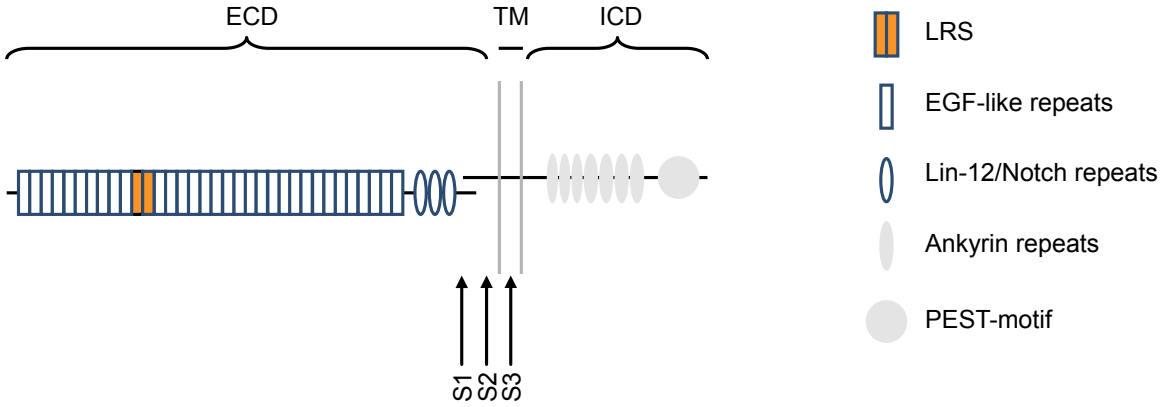

Figure 6: Schematic Notch3 structure. Notch3 is composed of an extracellular domain (ECD) with 34 epidermal growth factor (EGF)-like repeats including the ligand recognition site (LRS) in EGF-like repeats 10/11 (orange) and three lin-12/Notch repeats. The transmembrane domain (TM) is followed by the intracellular domain (ICD) comprising several ankyrin repeats and a PEST motif. The arrows indicate the cleavage sites S1-3.

The S1 cleavage is mediated by a furin-like convertase in the Golgi network and occurs during receptor transport to the plasma membrane. The cleavage products, among them the 210 kDa Notch-ECD fragment, remain associated non-covalently and are presented as heterodimers at the cell surface (Blaumueller et al., 1997). Signaling is initiated by membrane-bound ligands (e.g. Delta or Serrate) on neighboring cells which interact with the ligand binding domain located in EGF-like repeats 10/11 of the ECD (Figure 6). This triggers the S2 cleavage close to the plasma membrane by TNFα-converting enzyme (TACE), a metalloprotease also known as ADAM-17 (Brou et al., 2000). The Notch3-ECD is shedded and the remaining membrane-attached fragment becomes substrate for the γ-secretase catalyzing processing at the S3 site, an unusual cleavage occurring within the plasma membrane (Mumm et al., 2000). The resulting fragment, Notch-ICD, is released and translocates to the nucleus where it interacts with DNA binding proteins including RBP-Jk to regulate transcription of target genes (Fouillade et al., 2013).

Whereas invertebrates possess only one *NOTCH* gene, four isoforms are present in vertebrates. Notch3 plays essential roles in cell fate determinations during embryonic development and in adulthood (Artavanis-Tsakonas et al., 1999). It is mainly expressed in

vSMCs and pericytes regulating cell growth, migration and apoptotic death (Joutel et al., 2000, Prakash et al., 2002, Joutel et al., 2010). Notch3 knockout mice (Notch3$^{-/-}$) are viable and fertile demonstrating a non-essential role of the protein (Domenga et al., 2004, Belin de Chantemele et al., 2008). While arterial vSMCs of Notch3$^{-/-}$ mice are indistinguishable from wild type cells at birth, they have an abnormal shape and a smaller size in adult mice. Moreover, their reactivity to changes in arterial pressure and cerebral blood flow is compromised especially in small arteries (Domenga et al., 2004, Belin de Chantemele et al., 2008). Thus, Notch3 is believed to be required for arterial differentiation and maturation of vSMCs in cerebral arteries.

NOTCH3 mutations resulting in CADASIL exclusively localize to exons 2-24 encoding the 34 EGF-like repeats (Chabriat et al., 2009). Each repeat contains a conserved number of six cysteine residues forming three disulfide bridges between cysteines 1-3, 2-4 and 5-6 (Figure 7), which are required for the correct folding of the receptor (Simpson, 1997). 95 % of mutations lead to a single amino acid substitution, whereas in-frame deletions and splice site mutations are rarely observed. Substitutions predominantly affect cysteine residues within individual EGF-like repeats causing either the addition or the loss of a cysteine (Figure 7) (Joutel et al., 1997, Peters et al., 2005b). Today, more than 150 mutations are known and interestingly, a hotspot is found in EGF-like repeats 3 and 4, in which ~68 % of the mutations reside (Joutel et al., 1997, Peters et al., 2005b). Genetic testing for pathogenic *NOTCH3* mutations is the diagnostic gold standard, since its sensitivity is close to 100 % (Joutel et al., 1997).

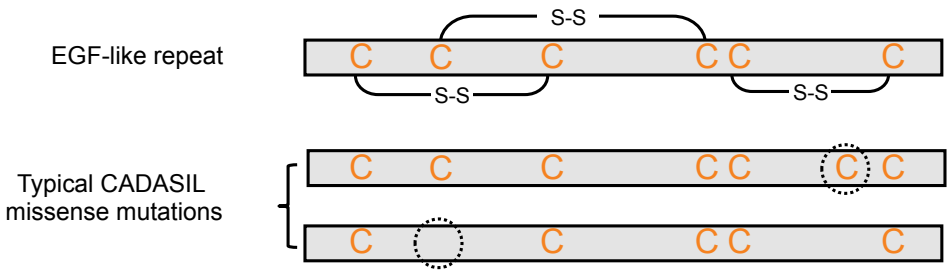

Figure 7: CADASIL mutations are highly conserved. Each EGF-like repeat bears a conserved number of six cysteines (orange) forming three disulfide bridges (S-S) between Cys 1-3, 2-4, 5-6. The lack or addition (dotted circle) leads to an odd number of cysteines. Adapted from Chabriat et al., 2009.

1.3.3 Pathology and pathomechanism

The gain or loss of a cysteine residue caused by CADASIL mutations generates an unpaired sulfhydryl group, which likely promotes disulfide bond formation between mutant Notch3-ECD proteins (Duering et al., 2011). This is believed to induce the

extracellular multimerization of shedded Notch3-ECD molecules leading to their accumulation in the tunica media of vessel walls (see below) (Dichgans et al., 2000, Joutel et al., 2000). Notch3-ECD aggregates can be detected by immunohistological staining and are believed to coincide with large electron-dense deposits known as granular osmiophilic material (GOM, Figure 8), an invariant feature of CADASIL-affected vessels (Joutel et al., 2000, Ishiko et al., 2006). GOM are non-amyloid, basophilic structures 0.2-0.8 µm in diameter (Kalimo et al., 2002, Tikka et al., 2009) mostly located in extracellular indentations of vSMC, but also in the thickened basement membrane. Although symptoms in CADASIL are exclusively neurological, GOMs can be found in vessel walls of many other organs, allowing diagnostic electron microscopy analysis of skin biopsies (Chabriat et al., 2009).

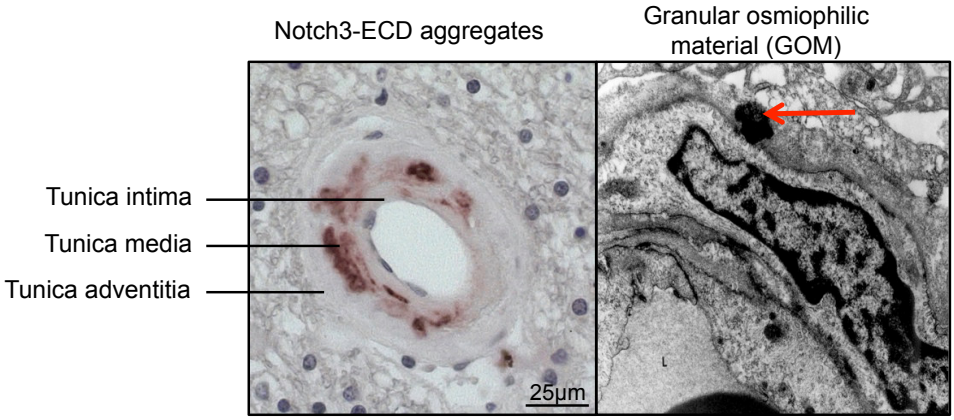

Figure 8: Pathological Notch3-ECD aggregates and granular osmiophilic material (GOM). Left: Section of a white matter arteriole immunostained for Notch3-ECD, showing the characteristic granular Notch3-ECD deposits within the thickened vascular wall in brown. Right: Electron micrograph of a dermal artery showing granular osmiophilic material (arrow) at the surface of a vascular smooth muscle cell (courtesy of Christian Opherk, ISD).

While both Notch3-ECD aggregates and GOM are hallmarks of CADASIL, other morphological changes of vessel walls are also common in sporadic SVD. They are mainly restricted to small perforating brain vessels in the white and deep grey matter, while the cortex is relatively spared. Arterioles show non-arteriosclerotic thickening of the vessel wall especially at the tunica intima and tunica adventitia causing luminal stenosis in pre-capillary arterioles (less than 50 µm diameter) (Miao et al., 2004). These fibrotic changes likely result from increased amounts of extracellular matrix proteins such as collagen type I, III, IV and VI (Miao et al., 2004, Miao et al., 2006, Dong et al., 2012), elastin (Caronti et al., 1998) and fibronectin (Oide et al., 2008), or debris from degenerating vSMCs (Kalaria, 1996, Ceroni et al., 2000, Miao et al., 2004). Additionally, CADASIL patients suffer from an irregular distribution of vSMCs in the tunica media (Miao et al., 2004), an alteration

possibly preceding the degeneration and loss of this cell type in later stages of the disease (Miao et al., 2004) (Okeda et al., 2002).

The molecular mechanisms underlying Notch3-ECD deposit formation and the pathological events leading to vessel dysfunction are incompletely understood. A variety of studies using cultured cells have failed to detect alterations in receptor maturation and signaling capacity of CADASIL-mutant Notch3 (Haritunians et al., 2002, Karlstrom et al., 2002, Joutel et al., 2004, Peters et al., 2004, Low et al., 2006). Moreover, data from several CADASIL mouse models using mutated *NOTCH3* (Dubroca et al., 2005, Monet-Lepretre et al., 2009, Joutel et al., 2010, Wallays et al., 2011) strongly suggested that loss-of-function is not the prevalent pathomechanism, although conflicting results have been reported (Arboleda-Velasquez et al., 2011). Only a few mutations located within the ligand-binding site (EGF-like repeats 10/11), occurring in roughly 4 % of all CADASIL patients (Monet-Lepretre et al., 2009), cause impairment in signal transduction (Joutel et al., 2004, Peters et al., 2004, Monet-Lepretre et al., 2009, Arboleda-Velasquez et al., 2011). However, since hypomorphic Notch3 allele carriers do not show signs of CADASIL pathology (Rutten et al., 2013), it is likely the alteration of the number of cysteines, which confers pathogenicity to these mutants. Thus, novel pathogenic roles for mutant Notch3 rather than compromised Notch3 function have been proposed as the primary determinant of the disease (Joutel, 2011).

The appearance of Notch3-ECD aggregates prior to neurological symptoms in CADASIL patients (Mayer et al., 1999, Lesnik Oberstein et al., 2003) suggests that they represent an early manifestation causative for disease development. This hypothesis is supported by experimental data from the TgNotch3^{R169C} mouse model, which carries a PAC (P1-derived artificial chromosome) clone containing the mutant (R169C) rat *NOTCH3* gene driven by the endogenous mouse Notch3 promoter (Joutel et al., 2010). In a time-dependent fashion, TgNotch3^{R169C} mice show an extracellular accumulation of Notch3-ECD (2 months), followed by GOM development (5 months), brain parenchyma lesions and astrogliosis (12 months) and progressive white matter degeneration (20 months). Since the mice do not display any ischemic attacks, they likely represent an early disease model. The initial appearance of Notch3-ECD deposits puts them at the beginning of a cascade of events eventually resulting in CADASIL pathology and it is currently believed that the co-aggregation of additional proteins is a major determinant of this process.

While Notch3-ECD aggregation has been well studied *in vivo*, little is known about the exact nature of the aggregation process. Using scanning for intensely fluorescent targets (SIFT), a confocal technique, which distinguishes single protein particles from aggregated forms allowing the quantitative monitoring of protein multimerization in solution (Giese et

al., 2005), our group has recently recapitulated the Notch3-ECD aggregation process *in vitro*. A purified recombinant Notch3 fragment comprising EGF-like repeats 1-5, the mutational hotspot region, only showed formation of higher order multimers when bearing a CADASIL-causing mutation (Opherk et al., 2009a, Duering et al., 2011), a mechanism mediated by disulfide bond formation (Duering et al., 2011). Moreover, co-aggregation of thrombospondin-2 (Duering et al., 2011), a known Notch3 interactor and regulator of ECM assembly (Meng et al., 2009), was observed providing first direct experimental evidence for a pathological co-aggregation mechanism, i.e. that other proteins may be sequestered into aggregates.

Further support for such a mechanism was provided by proteomic studies of both mouse and CADASIL patient material (Arboleda-Velasquez et al., 2011, Monet-Lepretre et al., 2013). Clusterin and collagen18α1/endostatin were identified as GOM components in the tunica media of CADASIL brain vessels collected by laser capture microdissection (Arboleda-Velasquez et al., 2011). Monet-Lepretre and co-workers extended this approach by enriching Notch3-ECD deposits from CADASIL brain material and TgNotch3^{R169C} vessels through sequential fractionation and analyzing the Notch-ECD-containing fraction (Monet-Lepretre et al., 2013). A variety of proteins predominantly from the ECM were found to co-fractionate with Notch3-ECD. For two of them, tissue inhibitor of metalloprotease 3 (TIMP3) and vitronectin, further evidence for their presence in Notch3-ECD aggregates was reported and disease-related roles proposed. Their abnormal recruitment was suggested to cause a dysregulation of their activity contributing to the impaired ECM homeostasis in small vessels (Monet-Lepretre et al., 2013).

1.4 Goals of this thesis

Notch3-ECD aggregation in CADASIL vessel walls likely represents the initiating event of a continuative process involving the recruitment and sequestration of ECM proteins with important roles in normal vessel function ultimately leading to multifactorial toxicity. Although initial efforts to identify co-aggregating factors have yielded a variety of candidate proteins, the pathological events resulting in vessel degeneration are still poorly understood. This thesis aimed to extend and refine previous data on Notch3-ECD aggregate components by analyzing potential candidate proteins in more detail. Due to the extracellular localization of Notch3 deposits and the crucial role the ECM plays in vessel homeostasis, five ECM and ECM-associated (matricellular) proteins were selected for this study: fibrillin-1 and fibronectin, two major structural ECM components; LTBP-1 and LTBP-4, two members of the latent transforming growth factor-β (TGF-β) binding protein (LTBP) family of TGF-β signaling regulators; and thrombospondin-2 (TSP-2), a

matricellular protein known to interact with Notch3 and to co-aggregate with CADASIL mutants. Approaches applied in this study include biochemical fractionation and immunohistochemical localization on CADASIL patient brain autopsy material as well as *in vitro* interaction and co-aggregation assays. Using these techniques, I sought to provide an in depth analysis of the roles ECM proteins play in Notch3-ECD deposition.

2 Materials and Methods

2.1 Equipment

37 °C incubator (Function line)	Heraeus
37 °C shaker (Certomat BS-1)	Sartorius
Agarose gel chamber (40-0708)	PEQLAB
Autoclave (VX 150, DX 65)	Systec
Cell culture CO_2 incubator (HERA Cell)	Heraeus
Cell culture flasks for purification (Nunclon Surface Triple Flasks 500cm²)	Nunc
Cell Strainer (40 µm)	BD Falcon
Centrifuge (Avanti J-26 XP) with swinging rotor (JS 7.5)	Beckmann Coulter
Clean bench (HeraSafe KS18)	Heraeus
Cooling centrifuge for small disposable tubes (5417R)	Eppendorf
Cooling centrifuge for large disposable tubes (Heraeus Megafuge 16R)	Thermo Scientific
Cooling Ultracentrifuge (Optima L-90K)	Beckman Coulter
Coverslides 22x50 mm #1 (Inverse microscopy)	Menzel Glas
Coverslides 24x60 mm # 1.5 (confocal microscopy)	Menzel Glas
Disposable Cell culture flasks T80	Nunc
Disposable Cryotube (1.8 mL)	Nunc
Disposable Culture well plates (6 and 24 well)	BD Falcon
Disposable tubes (0.5 ml; 1.5 ml; 2.0 ml)	Eppendorf
Disposable tubes (15 mL)	Thermo Scientific
Disposable tubes (50 mL)	BD Falcon
Disposable well plate for protein determination (96well Microplates PS, F-bottom)	Greiner bio-one
Electrophoresis cell (Mini-PROTEAN)	BioRad
Freezer -80° C (Hera Freeze Top)	Thermo Scientific

Homogenisator Tissue Lyser LT	Qiagen
Liquid Nitrogen Tank (Cryoplus 2)	Thermo Scientific
Microscope Axiovert 200M; Camera AxioCam MRm	Zeiss
Microscope slide (Superfrost Plus)	Menzel
Microscope, confocal (TCS SP5)	Leica
Microwave	Siemens
Needle with cannula (0,33x12 mm, Myjector U40)	Terumo
pH-Meter (Lab 850)	Schott Instruments
Power Supply (Power Pac 30)	PEGLAB
Rocking Shaker (ST5 CAT)	neoLab
Tissue grinder, Type Potter-Elvehjem with smooth pestle	Wheaton
Water bath (1005)	GFL

2.2 Chemicals

0,05 % Trypsin-EDTA	Gibco
2-Mercaptoethanol (β-ME) ≥ 99,0 %	Sigma
Acetone	Merck
Acrylamide: Ultra Pure Proto Gel (30 %) 37.5:1 Acrylamide/Bisacrylamide	National diagnostics
Agarose	Sigma
Albumin from bovin serum (BSA) 96 %	Sigma
Ammoniumpersulfat (APS)	Sigma
Ampicillin	Sigma
Boric acid	Sigma
Bromphenol Blue	Sigma
Protease inhibitor (complete Mini EDTA free cocktail tablets)	Roche
Dimethyl Sulfoxide (DMSO)	Sigma
Disodiumphosphate (Na_2HPO_4)	Merck
DMEM + GlutaMAX	Invitrogen

Ethylenediaminetetraacetic acid disodium (EDTA)	Roth
Ethanol 70 %; 96 %	Roth
Ethanol absolute, for analysis	Merck
Fetal Bovine Serum (FBS)	Gibco
Ficoll PM 400	Sigma
G418 Sulfate	Calbiochem
Glycerol ≥99,5 %	Roth
Glycin	Sigma
Hydrogen peroxide (H_2O_2) 30 %	Merck
Methanol ≥ 99%	Roth
Monopotassium phosphate (KH_2PO_4)	Merck
Orange G	Sigma
Paraformaldehyd (PFA) 4 % in PBS 7.4	Morphisto
Penicillin/Streptomycin (10000U/mL)	Invitrogen
Peptone (from Soja)	Roth
Select agar	Invitrogen
Skim milk powder	Fluka
Sodium bicarbonate ($NaHCO_3$)	Sigma
Sodium chloride (NaCl)	Roth
Sodium dodecyl sulfate (SDS) Pellets	Serva
Tetramethylethylenediamine (TEMED)	Roth
Tri-Sodiumcitrat-dihydrat ($Na_3C_6H_5O_7xH_2O$)	Roth
Tris (Tris(hydroxymethyl)-Aminomethane)	Merck
Trizma base	Sigma
Tween 20	Roth
Xylene Cyanole F.F	ICN
Xylol (Rotihistol)	Roth
Yeast extract	Roth

2.3 Recombinant Proteins

Fibronectin	Sigma
Human IgG_1-Fc	R&D Systems
Human Notch3-Fc Chimera, aa 40-467	R&D Systems

2.4 Human samples

2.4.1 Human brain tissue

Brain samples from twelve deceased elderly patients, frozen or paraffin-embedded, were obtained from various sources (Brain-Net, LMU, Munich [Thomas Arzberger]; INSERM Paris [Anne Joutel]; Leiden University Medical Center [Saskia Lesnik-Oberstein]). A total of six CADASIL patients, genetically confirmed (mean age 64,3 years) and six age- and sex-matched controls (mean age 61,3 years) were employed.

Table 2: Overview of all brain autopsies

Description	Sex	Age	Diagnosis	Mutation	Location
CAD 1	M	64	CADASIL	R110C	Gyrus frontalis medius
CAD 2	F	66	CADASIL	D239_D253del	Gyrus frontalis medius
CAD 3	M	68	CADASIL	C144S	Gyrus frontalis medius
CAD 4	F	60	CADASIL	R153C	Frontal lobe
CAD 5	F	70	CADASIL	C1261R	Frontal lobe
CAD 6	F	58	CADASIL	R153C	Frontal cortex
Ctrl 1	M	61	Control	-	Gyrus frontalis medius
Ctrl 2	F	55	Control	-	Gyrus frontalis medius
Ctrl 3	F	60	Control	-	Gyrus frontalis medius
Ctrl 4	F	73	Control	-	Gyrus frontalis medius
Ctrl 5	M	60	Control	-	Gyrus frontalis medius
Ctrl 6	F	59	Control	-	Gyrus frontalis medius

2.4.2 Brain vessel isolation

Phosphate buffered saline (PBS)
154 mM NaCl, 9.5 mM Na_2HPO_4, 1.7 mM KH_2PO_4, pH 7.4

50 mg brain tissue was homogenized with 15 mL cold Minimum Essential Media (MEM, Invitrogen) in a tissue grinder with a total of 60 up and down strokes. An equal volume of

30 % Ficoll in MEM was added and centrifuged at 6000 g, 4 °C for 20 min in a swinging rotor. The supernatant was discarded and the pellet suspended in 1 %BSA in PBS. Next, the homogenate was poured onto a 40 µm Nylon mesh (Corning Life Sciences) and extensively washed with PBS. By inversion of the nylon mesh, vessels were collected in a tube and pelleted for 5 min at 3000 g. The purity of the vessels was checked under a phase-contrast microscope.

2.5 DNA Techniques

2.5.1 Plasmids

Table 3: List of plasmids. EGF: epidermal growth factor, aa: amino acids.

Plasmid	**Description**	**Reference / Cloning Strategy**
pcDNA3.1 (-)	Mammalian expression vector	Invitrogen
pcDNA3_LTBP-1	Encodes human full length LTBP-1S with a CD5 signal peptide, an N-terminal HA-tag and a C-terminal V5-His tag	Nathalie Beaufort, ISD Munich
pSignal_LTBP-1ΔN_HA	Encodes N-terminally truncated LTBP-1 (aa 528-1395) with a C-terminal HA-tag	Jorma Keski-Oja, Helsinki, Finland (Saharinen et al., 1996)
pcDNA3_LTBP-1ΔN_V5	Encodes LTBP-1ΔN with a C-terminal V5-His tag	Generated by restriction with SnaBI and BbvCI of LTBP-1 (Vector) and LTBP-1ΔN_HA (Insert)
pTT5_N3EGF1-5 Wt_Halo	Encodes hNotch3 EGFR 1-5 with a Halo fusion Tag	Patrizia Hanecker, ISD Munich
pTT5_N3EGF1-5 C183R_Halo	Encodes hNotch3 EGFR 1-5 with a Halo fusion Tag, mutation C183R	Patrizia Hanecker
pcDNA3_LTBP-1ΔC_V5	Encodes a C-terminally truncated LTBP-1 (aa 1-689) with a C-terminal V5-His tag	Nathalie Beaufort

2.5.2 Agarose gel electrophoresis

Agarose Gels:
1 % (w/v) agarose in 1xTBE buffer, melted in a microwave

5x TBE buffer:
445 mM Trizma base, 445 mM boric acid, 10 mM EDTA, pH 8.0

6x DNA-loading buffer:
60 % (v/v) Glycerol, 10 mM Tris-HCl pH 7.6, 60 mM EDTA, 2.5 mg Xylene Cyanol, 2.5 mg Orange G

DNA fragments mixed with DNA-loading buffer were separated on a 1 % agarose Gel in 1x TBE buffer with the addition of SYBR Safe DNA Gel Stain (Invitrogen) diluted 1:10000, using a constant voltage of 80 V for roughly 1 h. As a molecular marker, PeqGOLD DNA Ladder-Mix (PEQLAB) was used. Finally, gels were visualized on a gel-doc Fusion FX7 (Vilber Lourmat).

2.5.3 Restriction enzyme treatment

Restriction enzymes (New England Biolabs):
SnaBI (5U/µL), BbvCI (2U/µL)

Restriction Enzyme Buffer (New England Biolabs):
NEB4

100x BSA (New England Biolabs):
diluted 1:10

Analytical restriction analysis was carried out in the following manner.

Table 4: Analytical restriction enzyme treatment

Component	Volume
Restriction enzyme	5 U
Restriction buffer	3 µL
DNA	0.6 µg
10x BSA	3 µL
H_20	ad 30 µL

Preparative restriction analysis for subsequent cloning experiments was carried out in the following manner

Table 5: Preparative restriction enzyme treatment

Component	Volume
Restriction enzyme	10 U
Restriction buffer	5 µL
10x BSA	5 µL
DNA	4 µg
H_20	ad 50 µL

All restriction digestion mixtures were incubated for 1 h at 37 °C. Afterwards, the DNA fragments were separated on an agarose gel, extracted and purified using the GeneJET Gel Extraction Kit (Fermentas) according to manufacturer's specifications.

2.5.4 Vector dephosphorylation

Phosphatase (New England Biolabs):
Antarctic Phosphatase (5 U/µL)

Phosphatase buffer (New England Biolabs):
10x Antarctic buffer

Table 6: Dephosphorilation of the vector

Component	Volume
Gel extract	20 µL
10x Antarctic buffer	3 µL
Antarctic phosphatase	1 µL
H_20	6 µL

In order to dephosphorylate the vector to prevent self-ligation, the gel extract was treated with a phosphatase for 30 min at 37 °C, followed by 5 min at 65 ° C to inactivate the enzyme.

2.5.5 DNA Ligation

Enzyme (New England Biolabs):
T4 DNA ligase (400 U/µL)

Buffer (New England Biolabs):
10x T4 DNA Ligase Reaction buffer

Table 7: DNA Ligation Mixture

Component	Volume
Vector	150 ng
Insert	50 ng
T4 Ligase	1 µL
T4 buffer	2 µL
H_20	ad 20 µL

Components to ligate vector and insert were mixed together and incubated 1 h at room temperature. 2 µL of the ligation mix was used for the subsequent transformation of competent bacteria.

2.5.6 Transformation of competent bacteria

LB-Medium:
0.5 % (w/v) Yeast extract, 1 % (w/v) Peptone, 0.5 % (w/v) NaCl, pH 7.0; autoclaved

LB Agar plates containing ampicillin:
LB Medium, 0.15 % (w/v) agar, autoclaved, 100 µg/mL ampicillin is added after chilling to roughly 50 °C.

2 µL ligation mix was added to 50 µL of competent bacterica (*E.coli DH5α*, present in the laboratory) and incubated for 30 min on ice. A heat shock at 42 °C for 90 sec allowed the plasmid to permeate into bacteria. After cooling down for 2 min on ice, 250 µL LB-Medium was added and incubated at 37 °C for 1h under gentle agitation. Subsequently, 200 µL transformation mix were plated on LB Agar plates containing ampicillin. After incubation overnight at 37 °C, several colonies were picked from the plates in 5 mL LB-Medium + 100 µg/mL ampicillin for small-scale DNA isolation.

2.5.7 DNA Isolation of bacteria

5 mL of transformed bacteria were used for small-scale DNA isolation with the NucleoSpin Plasmid Kit (Macherey-Nagel). The concentration and quality was checked using the Nanodrop ND-1000 (PEQLAB). Before the plasmid was sent for sequencing to GATC Biotech AG (Konstanz, Germany), analytical restriction analysis was carried out to ensure the correct buildup of the plasmid.

For large-scale DNA isolation, small amounts of transformed bacteria were diluted in 100 mL LB-Medium + 100 µg/mL ampicillin and cultured overnight while shaking. On the next day, plasmid DNA was isolated with the aid of the NucleoBond Xtra Midi Kit (Macherey-Nagel). Again, purity and concentration was analyzed using the Nanodrop.

2.6 Cell Culture

2.6.1 Cell lines

Table 8: List of cell lines. All cell lines were available in the laboratory. DMEM: Dulbecco's Modified Eagle Medium

Cell line	Description	Culture Medium+
HEK293T	Human embryonic kidney cells, expressing the SV40 large T antigen	DMEM+GlutaMax +10% FBS + 5 mL Penicillin/Streptomycin
HEK293E	Human embryonic kidney cells, transfected with the Epstein Barr Virus nuclear antigen 1 (EBVNA 1)	DMEM+GlutaMax +10% FBS + 5 mL Penicillin/Streptomycin + 25 µg/mL G418

2.6.2 Cell Cultivation

Cells were cultured in their respective media (see Table 8) as adherent monolayers at 37 °C in a humidified atmosphere of 5 % CO_2. As requested, cells were passaged twice a week. Therefore, cells grown to 70-80 % confluency were washed once with PBS, trypsinized and seeded in fresh medium after resuspending in the desired ratio (roughly 1:10). Microscopic analysis guaranteed the condition of the cells. Frequent analysis for microplasma using the Venor GeM One-Step Detection Kit for endpoint PCR (Minerva Biolabs) secured a microplasma-free environment.

2.6.3 Cell transfection for conditioned media

HEK293T cells were seeded into well plates in a defined number, totaled using an automated cell counter (TC20, Biorad). Transfection was performed with the Fugene HD Transfection Reagent (Roche) according to the manufacturer's manual. Briefly, plasmid and Fugene were mixed in OptiMEM (Invitrogen) and, after an incubation period of 15 min, added to serum-free medium. Following culturing in serum-free DMEM for 48 h,

the medium was collected and centrifuged 10 min at 1000 g to eliminate cell debris. Finally, the conditioned medium was stored at -20°C until further use.

2.6.4 Cell cryoconservation

Freezing Medium
FBS containing 10 % (v/v) DMSO

90 % confluent cells grown in a T 80 flask were trypsinized and pelleted. Pellets were re-suspended in freezing medium, transferred into a cryotube and allowed to gradually freeze in a Freezing Container (Mr. Frosty, Nalgene) kept in a - 80 ° freezer overnight. On the next day, cryotubes were transferred into a liquid nitrogen tank for long-term storage.

For thawing, cryotubes were allowed to quickly reach 37 °C in a water bath and subsequently collected in fresh medium. After centrifugation, the pellet was washed once with PBS and resuspended in fresh medium. Next, cells were transferred into a flask and allowed to sediment.

2.6.5 Large scale transfection for protein purification

First, two confluent T 80 flask of HEK293E cells were trypsinized and transferred into a triple flask with 90 mL of fresh medium. A total of four triple flasks for each purification were used. For the transfection on the next day, 75 µg plasmid and 300 µg poly-ethylenimine (Polyscience) in OptiMEM were prepared for each flask and incubated for 25 min. In the meantime, cells were washed twice with PBS. The transfection mix was added to 90 mL of fresh DMEM + 10 % FCS. Five hours later, cells were washed again twice and replaced by 90 mL serum-free medium. Conditioned medium from cells transfected with LTBP-1ΔC_V5 and LTBP-1ΔN_V5 was collected two or three days later, respectively and cleared from cell debris by centrifugation for 10 min at 1000 g. Afterwards, conditioned media were immediately subjected to dialysis.

2.7 Protein analysis

2.7.1 Antibodies

Respectively, Table 9 and Table 10 list all the primary and secondary antibodies that were used during this thesis.

Table 9: List of primary antibodies. WB: Western Blot; IF: Immunofluorescence, IHC: Immunohistochemistry, SPBA: Solid phase binding assay.

Antibody	Type	Application	Source/Reference
Anti-APP A4	Mouse monoclonal	WB 1:4000	Millipore
Anti-Collagen type IV	Goat polyclonal	IF 1:500	Southern Biotech
Anti-fibrillin-1	Rabbit polyclonal, affinity purified	IF/IHC 1:100 WB 1:1000	Lynn Sakai (Gayraud et al., 2000)
Anti-fibronectin	Mouse monoclonal	IHC 1:300	Sigma
Anti-fibronectin	Rabbit polyclonal, affinity purified	WB 1:10000	Sigma
Anti-LAP TGF-β1	Goat polyclonal	WB 1:500 IHC 1:50	R&D Systems
Anti-LTBP-1	Mouse monoclonal	WB 1:500 IF 1:50 SPBA 1:500	R&D Systems
Anti-LTBP-4	Rabbit polyclonal	WB 1:1000	Lynn Sakai, Portland, USA (Ono et al., 2009)
Anti-Notch3-ECD (2G8)	Rat monoclonal hybridoma supernatant	IF/IHC 1:10	Elisabeth Kremmer, Helmholz Zentrum, Munich
Anti-Notch3-ECD (3G6)	Rat monoclonal hybridoma supernatant	WB 1:20	Elisabeth Kremmer, Helmholz Zentrum, Munich
Anti-α-SMA	Mouse monoclonal, Cy3 (red) coupled	WB 1:10000	SIGMA
Anti-TSP-2	Mouse monoclonal	WB 1:1000	Santa Cruz
Anti-β-Tubulin	Mouse monoclonal, ascites fluid	WB 1:1000	Sigma
Anti-V5	Mouse monoclonal	SPBA 1:500 WB 1:1000	Invitrogen

Table 10: List of secondary antibodies. HRP: Horseradish peroxidase.

Antibody	Type	Conjugate	Application	Source
Donkey anti-goat	Purified	Cy2 (green)	IF 1:200	Jackson ImmunoResearch
Donkey anti-goat	Purified, $F(ab')_2$ Fragment	Rhodamine Red X (red)	IF 1:100	Jackson ImmunoResearch
Donkey anti-mouse	Purified, $F(ab')_2$ Fragment	Rhodamine Red X (red)	IF 1:50-1:100	Jackson ImmunoResearch
Donkey anti-rabbit	Purified	Cy3 (red)	IF 1:100	Jackson ImmunoResearch
Donkey anti-rabbit	Purified, $F(ab')_2$ Fragment	AF488 (green)	IF 1:50	Jackson ImmunoResearch
Donkey anti-rat	Purified, $F(ab')_2$ Fragment	Cy3 (red)	IF 1:50	Jackson ImmunoResearch
Goat anti-mouse	Polyclonal, purified	Biotinylated	IHC 1:200	Vector
Goat anti-mouse	Polyclonal	HRP	WB 1:5000-1:10000 SPBA 1:1000	DAKO
Goat anti-rabbit	Polyclonal	HRP	WB 1:5000-1:10000	DAKO
Goat anti-rabbit	Polyclonal, purified	Biotinylated	IHC 1:200	DAKO
Goat anti-rat	Purified	Fluorescein (green)	IF 1:50	Jackson ImmunoResearch
Horse anti-goat	Polyclonal purified	Biotinylated	IHC 1:200	Vector
Rabbit anti-goat	Polyclonal	HRP	WB 1:5000	DAKO
Rabbit anti-human	Polyclonal	HRP	SPBA 1:1000	DAKO
Rabbit anti-rat	Polyclonal	HRP	WB 1:5000	DAKO
Rabbit anti-rat	Polyclonal, purified	Biotinylated	IHC 1:200	DAKO

2.7.2 Sequential protein extraction

Tris Buffer:
0.05 M Tris-HCl pH 7.5 + Protease inhibitors

SDS Buffer:
Tris Buffer + 1 % (w/v) SDS + Protease inhibitors

β-ME Buffer
SDS Buffer + 5 % (v/v) β-ME + Protease inhibitors

5x Lämmli buffer:
375 mM Tris Base pH 6.8, 30 % (v/v) Glycerol, 6 % (w/v) SDS, 0.03 % (w/v) Bromphenol blue

All steps were carried out at 4 °C. 30 mg brain tissue or purified brain vessels were homogenized in a tissue homogenisator with a 5 mm metal-ball (Qiagen) for 3 min at 50 Hz in 100 µL Tris Buffer. After spinning down for 5 min at 13200 rpm, the "Tris-faction" was set aside and the pellet resuspended in 100 µL SDS Buffer. After lysing 30 min on ice, the homogenate was sedimented for 30 min at 13200 rpm. The supernatant (SDS fraction) was collected and the remaining pellet was further solubilized in 100 µL β-ME Buffer for 30 min on ice while passing though a 29 gauge needle at least 5 times. Repeated centrifugation for 30 min at 13200 rpm resulted in the last fraction, the "β-ME fraction". After the protein amount of the Tris and SDS fraction was determined, the samples were mixed with the appropriate amount of Lämmli-buffer. Due to the high amount of reducing agent, a protein determination in the β-ME fraction was not possible.

2.7.3 Protein Quantification

The Tris, as well as the SDS fraction of the sequential protein extraction were quantified using a bicinchoninic acid assay (Thermo Scientific) with a BSA standard (Quick Start BSA Assay, BioRad) according to the manufacturer's protocol.

2.7.4 Dialysis of conditioned media

Before conditioned medium was purified, it was fist dialyzed twice against 0.5x PBS for one hour and another two times against 0.5x PBS + 200 mM NaCl for one hour each.

2.7.5 Purification of proteins using Talon beads

Talon Wash buffer
50mM Phosphate, 300mM NaCl, pH 7.0

The following steps were carried out at room temperature and 4 °C for LTBP-1ΔC and LTBP-1ΔN, respectively. To the total amount of conditioned medium (360 mL), 2 mL (bead volume) TALON affinity resin (Clontech), washed three times with Talon washing buffer, was added and allowed to bind His-tagged proteins for one hour under gentle agitation.

Subsequently, the beads were spinned down for 10 min at 800 g, the supernatant was discarded and the beads were transferred onto a TALON 2 mL disposable gravity column (Clontech). After washing several times with Talon washing buffer, with and without adding 5mM imidazole (Fluka), the protein was eluted in PBS containing 100 mM EDTA in ten fractions. Protein amounts were evaluated using the Qubit protein assay (Life Technologies) according to the manufacturer's instructions. To check the protein quality, the samples were run on a SDS-PAGE and visualized by silver staining.

2.7.6 Solid-phase binding assay

5x Lämmli + β-ME
5x Lämmli + 5 % (v/v) β-ME

20 µg/mL recombinant proteins dissolved in PBS were coated onto Maxisorp 96-well plates (Nunc) overnight at 4 °C. On the next day, the wells were first washed four times with 300 µL PBS, blocked with 1 % BSA in PBS for 1 hand then washed again. Next, 50 µL conditioned media from HEK293T transfected cells (LTBP-1, LTBP-1ΔC_V5, or LTBP-1ΔN_HA) or 2 ng/µL purified LTBP-1ΔC_V5 was added for 1 h at room temperature. Mock transfected cells or PBS was used as a negative control. After washing, bound protein was detected with the appropriate first antibody (anti-V5 (detection of LTBP-1 with LTBP-1_ΔC) or anti-LTBP1 (detection of LTBP-1 with LTBP-1_ΔN) and secondary antibody (anti-mouse-HRP) diluted in PBS and sequentially added for 1 h at room temperature with an in-between washing step. Immune complexes were determined by incubation with TMB substrate solution (KPL) followed by the appropriate stop solution once the colorimetric reaction was visible. The optical density was measured at 560 nm and corrected with a measurement at 420 nm. For the calculation of the results, the unspecific binding was subtracted.

To recover bound proteins from the plate, 25 µL 1xLämmli + β-ME was added to the plates and heated for 15 min at 95 °C.

2.7.7 SDS-PAGE

10x Running buffer
0.25 M Tris, 1.92 M Glycin, 1 % (w/v) SDS

4x Lower Tris
1.5 M Tris pH 8.8, 0.4 % (v/v) SDS

4x Upper Tris
0.5 M Tris pH 6.8, 0.4 % (v/v) SDS

Proteins were separated using the sodium dodecyl sulfate polyacrylamide gel electrophoresis (SDS-PAGE) in a discontinuous system with a stacking and a separation gel in 1x running buffer. Table 11 shows the composition of these gels. 6 µL Precision Plus Protein All Blue Standards (BioRad) or 2 µL Precision Plus Protein Unstained Standards (BioRad) were used as molecular weight markers in case of further processing for Western Blots or silver staining, respectively. Electrophoresis was carried out using the minigel system (BioRad) at 80-120 V.

Table 11: Composition of two 1.0 mm stacking and separation gels. AA: acryl–bisacrylamide; Tris: tris(hydroxymethyl)aminomethane; TEMED: tetramethylethylenediamine; APS: ammmonium persulfate.

Solution	Stacking gel	Separation gel
H_20	5.88 mL	2.94 mL
40 % AA	3 mL	0.55 mL
4x Lower Tris	-	3 mL
4x Upper Tris	1.02 mL	-
APS	45 µL	100 µL
TEMED	4.5 µL	10 µL

2.7.8 Western Blotting

Blotting buffer
25 mM Tris, 192 mM Glycine, 20 % (v/v) Methanol

10x TBST
100 mM Tris pH 8.0, 1.5 M NaCl, 0.5 % (v/v) Tween 20

Blocking solution
4 % (w/v) skim milk powder in 1xTBST

After SDS-PAGE, proteins were transferred onto a Immobilon-P Transfer Membrane (Millipore) in blotting buffer with a constant current of 125 mA limited to 25 V for 60-90 min using the semi-dry system (Trans-Blot SD Semi-Dry Transfer Cell, BioRad). Afterwards, unspecific binding sites were inhibited in blocking solution for one hour at room temperature followed by incubation with the primary antibody in blocking solution under constant rotation at 4 °C overnight. The next day, spare antibody was removed by several washing steps using 1xTBST followed by incubation with the with horseradish peroxidase (HRP)–conjugated secondary antibody diluted in blocking solution for at least one hour. Subsequently, membranes were washed again in 1xTBST before developing with Immobilon Western Chemiluminescent HRP Substrate (Millipore) according to the

manufacturer's specifications. The chemiluminesence signal was digitalized using the Fusion camera for the required amount of time.

2.7.9 Silver staining

Silver staining was performed with the Roti-Black P Silver Staining Kit (Roth) as specified in the manufacturer's manual.

2.7.10 Histological stainings

2.7.10.1 Immunofluorescence on human Cryosections

Histo blocking buffer
5 % (v/v) normal donkey serum (Jackson ImmunoResearch) in PBS

Human tissue samples were cut on a Cryostat (CM1950, Leica) in 10 µm thickness and stored at -80 °C until further use. On the day of the experiment, sections were thawed to room temperature for 15 min. Tissue was either fixed for 10 min in ice–cold acetone followed by air-drying for 30 min or with PFA under gentle agitation for 15 min. Subsequently, sections were washed 3x5 min with PBS. Thereafter, unspecific binding sites were blocked with histo blocking buffer for 40 min at room temperature and primary antibodies were diluted in histo blocking buffer and incubated overnight at 4 °C. On the following day, sections were first washed, incubated with the secondary, fluorescence coupled antibody in Histo blocking buffer for 1 h at room temperature in the dark and then washed again. Afterwards, sections were mounted in ProLong Gold antifade reagent (Life Technologies) with coverslips and sealed with common nail polish to prevent exsiccation. Sections were analyzed either on a confocal or inverse microscope. As an appropriate negative control, the first antibody was omitted in each experiment.

2.7.10.2 AEC Staining of human paraffin sections

Citrate buffer
10 mM $Na_3C_6H_5O_7xH_2O$ in PBS, pH 6.0

Paraffin sections with a thickness of 8 µm, received from Thomas Arzberger (Brain-Net, LMU Munich), were first deparaffinized (2x5 min Xylol) and rehydrated in a descending alcohol series (2 min absolute ethanol, 2 min 96 % ethanol, 2 min 70 % ethanol, 5 min PBS). Afterwards, sections were boiled in citrate buffer for 30 min at 95 °C to unmask antigens. Slides were allowed to reach room temperature, washed 2x5min in PBS and nonspecific binding sites were blocked for 1 h in histo blocking buffer at room temperature. Thereafter,

primary antibodies were diluted in histo blocking buffer and incubated overnight at 4 °C. The next day, slides were first washed 3x10 min in PBS. Afterwards, endogenous peroxidases were blocked by incubation with 0.3 % hydrogen peroxide (v/v) in PBS. Sections were washed and appropriate biotinylated secondary antibody diluted in Histo blocking buffer were applied to sections and incubated for 1 h at room temperature. After washing, immunoreactivity was visualized with avidin/biotin-horseradish peroxydase complex (Vectastain ABC-HRP kit, Vector Laboratories) and developed with 3-amino-9-ethylcarbazole (AEC Peroxidase substrate Kit, Vector Laboratories). After washing 5 min in tap water, sections were counterstained with Mayer's hematoxylin Solution (Sigma) for 1 min to provide cytological detail and rinsed 10 min in tap water before mounting with ProLong Gold. Omission of primary antibodies served as a negative control. Sections were analyzed using a histology microscope (Zeiss).

2.7.11 Labeling of purified proteins for SIFT

SIFT buffer
50 mmol/l Tris HCl, pH 7.5

Prior to labeling the purified proteins (1.7 µM and 1.58 µM LTBP-1ΔC; 2.27 µM LTBP-1ΔN), samples were concentrated to 50 µL using a centrifugational filter device with a 3 kDa molecular cutoff (Amicon Ultra Centrifugal Filters-0.5 mL 3K, Millipore) according to the manufacturer's specifications. Afterwards, green fluorescence dye (Alexa Fluor 488 carboxylic acid succinimidyl ester, Invitrogen) was added in 2.5 fold excess, which covalently binds to free amines of the protein. To buffer the reaction, 100 mmol/L sodium bicarbonate (pH 8.5) was added and the mixture was incubated overnight at 4 °C in the dark.

On the next day, the unbound dye was removed by two gel filtration steps (Zeba desalt spin Columns, 0.5ml, Thermo Scientific) carried out according to the manufacturer's protocol. At the same time, the buffer was exchanged from PBS+EDTA to the SIFT buffer. Purity was checked using fluorescence correlation spectroscopy autocorrelation measurements (Insight Reader, Evotec-Technologies). All samples had roughly the same amount 70 %of unbound remaining dye. Finally, samples were aliquoted (4 µL), shock frozen in liquid nitrogen and stored until further use at -80 °C.

2.7.12 Scanning for intensely fluorescent targets (SIFT)

Scanning for intensely fluorescent targets (SIFT) is a method where single protein particles can be distinguished from aggregated proteins in a subpicomolar concentration. The

samples are composed of two proteins, one labeled in red, one in green, or a single protein with half of the molecule marked in red and the other half in green. The setup is confocal and the sample in a 398 well plate is excited by two lasers (green: 488 nm; red: 633 nm). They lasers are directed by an oscillating and moving beamsplitter and a moving sample table. The locomotion is necessary to achieve a higher sensitivity since aggregated proteins with a lager particle size are moving with a decreased diffusion rate. The emitted photons of each color are detected and represented in a two-dimensional (2-D) intensity distribution histogram (Figure 9). Each well is scanned 5 times and the detected fluorescence intensity of all measurements is summed up. Shown are particle brightness' for each fluorophore on the individual axis (x-axis in green; y-axis in red) in 0-250 photons/bin in dots. A bin is the sum of photons that are detected in a timeframe, here 40 µsec, in which the total measurement time is divided. Monomers with low particle brightness are found on the arbitrary origin while multimers and aggregates have higher bins thus are further away from this point. Mono-colored aggregates are found alongside the axis while dual colored aggregates are found in the middle of the histogram.

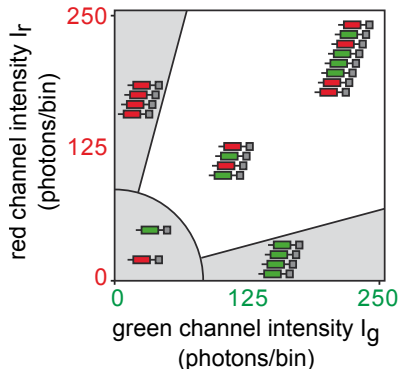

Figure 9: Schematic representation of SIFT data evaluation with a 2-D histogram. The y-axis shows photons/bin for the red channel while the x-axis represents green photons/bin. Monomers are located in the lower left corner. Higher order multimers of one color are distributed along the axis and multimers of both colors in the middle of the histogram.

After thawing aliquots, unspecific aggregates from the freezing process were removed by ultracentrifugation. Therefore, 4 µL samples were diluted with 100 µL SIFT buffer and centrifuged for 1 h at 100000 g at 4 °C. Particle amounts were checked using fluorescence correlation spectroscopy autocorrelation measurements and adjusted.

For spontaneous aggregation experiments, 50 µL of red-labeled protein was combined with 50 µL of green-labeled protein and samples were incubated for 24 hours at 37 °C and 500 rpm. Purified and green- or red-labeled Notch3EGF1-5 Wt or C183R were kindly provided by Patrizia Hanecker (ISD, Munich). Before the measuring on the SIFT Insight reader, 3 µL of sample was diluted in 20 µL SIFT buffer in a 384-well measurement plate

(Sensoplate, Greiner Bio-One). Each well was measured in triplicate with five meander per well with a total measurement time of 10 sec/well. Scanning parameters were set to 50 Hz beam scanner, 100 mm scan path length and 2000 mm positioning table movement. Results were evaluated with a 2D-SIFT software module (Evotec-Technologies)

2.8 Statistical analysis

Data generated with the solid phase binding assay were represented with mean values and standard error of the mean (SEM). Statistical analysis was performed applying the Mann-Whitney Test with the Sigma Plot 12.5 software. Significance is depicted with stars: *: $p<0.05$; **: $p<0.01$; ***: $p<0.001$.

3 Results

As a central event in CADASIL, mutant Notch3-ECD accumulates at the surface of vascular smooth muscle cells (vSMCs) in the tunica media of vessel walls, which likely promotes the abnormal recruitment of functionally relevant ECM proteins (Monet-Lepretre et al., 2013). In this thesis, potential candidates introduced below were studied in order to identify aggregate constituents involved in mediating Notch3-ECD toxicity using *post-mortem* brain material from CADASIL patients and controls.

3.1 Human post-mortem brain samples

A total of six CADASIL brain samples (mean donor age: 64.3 years) were compared to six age- and sex-matched controls (mean donor age: 61.3 years) with no known cerebrovascular disorders (Table 12). Since CADASIL mainly affects the white matter, regions of the frontal sub-cortex (gyrus frontalis medius and frontal lobe) were used except for patient 6 (CAD 6), for whom only a sample from the frontal cortex was available. The analysis techniques used were limited by the amount and type (frozen or paraffin-embedded) of the obtained material (Table 12).

For all patients, genomic sequencing of *NOTCH3* exons resulted in the detection of previously described Notch3 mutations genetically confirming the diagnosis CADASIL. All mutations led to the gain or loss of one or more cysteines within a single epidermal growth factor (EGF)-like repeat resulting in an odd number of this amino acid residue as observed for the vast majority of CADASIL mutations. The patient samples display a representative spectrum of characteristic mutations: the missense mutations C144S, R153C (both within EGF-like repeat 3) and R110C (within EGF-like repeat 2) are located in exon 4 (Joutel et al., 1997, Dichgans et al., 2000) and exon 3 (Joutel et al., 1997), respectively. The more rare deletion D239_D253del (within EGF-like repeat 6) locates in exon 5 and causes the loss of 15 amino acids including three cysteines (Cys240, Cys245 and Cys251) (Dichgans et al., 2001). Whereas all these mutations are situated within the mutational hotspot in exons 2 through 6 encompassing 86% of all CADASIL mutations (Peters et al., 2005a), the rare missense mutation C1261R resides in EGF-like repeat 32 close to the Notch3 transmembrane domain (Joutel et al., 1997).

Table 12: Overview of *post-mortem* brain samples. CAD: CADASIL, Ctrl: Control.

Description	Sex	Age	Mutation	Application
CAD 1	M	64	R110C	Histological stainings, Immunoblot
CAD 2	F	66	D239_D253del	Histological stainings, Immunoblot
CAD 3	M	68	C144S	Histological stainings, Immunoblot
CAD 4	F	60	R153C	Immunoblot
CAD 5	F	70	C1261R	Immunoblot
CAD 6	F	58	R153C	Immunoblot
Ctrl 1	M	61	-	Histological stainings, Immunoblot
Ctrl 2	F	55	-	Histological stainings, Immunoblot
Ctrl 3	F	60	-	Histological stainings, Immunoblot
Ctrl 4	F	73	-	Immunoblot
Ctrl 5	M	60	-	Immunoblot
Ctrl 6	F	59	-	Immunoblot

3.2 Analysis of Notch3 aggregates by biochemical fractionation

3.2.1 Notch3-ECD accumulates in CADASIL-affected brains

In a first approach, sequential protein extraction from brain samples was performed to enrich Notch3-ECD and potential co-aggregating proteins (Figure 10). Efficient solubilization of mutant Notch3-ECD requires a combination of sodium dodecyl sulfate (SDS) and β-mercaptoethanol (β-ME) (Duering et al., 2011, Monet-Lepretre et al., 2013). Therefore, a modified version of a previously established extraction protocol using increasing solubility strength was applied, which allows the enrichment of Notch3-ECD deposits. The procedure is described in detail in figure 10 A and yielded three fractions (Tris, SDS, β-ME), which were subsequently analyzed by immunoblotting. Analysis of one CADASIL (CAD 1) and one control (Ctrl 1) sample using an anti-Notch3-ECD antibody revealed the presence of a ~210 kDa band in the β-ME fraction of patient, but not control material confirming the enrichment of disulfide-bridged Notch3-ECD in CADASIL-affected tissue by the sequential extraction procedure. β-tubulin served as a loading control since it exists in a soluble monomeric as well as polymerized form and is thus present in each fraction (Mandelkow and Mandelkow, 1992).

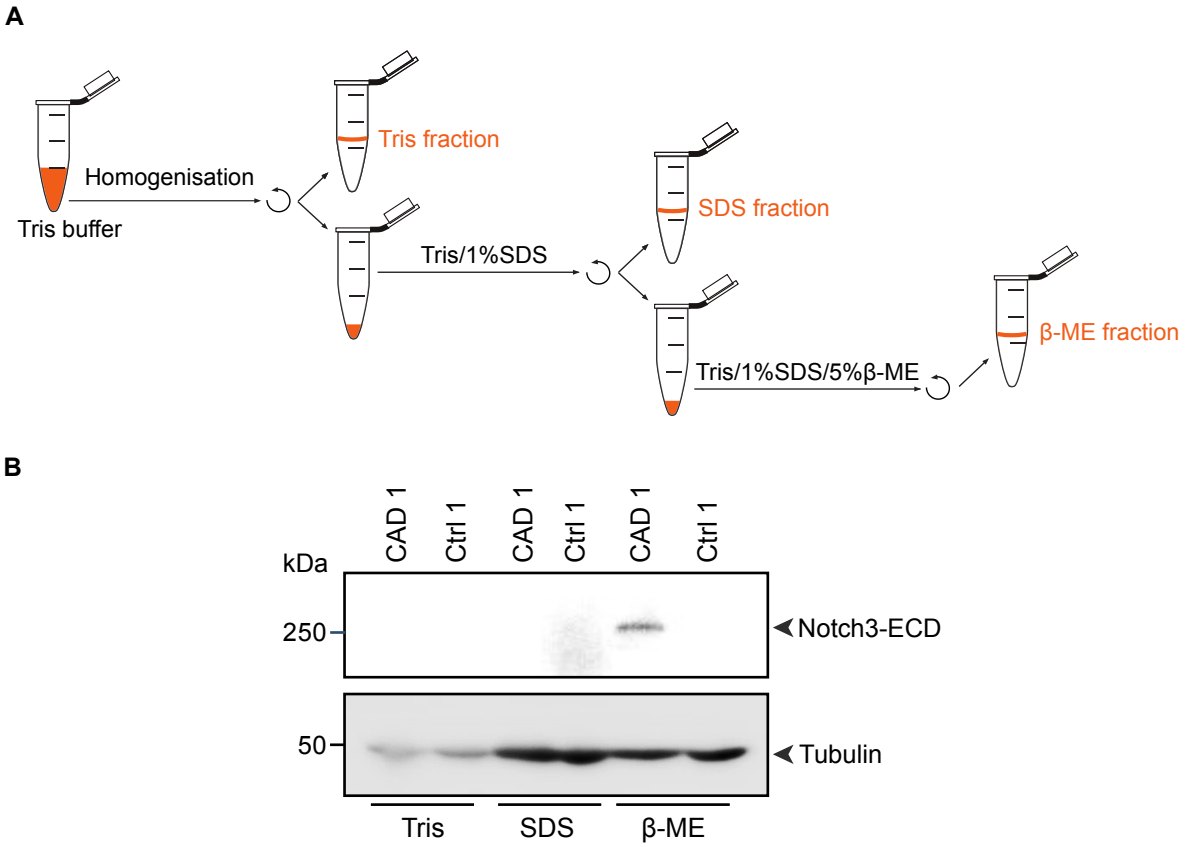

Figure 10: Sequential extraction of human brain samples. A) Schematic representation of the extraction procedure. Briefly, 30 mg of brain tissue was homogenized in 50 mM Tris pH 7.5, centrifuged and the resulting supernatant (Tris fraction) collected. After solubilization of the pellet in Tris buffer/1 % SDS and re-centrifugation, the SDS-soluble fraction was obtained. Detergent insoluble material was finally resuspended in Tris buffer/1 % SDS/5 % β-ME and clearance by centrifugation yielded the β-ME fraction. B) All three fractions obtained from an extraction of a CADASIL patient (CAD) and a control (Ctrl) sample were subjected to SDS-PAGE and immunoblotted with anti-Notch3-ECD 3G6 and anti-β-tubulin antibodies. Because of the impossibility of determine the protein concentrations in β-ME fractions, equal loading was ensured by adjusting protein amounts following Coomassie staining. Shown is a representative immunoblot from at least five independent extractions of three CADASIL and three control autopsies each.

3.2.2 TSP-2 and LTBP-4 are enriched in CADASIL brain samples

Having established this effective protein extraction procedure, potential Notch3-ECD aggregate constituents in the β-ME fraction were analyze expecting that co-aggregating proteins co-distribute in this fraction. Since Notch3-ECD deposits are extracellular structures located at the surface of vSMCs, the focus was set on ECM and matricellular (ECM-associated) proteins. This approach was supported by the recent results from a study by Monet-Lepretre et al., which reported the preferential enrichment of ECM constituents

in a proteomic analysis of a Notch3-ECD enriched fraction from CADASIL brain material (Monet-Lepretre et al., 2013).

First, two matricellular proteins, thrombospondin-2 (TSP-2) and latent transforming growth factor-β (TGF-β) binding protein 4 (LTBP-4), were selected for analysis. TSP-2 has been shown to interact with the shedded Notch3-ECD to mediate its re-uptake into neighboring cells (Meng et al., 2009, Meng et al., 2010). Moreover, our group previously demonstrated that TSP-2 co-aggregates with CADASIL-relevant mutant Notch3 fragments *in vitro* providing experimental evidence for a pathological co-aggregation (Duering et al., 2011). LTBP-4 was among the proteins identified in the study by Monet-Lepretre et al. as component of Notch3 aggregates isolated from a CADASIL mouse model. It is a member of the LTBP family, which regulates TGF-β signaling, a key pathway of the cerebral microvasculature involved in cell proliferation, differentiation, apoptosis and extracellular matrix production (Ruiz-Ortega et al., 2007).

The two candidate proteins were analyzed by immunoblotting for their distribution in the Notch3-ECD-enriched β-ME fractions of CAD 1-2 and Ctrl 1-2, the four samples available in this early phase of the project. Analysis of TSP-2 yielded a strong immunoreactivity in patient but not control material (Figure 11 A). For LTBP-4, although present in controls, a clear increase in patient samples was observed (Figure 11 B). This demonstrated co-fractionation of both proteins with mutant Notch3-ECD indicating their association with Notch3-ECD deposits. However, due to a lack of appropriate antibodies, co-localization studies on paraffin-embedded or frozen tissue sections could not be performed (see below). Thus, definite proof for the role of TSP-2 and LTBP-4 in Notch3-ECD deposition could not be provided during this work.

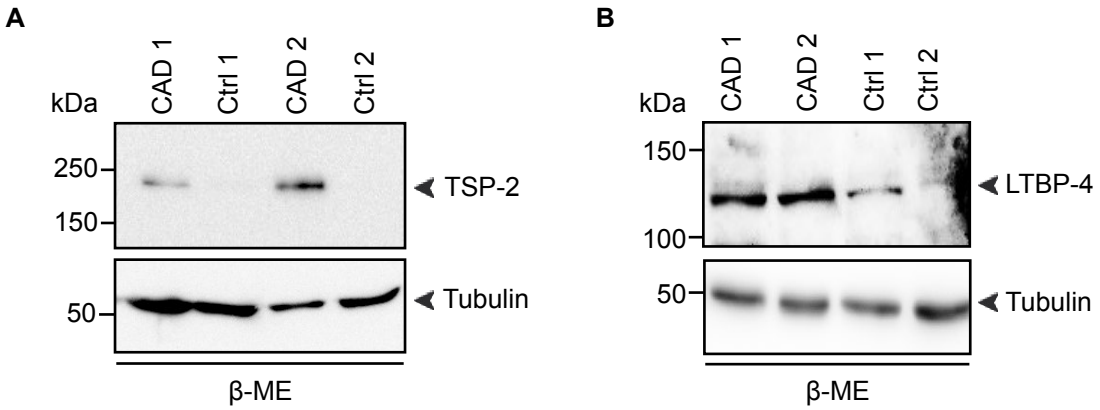

Figure 11: TSP-2 and LTBP-4 co-fractionate with Notch3-ECD in the β-ME fraction of CADASIL brains. Brain samples were sequentially extracted and the β-ME fraction was immunoblotted with A) anti-TSP-2 and B) anti-LTBP-4 as well as anti-β-tubulin antibodies. Representative blots from at least three independent extractions of three CADASIL and three control subjects are shown.

3.2.3 Isolation of brain vessels

During the initial analyses, immunoblotting for α-smooth muscle actin (α-SMA), a vSMC marker protein present in the β-ME fraction indicative for the amount of vessel tissue in the different samples, was also performed. As depicted in Figure 12, large heterogeneities in α-SMA amounts were observed despite relatively homogenous β-tubulin intensities. Moreover, the strongest signal was observed in one of the patient samples (CAD 2), which is expected to contain reduced α-SMA levels due to the well-known loss of vSMCs in CADASIL-affected vessels (Okeda et al., 2002). This indicated varying amounts of vessels in each brain extract although tissue samples from similar brain regions were used for the sequential extractions. Since the aim was to study differences in vessel proteins, the presence of roughly comparable amounts of vessels in each extract was desirable.

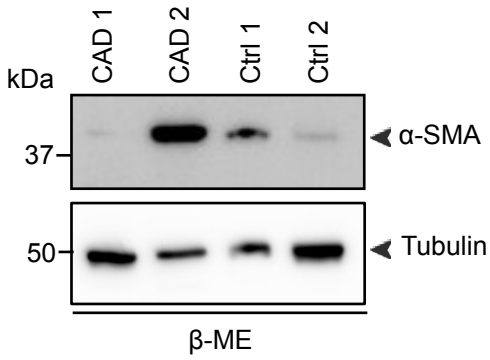

Figure 12: Brain lysates show varying contents of vessel marker α-SMA. Human brain homogenates were sequentially extracted and the β-ME fraction was immunoblotted with anti-α-SMA and anti-β-tubulin antibodies. Shown is a representative immunoblot from at least five independent extractions. α-SMA: smooth muscle actin.

Therefore, a previously described method (Monet-Lepretre et al., 2013) to isolate vessels including intraparenchymal arteries and arterioles, veins and capillaries from brain samples was established. The main steps of the isolation procedure are described in Figure 13A. It allows the removal of brain parenchymal tissue including myelin resulting in highly pure preparations of brain vessels as demonstrated by light microscopical analysis (Figure 13 B).

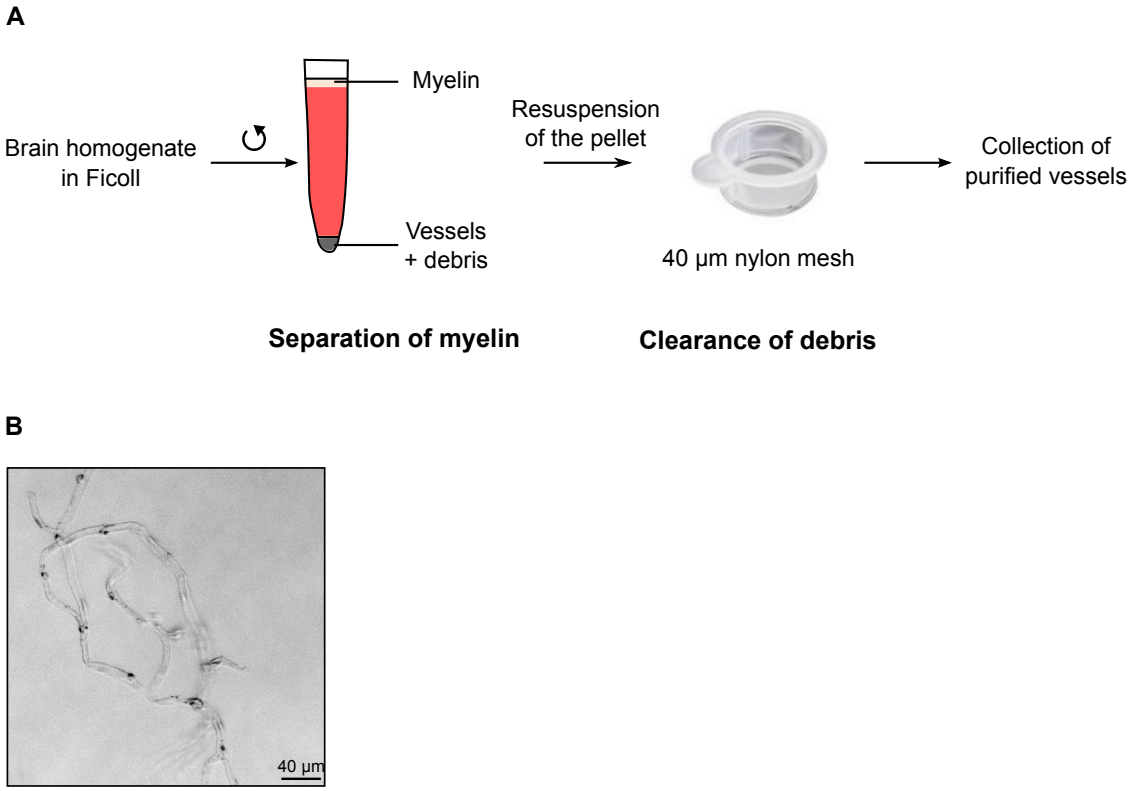

Figure 13: Vessel isolation from brain samples. A) 50 mg of brain tissue was homogenized in a tissue grinder with a smooth pestle allowing vessels to stay intact. Subsequent density gradient centrifugation in 15 % Ficoll resulted in pelletizing of vessels and cell debris, while myelin was floating on top of the gradient. After discarding the supernatant, the pellet was transferred onto a 40-µm nylon mesh, abundantly washed and purified vessels were collected by inversion of the mesh. B) Microscopic examination demonstrated the purity of the preparation.

Isolated vessels were subjected to sequential fractionation as described in chapter 3.2.1. Western Blotting of the β-ME fractions from three patients and three controls for α-SMA demonstrated the sample homogeneity and the expected reduction of α-SMA expression in CADASIL-affected vessels could be observed in all patient samples (Figure 14 A). Analysis of Notch3-ECD expression in the β-ME fractions of all available samples demonstrated the enrichment of Notch3-ECD in all patient, but not control vessels (Figure 14 B). The low intensity of the band in the CAD 2 sample is due to the low total protein amounts loaded (compare tubulin signals), a consequence of the impossibility to determine the protein concentration in the β-ME fractions. A repetition of immunoblots with adjusted protein amounts was not always possible due to the scarceness of the available brain material. However, accumulation of Notch3-ECD in the CAD 2 sample had already been demonstrated using whole brain material. Thus, the presence of Notch3-ECD deposits could be confirmed in all patients.

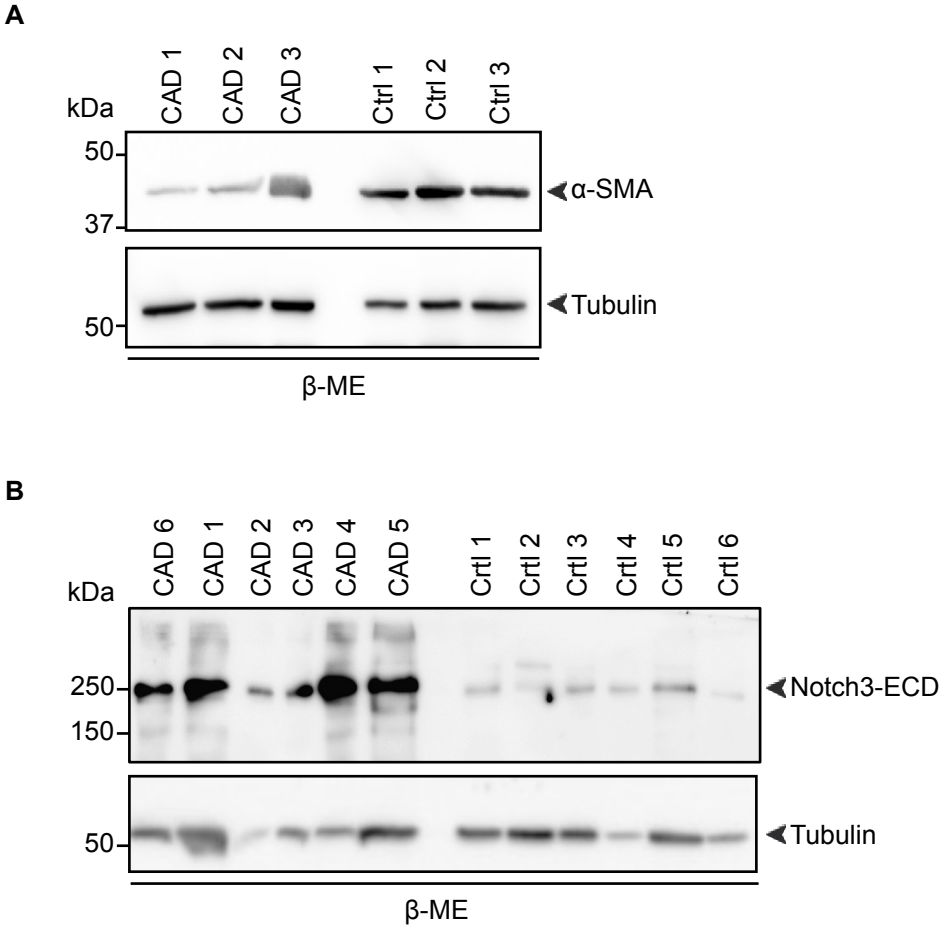

Figure 14: Immunoblot analysis of β-ME fractions from purified brain vessels. A) Vessel isolation allows the precise study of vessel-related proteins. Purified brain vessels were sequentially extracted and the β-ME fraction immunoblotted with anti-α-SMA and anti-β-tubulin antibodies. B) Notch3-ECD is specifically enriched in the β-ME fraction of purified patient vessels. Shown is an immunoblot of the β-ME fraction with anti-Notch3-ECD 3G6 and anti-β-tubulin antibodies with all available samples.

To validate the specificity of the sequential extraction method, amyloid precursor protein (APP) was analyzed, which plays no known role in CADASIL (Paquet et al., 2010) and, like Notch3, represents a type I transmembrane receptor with a large extracellular domain that undergoes the same proteolytic cleavages. Immunoblotting of the β-ME fractions revealed the presence of APP in both patient and control samples, albeit at varying levels with no disease-related trend (Figure 15). Based on this finding, an artificial enrichment of plasma membrane proteins by the sequential extraction method is unlikely. It was therefore concluded that the vessel isolation method is suited to identify new potential Notch3-ECD aggregate constituents.

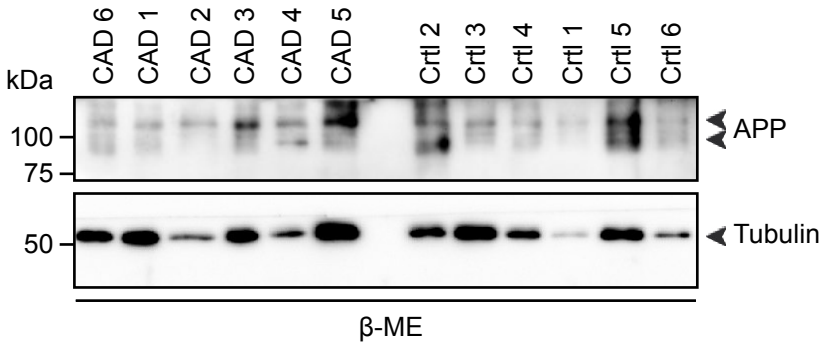

Figure 15: APP displays no CADASIL-related differences in the β-ME fraction of purified vessels. Purified brain vessels were sequentially extracted. Shown is an immunoblot of the β-ME fraction with anti-APP and anti-β-tubulin antibodies. APP: amyloid precursor protein.

3.2.4 Fibronectin and LTBP-1 co-fractionate with Notch3-ECD in CADASIL-affected vessels

Since the role of the initially identified factors TSP-2 and LTBP-4 in Notch-ECD deposition could not be further investigated due to the lack of appropriate antibodies (see 3.2.2), alternative candidates were explored. Among the four members of the LTBP family of TGF-β signaling regulators, LTBP-1 has by far been studied most extensively and shown to bind to all three TGF-β isoforms (TGF-β1, TGF-β2, TGF-β1) with similar efficiency (Saharinen and Keski-Oja, 2000). It mediates TGF-β sequestration by interacting with fibronectin and fibrillin-1, key structural components of blood vessel ECM, which had also been identified in the proteomic study on CADASIL brains (Monet-Lepretre et al., 2013). Moreover, fibrillin-1 and LTBP proteins, like Notch3, contain cysteine-rich domains including EGF-like repeats, which could possibly be involved in pathological disulfide bond-mediated aggregation processes. Based on these considerations, LTBP-1, fibronectin and fibrillin-1 were selected for further investigation.

For immunoblotting experiments the β-ME fractions of purified vessels from four patients and four controls were used. Staining for fibrillin-1 with various antibodies did show conclusive results neither in control nor in patient samples (data not shown). In contrast, fibronectin and LTBP-1 were clearly seen in patient, but almost absent in control material. Staining intensities within patient samples varied considerably, with the most prominent signals in CAD 4 and 5. A similar pattern had already been observed for Notch3 (see Figure 14). Thus, both fibronectin and LTBP-1 are strongly enriched in CADASIL-affected brain vessels and the extent of their accumulation within individual samples parallels that of Notch3-ECD. This clearly demonstrated co-fractionation with Notch3-ECD indicating a role in Notch3-ECD deposition.

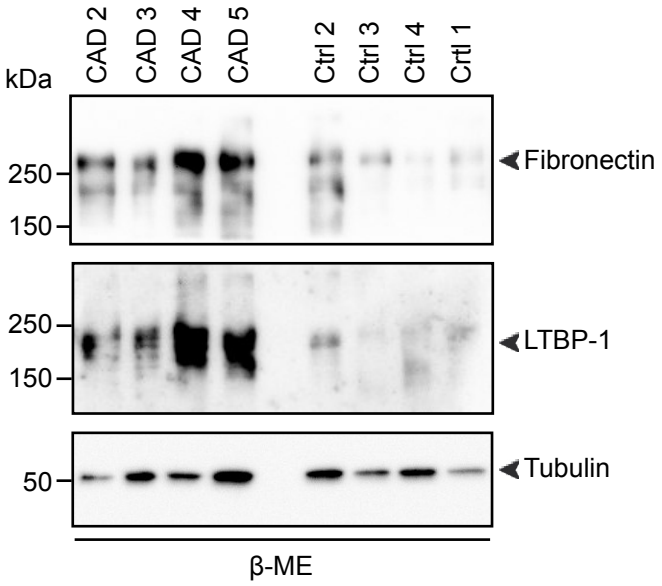

Figure 16: Fibronectin and LTBP-1 are increased in the β-ME fraction of CADASIL vessels. Purified vessels were sequentially extracted and the β-ME fraction was immunoblotted with anti-fibronectin, anti-LTBP-1 and anti-β-tubulin antibodies. A representative blot from two independent extractions of six CADASIL and control subjects is shown.

3.3 Co-localization analysis in human brain sections

Biochemical co-fractionation might occur independently of Notch3-ECD aggregates, especially with ECM proteins exhibiting poor solubility. Thus, additional evidence for a possible connection of the examined proteins with mutant Notch3-ECD was required. Therefore, immunohistochemical studies on human brain sections from CAD 1-3 and Ctrl 1-3 were performed to study their spatial distribution with respect to Notch3-ECD deposits. The latter can be visualized nicely by immunohistochemical staining of paraffin-embedded as well as frozen tissue (Joutel et al., 2000).

To confirm the presence of Notch3 deposits in the CADASIL patients, paraffin-embedded tissue was stained with a monoclonal anti-Notch3-ECD antibody. While Notch3-ECD could not be detected in control sections, it displayed elevated immunoreactivity in the tunica media of patient arterioles (Figure 17). Since Notch3 is exclusively expressed in vSMCs and pericytes of the tunica media, the extracellular deposits are located at the surface of these cells marking the tunica media and allowing a rough distinction of the three vessel layers (Joutel et al., 2000). In addition to Notch3-ECD deposits, the characteristic pathologic thickening of the tunica intima and tunica adventitia was observed (Figure 17 upper panels).

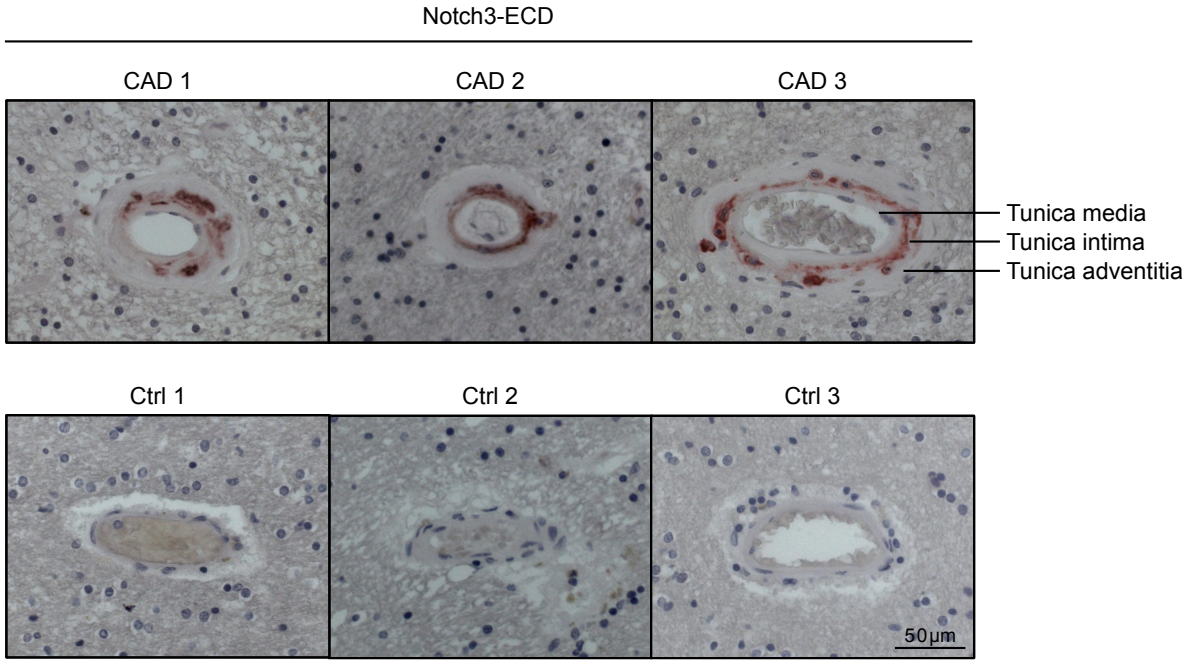

Figure 17: Notch3-ECD deposits are located in the tunica media in CADASIL arterioles. Paraffin-embedded brain sections were stained with the anti-Notch3-ECD 2G8 antibody and visualized with AEC (reddish brown). Nuclei were counterstained with hematoxylin (blue). The images are representatives of two independent experiments.

Immunofluorescence analysis allows an even more precise visualization of individual Notch3-ECD aggregates (Joutel et al., 2000) and co-localization analyses with additional proteins. Frozen tissue sections of CAD 1 and Ctrl 1 were co-stained for Notch3-ECD and collagen type IV, a basement membrane marker used to visualize vessels. As observed on paraffin sections, Notch3-ECD was not detectable in control tissue due to low expression. However, the focal enrichment of Notch3-ECD immunoreactivity indicative of deposits was observed in CADASIL arterioles (Figure 18 A) and, even more pronounced, in small capillaries (Figure 18 B)

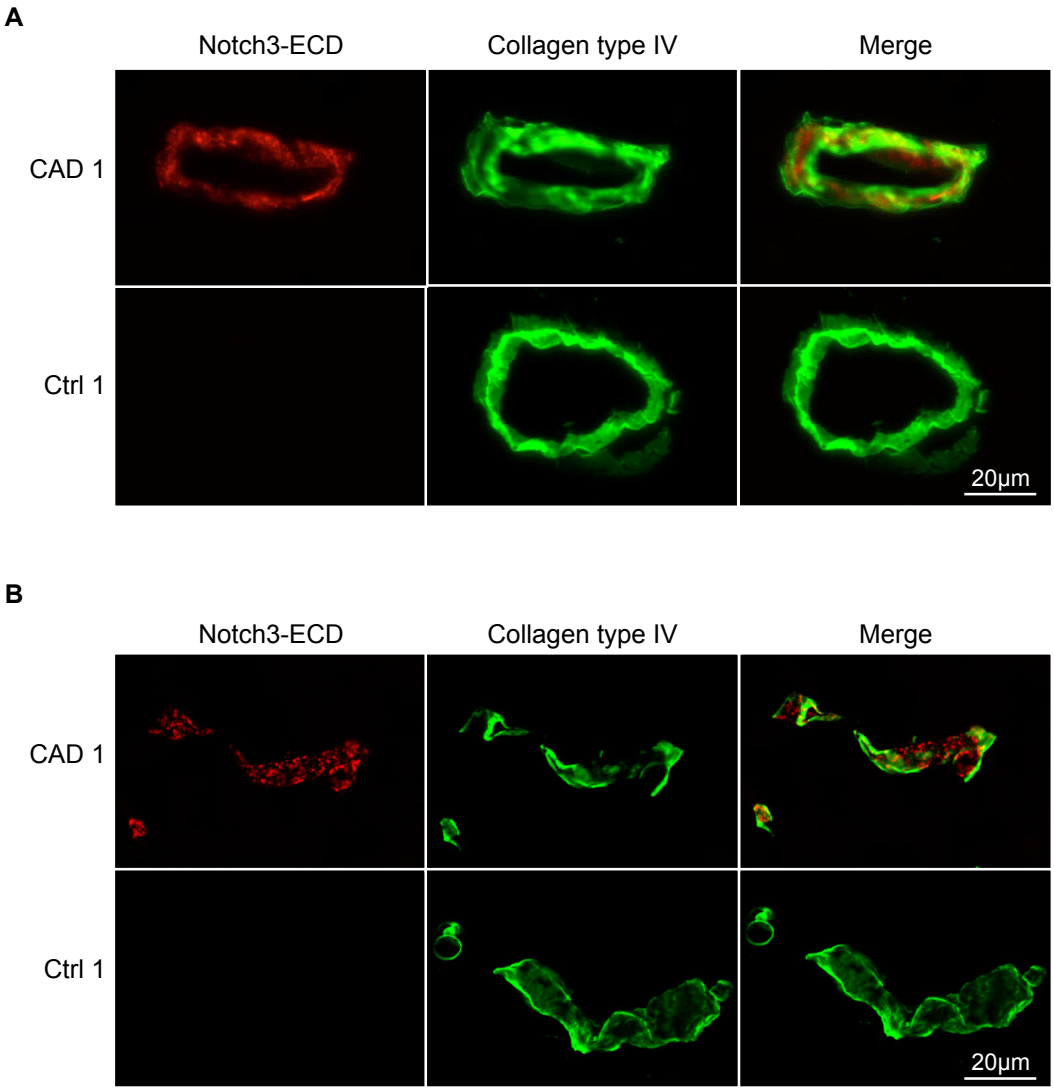

Figure 18: Notch3-ECD is observed as granular deposits in CADASIL vessels. Frozen brain sections of a patient (CAD 1) and a control (Ctrl 1) were stained with the anti-Notch3-ECD 2G8 and anti-collagen type IV antibody, a basement membrane marker, and analyzed by immunofluorescence. Images are representatives for least five different experiments with three CADASIL and control samples each. Pictures showing arterioles (A) and small capillaries (B) were taken with an inverse fluorescence and confocal microscope, respectively.

3.3.1 Fibronectin and fibrillin-1 accumulate in CADASIL vessels independently of Notch3-ECD deposits

To study the localization of fibronectin, paraffin-embedded brain sections were stained with an anti-fibronectin antibody. In control vessels, fibronectin was detected in moderate amounts as a fine lining of the tunica intima and adventitia (Figure 19), where it is abundantly expressed (Wagenseil and Mecham, 2009). In contrast, a dramatic increase was

observed in the thickened tunica adventitia of CADASIL vessels in agreement with the increased fibronectin levels observed in immunoblot experiments (see Figure 16). However, the staining pattern clearly differed from that of Notch3-ECD (Figure 19 right panel) arguing against a co-localization with Notch3-ECD aggregates.

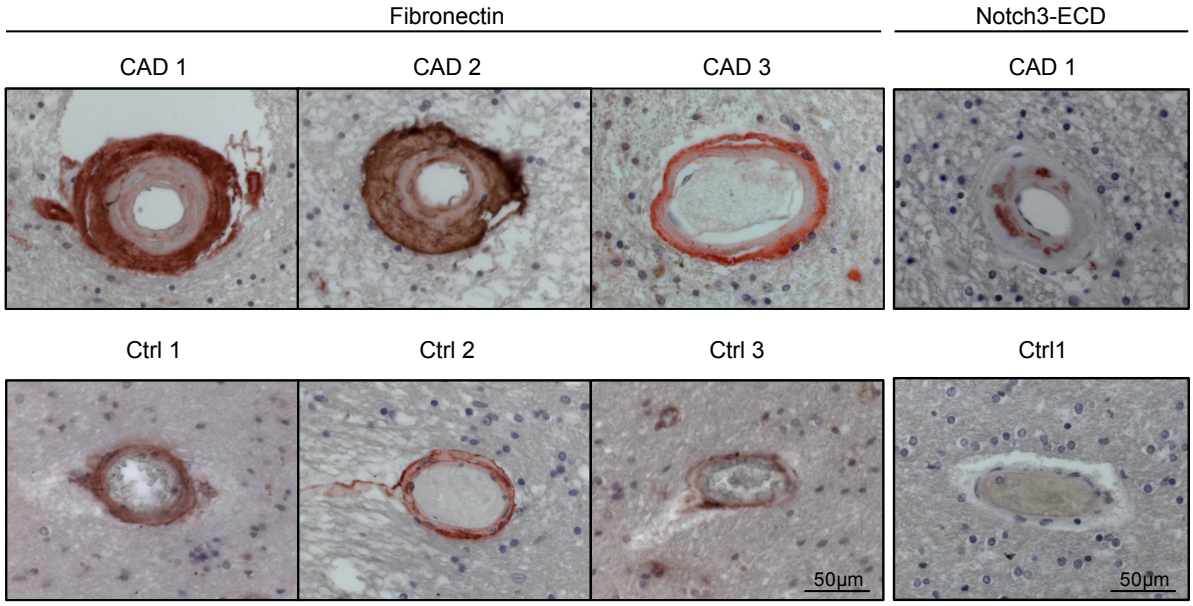

Figure 19: Fibronectin is increased in the tunica adventitia and intima of CADASIL patients while Notch3-ECD is located in the tunica media. Paraffin brain sections were stained with anti-fibronectin or anti-Notch3 2G8 antibodies and visualized with AEC (reddish brown). Cell nuclei were counterstained with hematoxylin (blue). Shown are representative images of three experiments.

In contrast to immunoblot analysis, the fibrillin-1 antibody worked excellently in immunohistochemical analyses. It revealed weak immunoreactivity in control vessels of paraffin-embedded tissue sections showing a fibrillar structure within the tunica adventitia (Figure 20). In CADASIL patients, a markedly elevated signal intensity was observed resulting in the continuous labeling of a thin layer at the perimeter of the tunica adventitia (Figure 20). This finding was confirmed by immunofluorescence stainings on frozen tissue sections, where the signal for fibrillin-1 showed a fibrous pattern, which was strongly increased in CADASIL vessels. Additionally, fibrillin-1 is also detected at the tunica intima with a lower intensity (Figure 20), since fibrillin-1 microfibrils are also found at the tunica elastica interna (Wagenseil and Mecham, 2009).

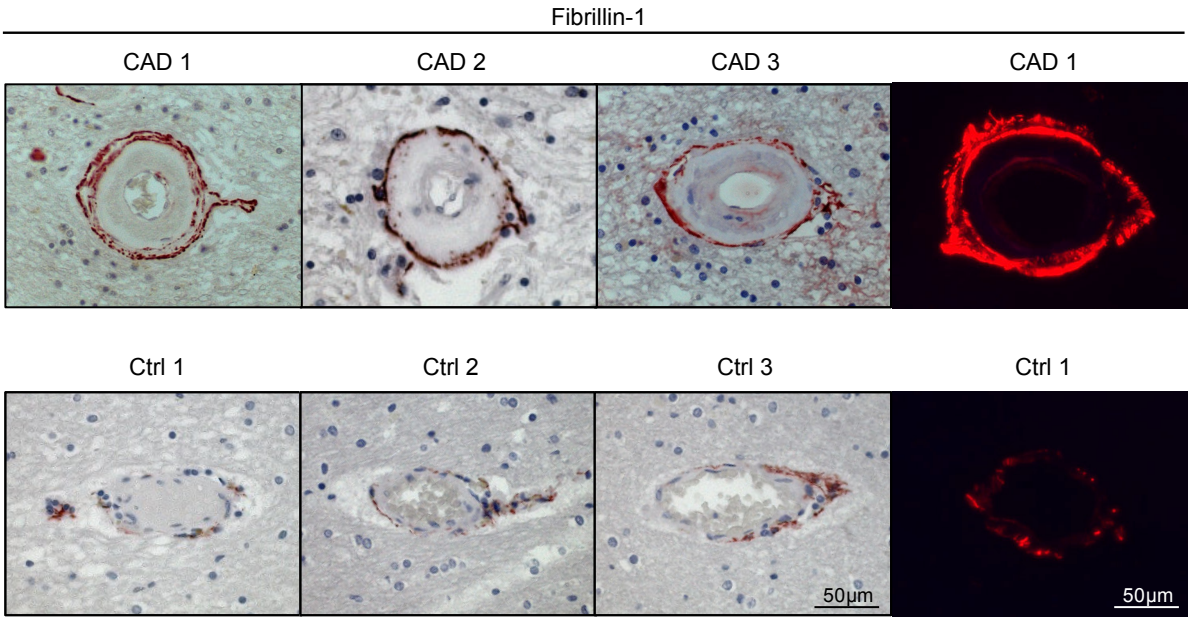

Figure 20: Fibrillin-1 is increased in the tunica adventitia of CADASIL patients. Paraffin-embedded brain sections were stained with an anti-fibrillin-1 antibody and visualized with AEC (reddish brown). Cell nuclei were counterstained with hematoxylin (blue). Frozen brain sections were stained with the anti-fibrillin-1 antibody and analyzed by immunofluorescence. Shown are representative images of two experiments with three CADASIL and three control samples.

For fibrillin-1, a co-localization could be studied more directly by performing co-staining with Notch3-ECD on frozen sections of CADASIL patients (for fibronectin this was not possible due to the lack of an appropriate antibody). The fibrous pattern for fibrillin-1 is clearly distinct from the granular Notch3-ECD immunoreactivity confirming the lack of spatial overlap between both proteins (Figure 21).

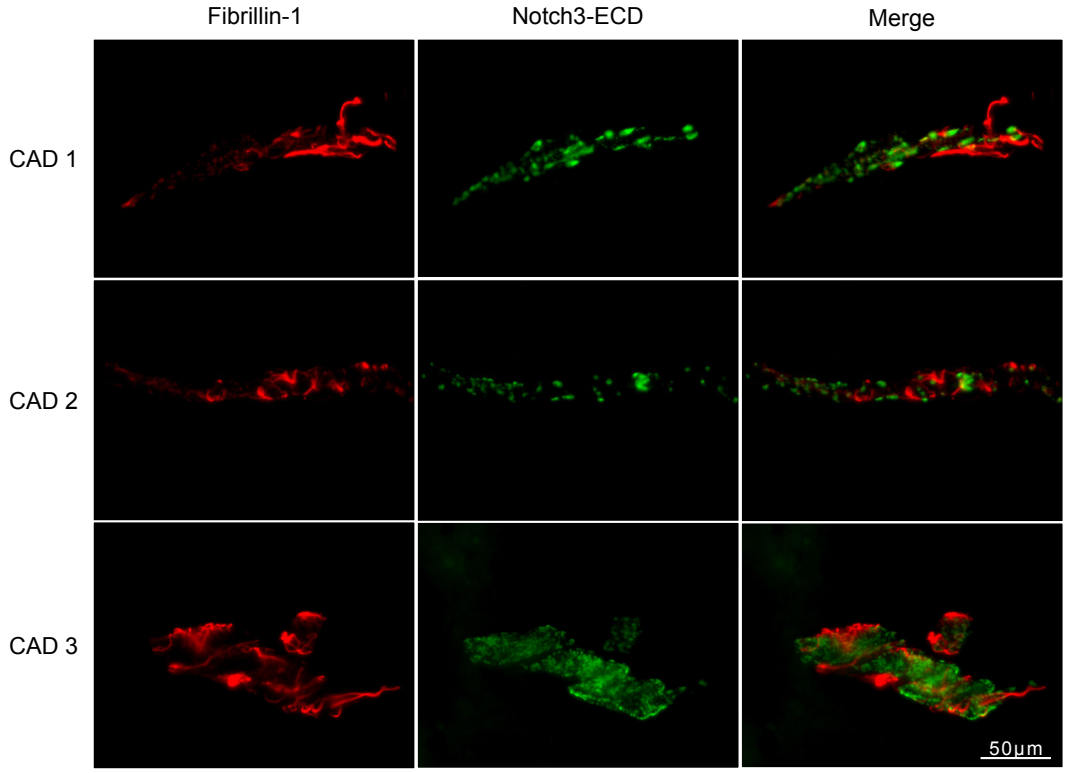

Figure 21: Fibrillin-1 does not co-localize with Notch3-ECD. Frozen brain sections were stained with the anti-fibrillin-1 and anti-Notch3-ECD 2G8 antibodies and analyzed by immunofluorescence. Shown are representative images from three experiments.

In summary, these findings suggested that the accumulation of fibrillin-1 and fibronectin in CADASIL vessels occurs independently of Notch3-ECD likely representing a fibrotic process secondary to deposit formation. Therefore, both proteins were excluded as direct participants in Notch3-ECD deposition.

3.3.2 LTBP-1 is recruited to Notch3-ECD deposits

To study the localization of the third candidate protein, LTBP-1, in CADASIL vessels, only immunoflouresence stainings on frozen tissue sections could be performed due to the lack of a suitable antibody for paraffin–embedded material. In control brain sections, arterioles (Figure 22 A) as well as capillaries (Figure 22 B), visualized by collagen type IV staining, showed a weak immunoreactivity for LTBP-1. In contrast, LTBP-1 levels were markedly increased in sections of CAD 1 recapitulating the enrichment observed in β-ME fractions after biochemical fractionation (see Figure 16). Most importantly, LTBP-1 in CADASIL vessels appeared not uniform but restricted to focal granules reminiscent of Notch3-ECD deposits, as most clearly seen in capillaries (Figure 22 B).

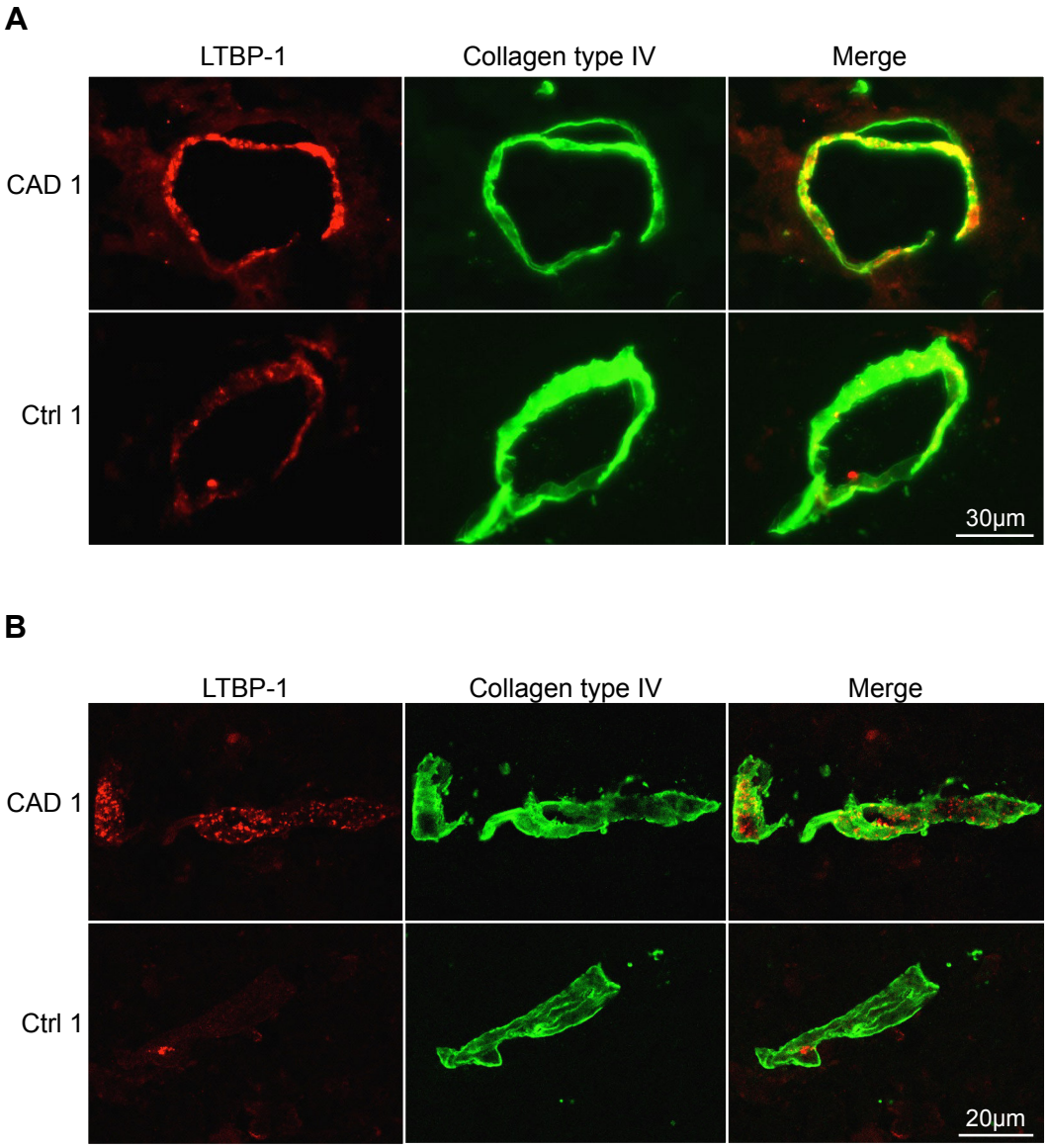

Figure 22: LTBP-1 shows a focal enrichment in CADASIL vessels. A-B) Frozen brain sections were stained with anti-LTBP-1 and anti-collagen type IV antibodies and analyzed by immunofluorescence. Shown are representative images from at least four experiments taken with A) an inverse microscope and B) a confocal microscope.

Therefore, co-stainings were performed and analyzed by confocal microscopy. Indeed, LTBP-1 and Notch3-ECD yielded almost completely overlapping signals in all examined patients (Figure 23) demonstrating co-localization. This result strongly suggested specific LTBP-1 sequestration within Notch3-ECD aggregates. The occurrence of this finding in three independent patients carrying different NOTCH3 mutations argued for its specificity.

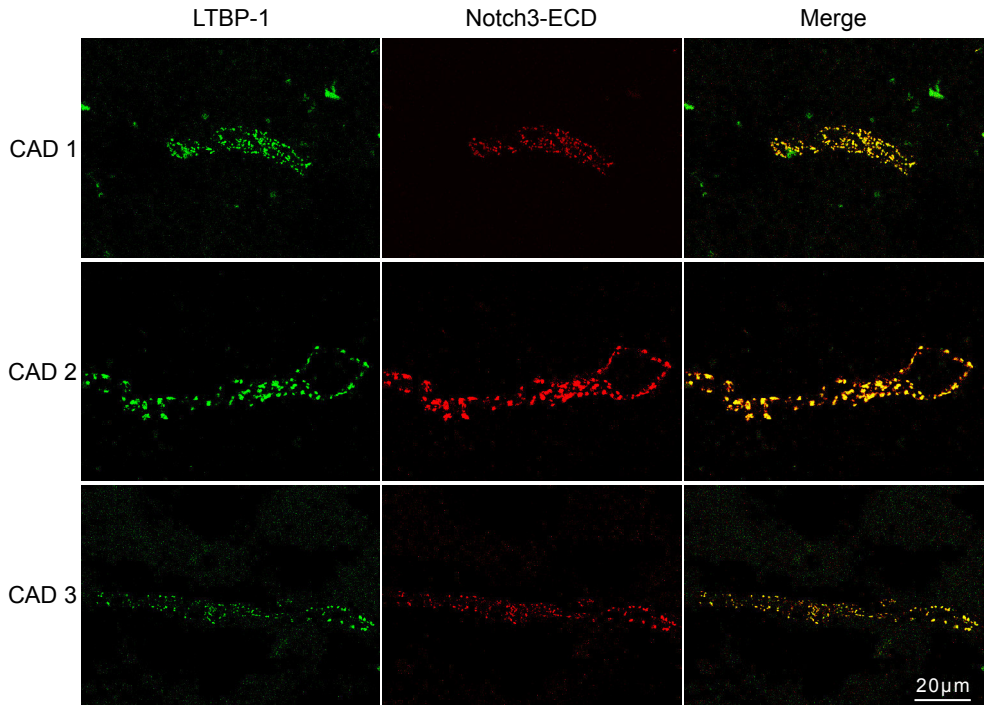

Figure 23: LTBP-1 co-localizes with Notch3-ECD aggregates. Frozen brain sections were stained with anti-LTBP-1 and anti-Notch3-ECD 2G8 antibodies and analyzed by immunofluorescence. Shown are representative images from at least four experiments with three CADASIL and three control brains taken with a confocal microscope.

LTBP-1 represents a key mediator of the pro-fibrotic cytokine TGF-β, a well known regulator of microvasculature function (Doyle et al., 2012), and its recruitment into Notch3-ECD deposits implicates a potential involvement of the TGF-β pathway in CADASIL. Notably, dysregulation of TGF-β signaling has been demonstrated in a number of inherited vascular diseases (ten Dijke and Arthur, 2007) including cerebral autosomal recessive arteriopathy with subcortical infarcts and leukoencephalopathy (CARASIL), a recessive hereditary SVD with a CADASIL-like pathology (Hara et al., 2009,). Moreover, TGF-β signaling has been suggested as an important contributor to vascular remodeling in sporadic SVD (Thompson and Hakim, 2009). Therefore, signs of altered TGF-β activity in the brain samples were investigated.

3.3.3 LAP accumulates in the tunica media of CADASIL vessels

The TGF-β pro-protein is processed in the cell into two fragments, the mature TGF-β, a dimer linked by disulfide bridges, and its pro-domain, the latency-associated peptide (LAP) (Dubois et al., 1995) (Figure 24). LAP keeps TGF-β in an inactive state (Shi et al., 2011) and mediates the interaction with LTBP proteins, which upon secretion of this complex promote its attachment to the ECM via interactions with fibronectin and fibrillins.

The mature TGF-β ligand can be released from the ECM by a variety of mechanisms (Olofsson et al., 1995, Isogai et al., 2003).

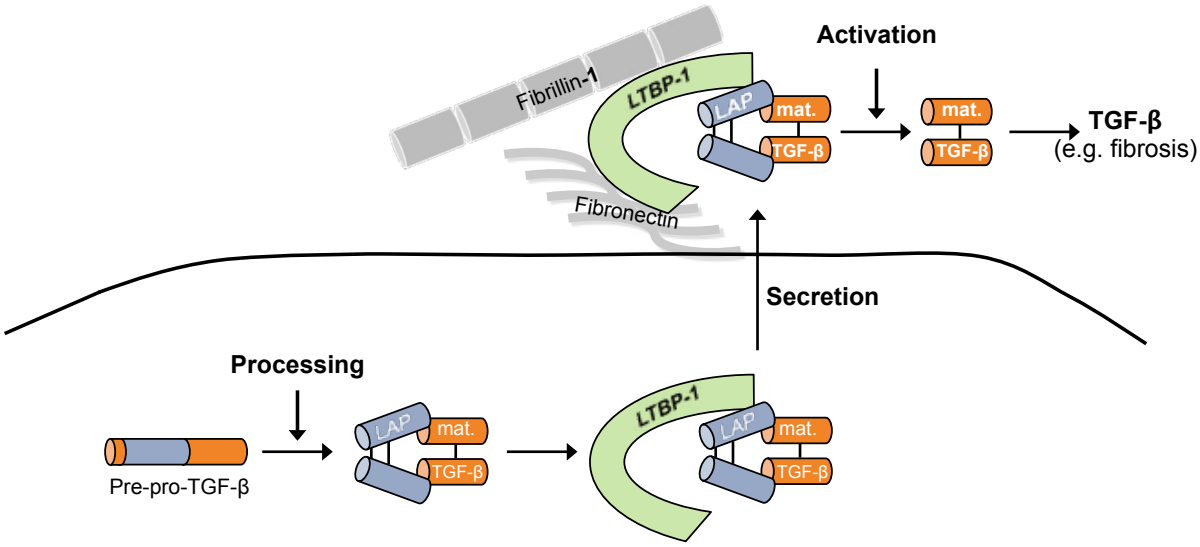

Figure 24: Schematic representation of latent TGF-β synthesis and secretion. See text for details. LAP and mature TGF-β are non-covalently attached, while LTBP-1 and LAP are cross-linked via a disulfide-bridge. Orange/blue bar: pre-pro TGF-β; blue dimer: LAP (latency associated peptide); orange dimer: mature TGF-β (transforming growth factor-β); green hemicycle: LTBP-1 (latent TGF-β binding protein-1); grey waved lines: fibronectin; grey bar: fibrillin-1.

Therefore, expression levels and localization of LAP were studied in the brain samples. First, protein levels were analyzed by immunoblotting of the β-ME fractions from purified vessels of CAD 2-5 and shown to be increased in all four CADASIL patients examined suggesting a specific enrichment (Figure 25 A). Next, immunohistochemical studies on paraffin-embedded tissue of CAD 1-3 and Ctrl 1-3 were performed to study the localization of LAP. While in controls expression could not be observed, LAP was strongly increased in CADASIL vessels (Figure 25 B). Most importantly, the immunoreactivity was restricted to the tunica media, the vessel layer containing Notch3-ECD aggregates. Due to the ineptitude of the anti-LAP antibody, immunofluorescence staining could not be performed preventing co-localization studies. Nevertheless, these findings suggest an LTBP-1-mediated enrichment and sequestration of immature TGF-β within Notch3-ECD aggregates. It remains to be determined whether this finding has implications on TGF-β signaling in CADASIL pathogenesis.

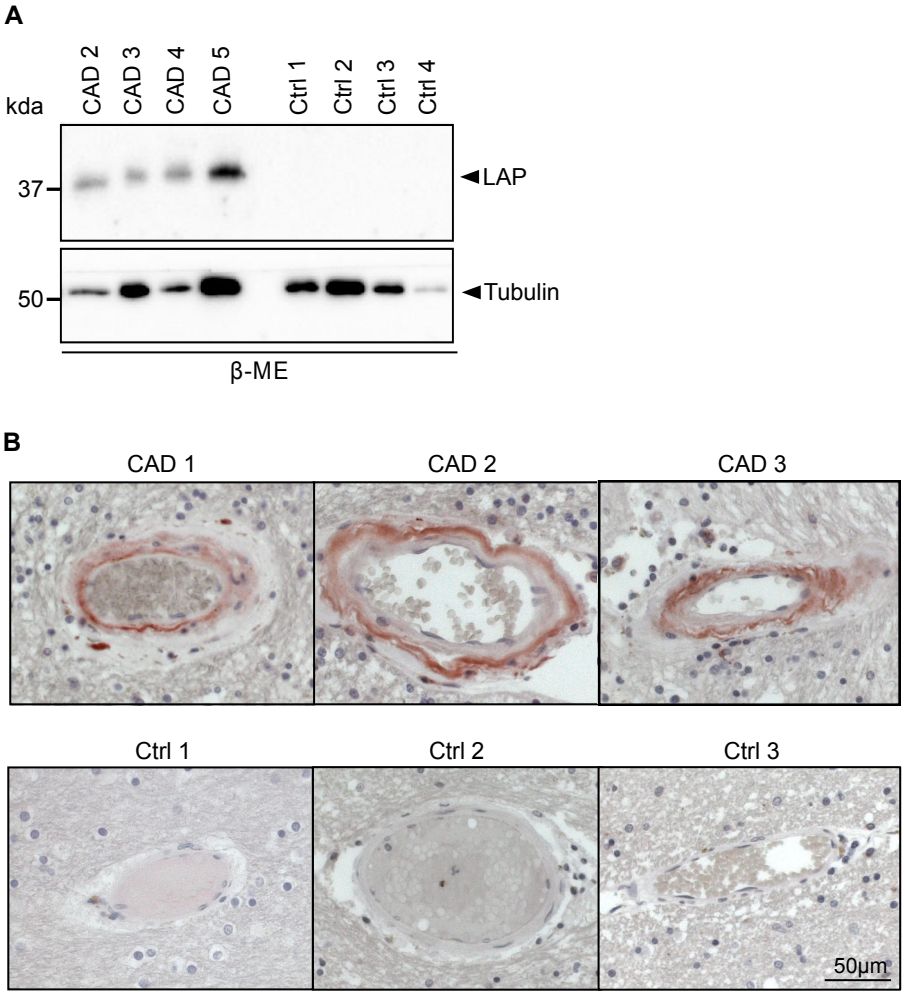

Figure 25: LAP is increased in CADASIL brain vessels. A) The β-ME fraction of sequentially extracted purified brain vessels were immunoblotted with anti-LAP and anti-β-tubulin antibodies. Shown is a representative image of two independent experiments. B) Paraffin-embedded brain sections were stained with the anti-LAP antibody and visualized with AEC (reddish brown). Nuclei were counterstained with hematoxylin (blue). Shown are representative images of two experiments.

3.4 LTBP-1 directly interacts with Notch3 *in vitro*

From the studies on brain samples LTBP-1 emerged as highly promising candidate for a role in Notch3-ECD aggregation. To investigate this more directly, *in vitro* approaches were employed. Since recruitment of ECM proteins into Notch3-ECD deposits might be facilitated by direct protein-protein interactions (Monet-Lepretre et al., 2013), the binding of LTBP-1 to Notch3-ECD was investigated by applying a solid-phase binding assay, an approach successfully used in the past to analyze interaction partners of both proteins (Meng et al., 2009, Massam-Wu et al., 2010). Since correctly folded full-length Notch3-ECD cannot be purified (Duering et al., 2011), a recombinantly generated Notch3 fragment

harboring the first 11 EGF-like repeats was chosen (N3EGF1-11-Fc). For efficient expression and purification this fragment contained a carboxy-terminally IgG-Fc affinity tag. As a soluble ligand, LTBP-1 conditioned medium derived from transiently transfected HEK293T cells was used. There are two LTBP-1 isoforms, LTBP-1L (long) and LTBP-1S (short), generated by the alternative use of two separate promoters within the same gene (Koski et al., 1999). Whereas LTBP-1L is mainly expressed during development, LTBP-1S is the major isotype in adult life and was thus selected for this study (in the following termed LTBP-1) (Todorovic and Rifkin, 2012).

To perform this assay, N3EGF1-11-Fc or the control ligand IgG-Fc were immobilized to microtiter plate wells and LTBP-1 conditioned medium was added. Subsequently, antibody-mediated labeling of bound LTBP-1 allowed quantification by a colorimetric detection procedure. An almost fivefold and highly significant increase in LTBP-1 binding to N3EGF1-11-Fc compared to the control was observed (Figure 26 A).

To verify the binding of LTBP-1 to immobilized N3EGF1-11-Fc by immunoblotting, the bound proteins were recovered from microtiter plates after assay completion. Equally efficient immobilization of N3EGF1-11-Fc and IgG-Fc was demonstrated by comparing the blotting signals of recovered proteins with that of a defined amount of purified protein (Figure 26 B). Immunoblotting for LTBP-1 in the recovered samples revealed its presence only in the N3EGF1-11-Fc, but not IgG-Fc lane confirming the specificity of the binding. LTBP-1 appeared as a high-molecular-weight band, which most likely represents oligomeric LTBP-1 not dissolved under the solubilization conditions used (Figure 26 C).

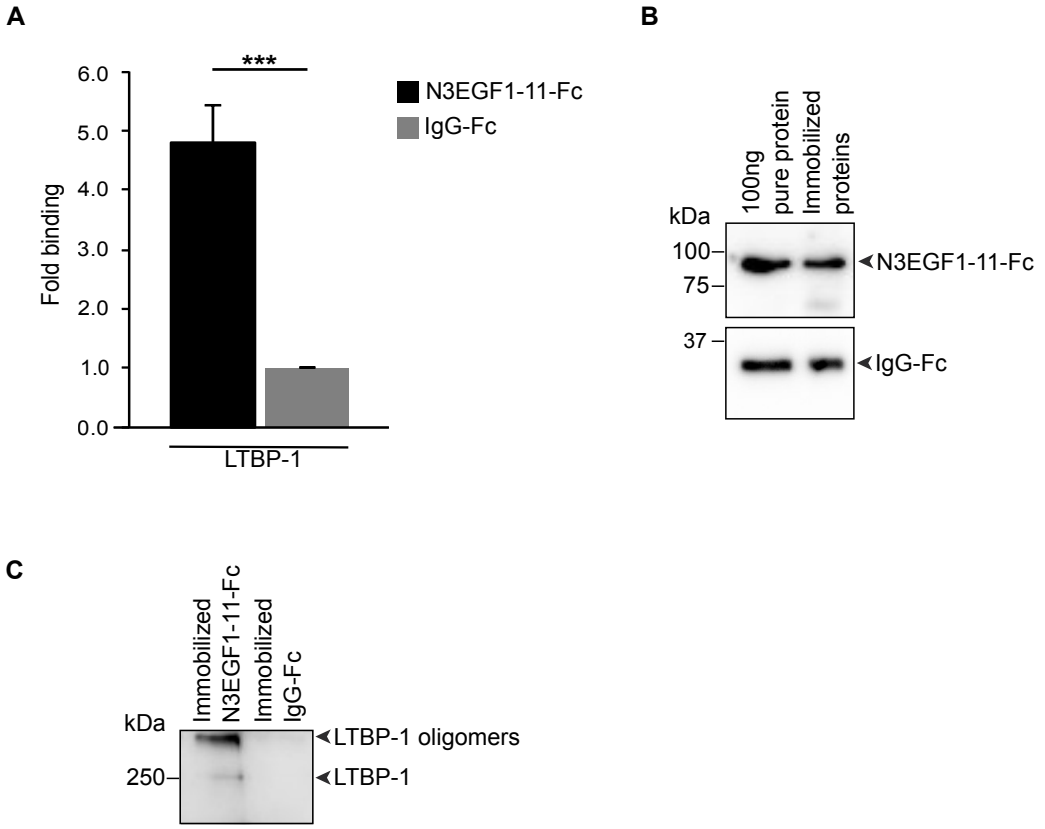

Figure 26: LTBP-1 binds to immobilized Notch3. A) Binding of full-length LTBP-1 derived from HEK293T cell conditioned medium to immobilized Notch3 (N3EGF1-11-Fc) or control ligand (IgG-Fc) was measured by immunodetection using an anti-LTBP-1 antibody. Upon incubation with a peroxidase-coupled secondary antibody, the substrate was added allowing a colorimetric measurement. Background absorbance of conditioned media from mock-transfected HEK293T cells was subtracted and relative amounts of bound LTBP-1 are shown. Binding of LTBP-1 to the control was set to 1 and results are expressed as mean +SEM of 7 independent experiments. *** $p<0.001$; Mann-Whitney Test. B-C) Bound proteins were recovered from wells by the addition of Lämmli buffer after assay completion. B) Immobilized proteins bind comparably to well plates. 100 ng pure protein and recovered N3EGF1-11-Fc (top panel) or IgG-Fc (lower panel) were immunodetected using an anti-human-IgG antibody. C) Bound LTBP-1 was evaluated by immunoblotting with an anti-LTBP-1 antibody and predominantly detected in oligomeric form. Shown are representative blots from at least three independent experiments.

To demonstrate the relevance of the solid phase binding assay, fibronectin was chosen as a control immobilizing partner, since its interaction with LTBP-1 is well established (Dallas et al., 2005). Fibronectin was immobilized with similar efficiency to microtiter plate wells as demonstrated by Western Blotting (Figure 27 A). Quantitation of the binding revealed a 3.5-fold increase in LTBP-1 binding to fibronectin (Figure 27 B), indicating that the assay adequately reflects *in vivo* conditions.

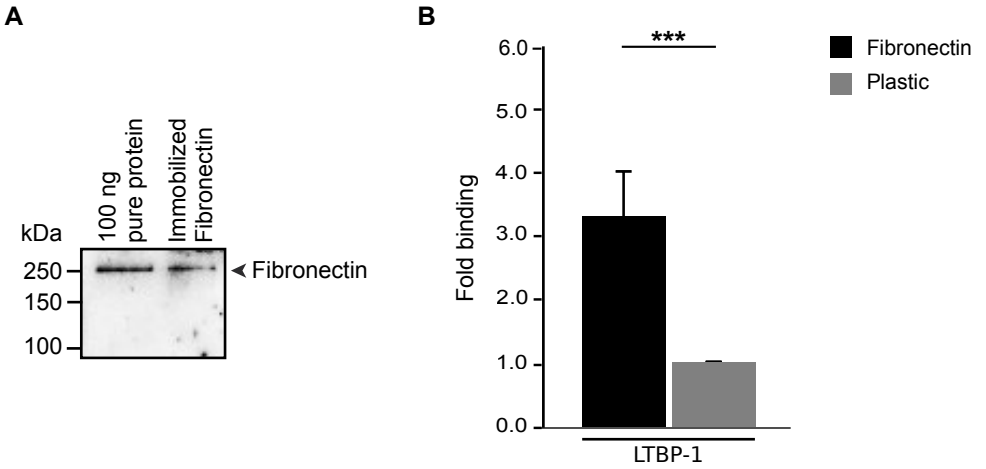

Figure 27: LTBP-1 binds to the known interactor fibronectin with a similar affinity than to Notch3. A) Bound fibronectin was recovered from microtiter well plates after assay completion by the addition of Lämmli buffer and compared to 100 ng pure protein. Shown is a representative immunoblot of two independent experiments detected with an anti-fibronectin antibody. B) Binding of LTBP-1 conditioned media to immobilized fibronectin or plastic was colorimetrically measured using the anti-LTBP-1 antibody for detection. Results are expressed as mean +SEM of 7 independent experiments. *** $p<0.001$; Mann-Whitney Test.

To map the Notch3 binding domain within LTBP-1, two truncated and epitope-tagged LTBP-1 expression constructs were generated. They either lack the N-terminus with the fibronectin interaction domain (LTBP-1ΔN) or the C-terminus containing the LAP and fibrillin-1 binding site (LTBP-1ΔC_V5) (Figure 28 A). LTBP-1ΔN was generated in two versions: HA-tagged LTBP-1ΔN_HA, which was used in assays with cell supernatants and V5-His-tagged LTBP-1ΔN_V5 for assays requiring purified LTBP-1. Immunoblotting with an anti-V5 antibody revealed molecular masses of ~220 kDa, ~120 kDa and ~140 kDa for LTBP-1, LTBP-1ΔC_V5 and LTBP-1ΔN_V5, respectively (Figure 28 B).

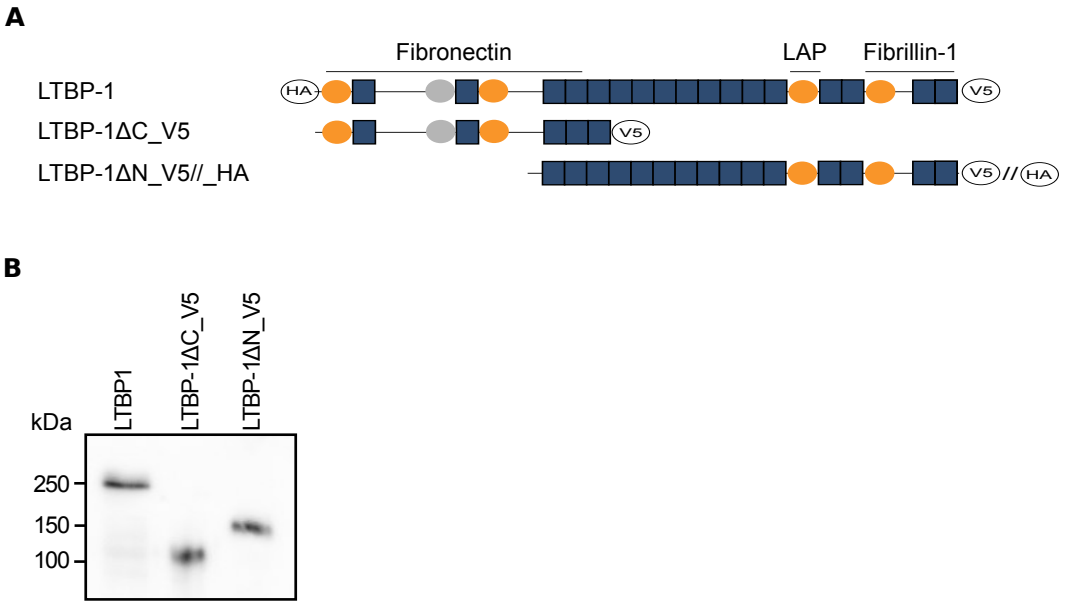

Figure 28: LTBP-1 deletion constructs. A) Schematic representation of the used LTBP-1 constructs and their domain organization including cysteine rich repeats (orange circles), a hybrid domain (grey circle), EGF-like repeats (blue squares) and V5-His or hemagglutinin (HA) tags (open circles). The fibronectin, LAP/TGF-β and fibrillin-1 binding regions are indicated. Note that LTBP-ΔC-HA was used in assays with cell supernatants and LTBP-ΔC-V5 in assays requiring purified LTBP-1. Adapted from Todorovic and Rifkin, 2012. B) Immunoblotting of LTBP-1, LTBP-1ΔC_V5 and LTBP-1ΔN_V5 from HEK293T cell-derived conditioned media with an anti-V5 antibody.

To assess the binding capacities of these LTBP-1 deletion fragments, they were transiently transfected into HEK293T cells and conditioned media were used in the binding assay. While the loss of the LTBP-1 N-terminus completely abrogated binding, LTBP-ΔC_V5 retained the ability to bind N3EGF1-11-Fc (Figure 29). To exclude an indirect interaction mediated by other factors present in the conditioned media, LTBP-1ΔC_V5 was purified using an affinity chromatography approach (see 3.5). Indeed, the binding of purified LTBP-1ΔC_V5 was as efficient as the corresponding conditioned medium (Figure 29) demonstrating that the interaction is direct.

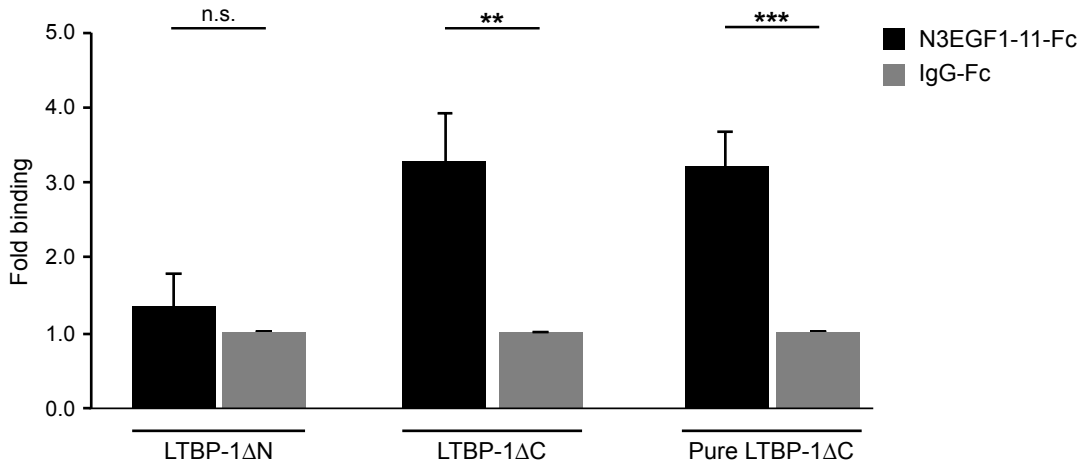

Figure 29: LTBP-1 binding to Notch3 is mediated by its N-terminus. Binding of conditioned media from HEK293T cells transfected with LTBP-1ΔN_HA and LTBP-1ΔC_V5 or purified LTBP-1ΔC_V5 to immobilized N3EGF1-11-Fc or IgG-Fc was immunodetected using anti-LTBP-1 (LTBP-1ΔN_HA) or anti-V5 (LTBP-1ΔC_V5) antibodies respectively. Background absorbance of conditioned media from mock-transfected HEK293T cells or PBS was subtracted. Relative amounts of bound LTBP-1 are shown. Results are expressed as mean + SEM of five (LTBP-1ΔC_V5) and four (LTBP-1ΔN_HA) independent experiments. n.s.: not significant, *** $p<0.001$; ** $p<0.01$; Mann-Whitney Test.

In summary, the data suggest that the sequestration of LTBP-1 into Notch3-ECD deposits is mediated by a direct interaction involving a region within the first 11 EGF-like repeats of the Notch3-ECD and the amino-terminal 1-689 aa of LTBP-1.

3.5 LTBP-1ΔC co-aggregates with mutant Notch3

To provide proof for a direct participation of LTBP-1 in the Notch3-ECD aggregation process, a previously established *in vitro* assay recapitulating the multimerization of mutant Notch3 was used (Opherk et al., 2009a, Duering et al., 2011). This assay is based on scanning for intensely fluorescent targets (SIFT), a unique technique, which distinguishes single protein particles from aggregated multimers in a confocal setup permitting the quantification of *de novo* protein aggregation in solution (Giese et al., 2005). Purified proteins are labeled with different fluorescent dyes (red or green) and pairwise incubated to allow the formation of multimeric particles. Dye intensities reflecting particle composition and size are measured via a light detector following dual-laser excitation and results are plotted in a two-dimensional graph. As depicted in Figure 31 A, monomers and low-molecular-weight oligomers appear as low-intensity signals in the lower left corner of the plot, whereas homomeric and heteromeric multimers are represented as mono-colored or dual-colored high-intensity signals, respectively.

For analyses, the previously described wild-type and R183C mutant-carrying Notch3 fragments encompassing EGF-like repeats 1-5 (N3EGF1-5) (Duering et al., 2011) as well as the LTBP-1 deletion variants LTBP-1ΔN and LTBP-1ΔC were used. The Notch3 EGF1-5 fragment harbors the mutational hotspot region (Peters et al., 2005a) and is efficiently secreted by HEK293E cells and thus correctly folded (larger Notch3-ECD fragments are incompletely folded and invariably retained within cells) (Duering et al., 2011). Purified red- and green-labeled Notch3 fragments were provided by Patrizia Hanecker (Institute for Stroke and Dementia Research, Munich) who also assisted in performing the following experiments.

For the purification of LTBP-1 deletion variants, conditioned medium from HEK293E cells transiently transfected with LTBP-1ΔC_V5 or LTBP-1ΔN_V5 was dialyzed and subsequently affinity-purified using their C-terminal V5-His tag. Silver staining of eluted fractions demonstrated sufficient purity of both fragments with LTBP-1ΔC_V5 showing a slightly better quality (Figure 30). For fluorescent labeling, elution fraction 4 of LTBP-1ΔC_V5 and combined fractions 4 and 5 of LTBP-1ΔN_V5 were used. To assess their co-aggregation potential, they were incubated in combination with wild-type or mutant N3EGF1-5 fragment for 1, 3 and 5/6 days to allow aggregation and subsequently analyzed by SIFT. Representative data of a day 1 experiment are depicted in Figure 31 B.

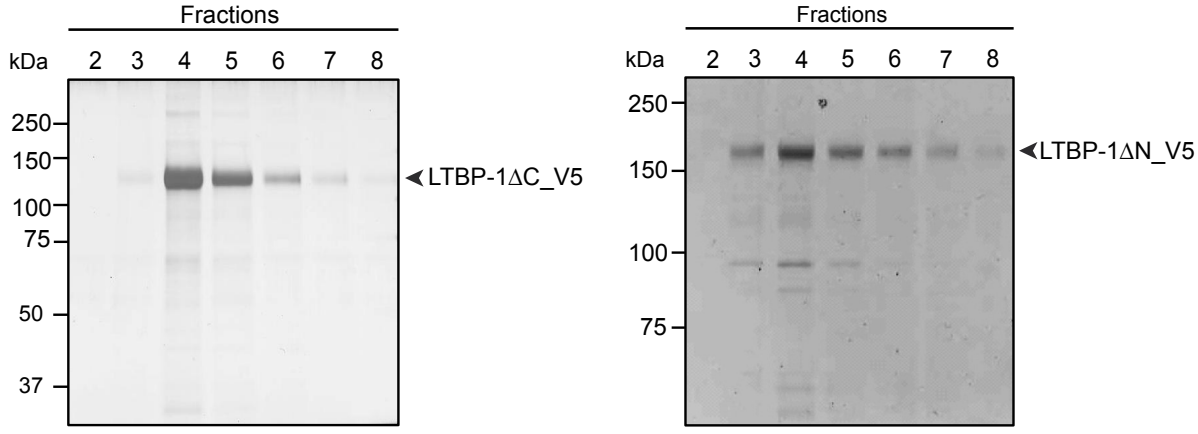

Figure 30: Silver Staining of purified LTBP-1 fragments. Conditioned media from transiently transfected HEK293E cells with LTBP-1ΔC_V5 or LTBP-1ΔN_V5 were dialyzed and proteins were purified via their His-Tag using the Talon System. Eluted fractions 2-8 were separated by SDS-PAGE and visualized by silver staining. Three different batches of LTBP-1ΔC_V5 and one for LTBP-1ΔN_V5 were prepared.

In line with our published data (Duering et al., 2011), N3EGF1-5 R183C formed higher-order dual-color multimers, while the corresponding wild-type fragment did not show this tendency (Figure 31 B, C). When LTBP-1ΔC or LTBP-1ΔN were analyzed in combination

with N3EGF1-5 wild-type, no formation of dual-colored aggregates was observed. However, single-color LTBP-1 multimers were detected indicating self-aggregation, a finding already observed in the solid-phase binding assay (see Figure 26 C). Similarly, predominantly mono-colored multimers were formed when LTBP-1ΔN_V5 was combined with mutant N3EGF1-5 (Figure 31 B). In contrast, the combination of LTBP-1ΔC and mutant N3EGF1-5 yielded higher-order dual-color multimers with a distribution typical for mutant Notch3EGF1-5 fragments suggesting the generation of aggregates containing both proteins (Figure 31 B).

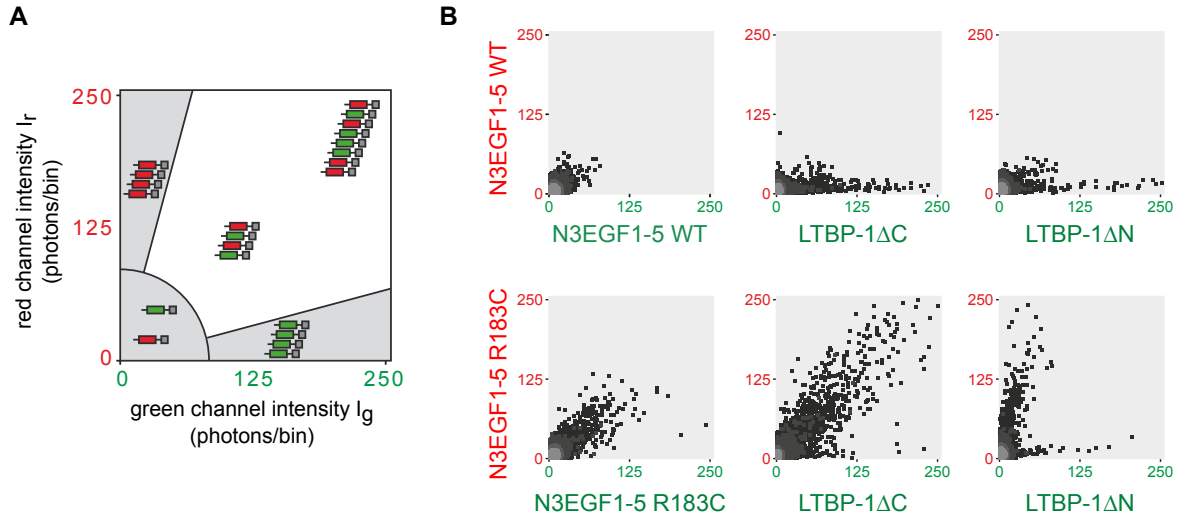

Figure 31: LTBP-1ΔC specifically co-aggregates with mutant Notch3. A) Schematic representation of SIFT data evaluation with a 2-D histogram. Shown are particle brightnesses for each fluorophore on the individual axis (x-axis in green; y-axis in red) in 0-250 photons/bin in dots (a bin is the sum of photons that are detected in a timeframe). Adapted from Duering et al., 2011. B) Purified proteins were fluorescently labeled and incubated 24 h at 550rpm and 37 °C. SIFT analysis was performed in order to analyze the aggregational behavior of different combinations. Shown are representative images of 2-5 experiments with two separately purified and labeled LTBP-1ΔC_V5 batches and one batch of LTBP-1ΔN_V5. WT: Wild-type.

In summary, it was concluded that LTBP-1 can multimerize with mutant Notch3, a process dependent on the presence of the interaction domain. These results further support the hypothesis that a direct interaction promotes co-aggregation. In combination with the findings on brain samples, they strongly suggest that LTBP-1 represents a component of Notch3-ECD deposits with a key role in CADASIL-relevant aggregation processes.

4 Discussion

The extracellular accumulation and deposition of excess Notch3-ECD in small brain vessels penetrating the white and deep gray matter is an early manifestation and hallmark of CADASIL (Mayer et al., 1999). This process is considered the starting point of a chain of pathological events involving the recruitment and sequestration of functionally important ECM and ECM-associated (matricellular) proteins and eventually resulting in brain vessel dysfunction (Joutel, 2011). Using a candidate-based approach several ECM components with potential disease-specific roles were investigated using CADASIL patient and control brain samples. Five proteins were selected for analysis based on their role in ECM function.

4.1 Thrombospondin-2

Thrombospondin-2 (TSP-2) is an adhesive glycoprotein involved in ECM assembly and cell-to-matrix interactions (Calabro et al., 2014). It was selected for analysis since several previous studies had suggested a role in Notch3 biology (Meng et al., 2009, Meng et al., 2010). TSP-2 binds directly to Notch3-ECD and potentiates Notch3/Jagged1 signaling (Meng et al., 2009). Moreover, it associates with low density lipoprotein receptor-related protein-1 stimulating Notch3-ECD endocytosis and clearance from the extracellular space (Meng et al., 2010). Most importantly with respect to CADASIL, our group previously demonstrated co-aggregation of TSP-2 with mutant Notch3 fragments in an *in vitro* aggregation assay (Duering et al., 2011). In the present study, an enrichment of TSP-2 in the β-ME fraction upon sequential extraction was observed indicating co-fractionation with Notch3 deposits. However, due to the lack of an appropriate antibody, immunohistochemical analyses in order to proof a spatial overlap could not be performed. Assumingly, co-aggregation of mutant Notch3-ECD and TSP-2 prevents the TSP-2-mediated recycling of Notch3. The impaired clearance from the extracellular space in turn could promote the aggregation process resulting in a build-up of extracellular deposits over time. However, further studies are required to elucidate the precise role of TSP-2 in CADASIL development.

4.2 Fibronectin and fibrillin-1

Fibronectin and fibrillin-1 are major structural ECM components. While fibronectin is a dimeric protein interacting with other ECM components allowing the formation of an interconnected network and stable matrix, fibrillin-1 polymerizes into microfibrils to form a microfibrillar network (Raines, 2000). They are synthesized by vSMCs and fibroblasts and

mediate the interaction of vSMCs with the ECM influencing their adhesion, migration and survival in the arterial wall. Alterations in their functionality are known to have deleterious effects on ECM homeostasis (Judge and Dietz, 2005, White and Muro, 2011). Accumulation of fibronectin has previously been reported in a single CADASIL case (Oide et al., 2008). In the present thesis, this finding is now confirmed and extended and the abnormal enrichment of fibronectin as well as fibrillin-1 in brain vessels of three independent patients carrying different Notch3 mutations was demonstrated. However, the accumulation is observed within the tunica adventitia and intima, but not in the tunica media where Notch3-ECD aggregates are located. Immunofluorescent co-staining of fibrillin-1 and Notch3 clearly showed the difference in localization. This finding is interpreted as an indication against a direct involvement of fibronectin and fibrillin-1 in Notch3-ECD aggregation. It rather implies excess ECM production, which is known to occur during fibrosis, a pathological process also observed in CADASIL pathogenesis. Therefore, fibronectin and fibrillin-1 accumulation is considered as an event occurring secondary to Notch3-ECD deposition. A similar enrichment has been reported for various types of collagens (type I, III and VI) in the massively thickened tunica adventitia of CADASIL patients (Miao et al., 2004, Miao et al., 2006, Dong et al., 2012). Moreover, in the proteomic study by Monet-Lepretre et al., a number of additional matricellular proteins such as nidogen-1, laminin and perlecan were identified, which might accumulate due to arterial wall thickening (Monet-Lepretre et al., 2013).

The excessive production, deposition and contraction of ECM are distinctive features of fibrotic diseases and usually advance over many months and years (Leask and Abraham, 2004). Fibrosis occurs in a variety of vascular conditions including hereditary hemorrhagic telangiectasia, Marfan and Loeys-Dietz Syndrome and pulmonary arterial hypertension (ten Dijke and Arthur, 2007). The common denominator of all these vascular disorders is a dysregulation of transforming growth factor-β (TGF-β) signaling contributing to vessel wall malformations (Goumans et al., 2009). It was therefore decided to continue the candidate analysis by selecting extracellular factors involved in the TGF-β pathway.

4.3 Latent TGF-β-binding proteins

TGF-β, a well-described regulator of blood vessel formation and homeostasis, is secreted from cells as inactive complex and stored in the ECM. This complex, also termed large latency complex (LLC), consists of mature TGF-β, latency-associated peptide (LAP) and a member of the latent TGF-β binding protein (LTBP) family (Pardali and Ten Dijke, 2012). LAP keeps the mature ligand in a biologically inactive state and covalently links it to LTBP-1, -3 or -4 by a disulfide bond (Ramirez et al., 2007, Shi et al., 2011). Sequestration

within the ECM is mediated by interactions between LTBPs, fibronectin and fibrillin-1 generating a reservoir of inactive TGF-β.

Using mass spectrometry, Monet-Lepretre and colleagues identified LTBP-2 and LTBP-4 in human and murine Notch3-ECD enriched preparations, respectively (Monet-Lepretre et al., 2013). Thus, LTBPs as regulators of TGF-β bioavailability represent promising candidate molecules for a role in CADASIL pathogenesis. Since LTBP-2 does not bind TGF-β, the focus was set on LTBP-4 and LTBP-1, the latter being the best studied family member, binding equally efficient to all three TGF-β ligands (TGF-β1, TGF-β2, TGF-β1) (Saharinen and Keski-Oja, 2000). For both LTBPs, Western Blotting demonstrates a specific enrichment and co-fractionation with Notch3-ECD deposits in CADASIL samples. For LTBP-4, however, immunohistological analysis data could not be interpreted due to unclear antibody specificity and thus, a final conclusion about its role in Notch3-ECD aggregation could not be drawn. In contrast, LTBP-1 displayed an accumulation as well as a striking co-localization with Notch3-ECD deposits in CADASIL-affected vessels. The presence of this observation in three unrelated patients carrying different *NOTCH3* mutations argued for its specificity and suggested a role for LTBP-1 in Notch3 deposit formation.

This finding prompted us to investigate the relationship between LTBP-1 and Notch3 in more detail. Monet-Lepretre and collegues proposed that a direct interaction is required for the recruitment of matricellular proteins into Notch3-ECD aggregates. Particularly, they established tissue inhibitor of metalloproteinase 3 (TIMP3) as a Notch3-ECD interactor and aggregate constituent, which is not affected by CADASIL mutations (Monet-Lepretre et al., 2013). Therefore, a possible interaction between Notch3 and LTBP-1 was investigated using a solid-phase binding assay, an approach previously used to identify binding partners of both factors (Meng et al., 2009, Massam-Wu et al., 2010). Indeed, an interaction between the LTBP-1 N-terminal domain and the first 11 EGF-like repeats of Notch3-ECD was discovered. Since a purified mutant Notch3-ECD EGF1-11 fragment was not available and the mutant EGF1-5 fragments used in the co-aggregation assay (see below) could not be used as ligands due to their low stickiness, the effect of CADASIL mutations on the interaction could not be investigated. However, the data from Monet-Lepretre et al. and the present results from a co-aggregation assay (see below) suggest that LTBP-1 binding is preserved in Notch3 mutants.

To provide proof for a direct participation of LTBP-1 in the Notch3-ECD aggregation process, a previously established *in vitro* assay based on scanning for intensely fluorescent targets (SIFT) was applied, which allows the quantitative monitoring of *de novo* aggregation of mutant Notch3 in solution (Opherk et al., 2009a, Duering et al., 2011). It so far represents

the only assay in which Notch3 aggregation can be analyzed under controlled conditions and it has been successfully used to demonstrate the disulfide dependency of mutant Notch3-ECD multimerization. Proteins used in this assay need to be purified in a correctly folded form and are therefore obtained from conditioned supernatants of transfected cultured cells. Since longer Notch3-ECD fragments are poorly secreted, a shorter Notch3 fragment containing EGF-like repeats 1-5, the mutational hotspot region of CADASIL, are analyzed. As mentioned above, co-aggregation of TSP-2 with mutant Notch3 was demonstrated in this assay providing the first experimental evidence for a pathological co-aggregation mechanism (Duering et al., 2011). The present thesis demonstrated that while the LTBP-1 deletion variant containing the Notch3 binding site showed strong co-aggregation with the archetypal Notch3 mutant R183C, this tendency was not observed with the variant lacking the Notch3 interaction domain. Altogether, these results strongly suggest the recruitment of LTBP-1 into Notch3-ECD deposits by a co-aggregation mechanism requiring a direct interaction.

These observations support and extend the previous results on the gain-of-toxic-function hypothesis by Monet-Lepretre and co-workers involving the recruitment of matricellular proteins into Notch3-ECD deposits. For TIMP3, they were able to demonstrate a clear increase in its protease activity providing first hints for a disease-related role. This matricellular protein is an inhibitor of ECM-degrading metalloproteases and TIMP3 activity alterations were suggested to contribute to the impaired ECM homeostasis and fibrosis in small vessels in CADASIL patients (Monet-Lepretre et al., 2013). Here, LTBP-1 is demonstrated as a novel Notch3-ECD aggregate constituent (Figure 32). Together with the present data, this suggests that while structural components of the ECM such as fibrillin-1, fibronectin and collagens rather ubiquitously accumulate within CADASIL-affected vessels, direct Notch3-ECD interactors such as the matricellular proteins TIMP3 and LTBP-1 can be specifically trapped in Notch3-ECD aggregates. Likely, the sequestration of additional proteins into Notch3-ECD deposits triggers a snowball effect continuously promoting the recruitment of more proteins, generating new interaction surfaces and increasing their toxic potential.

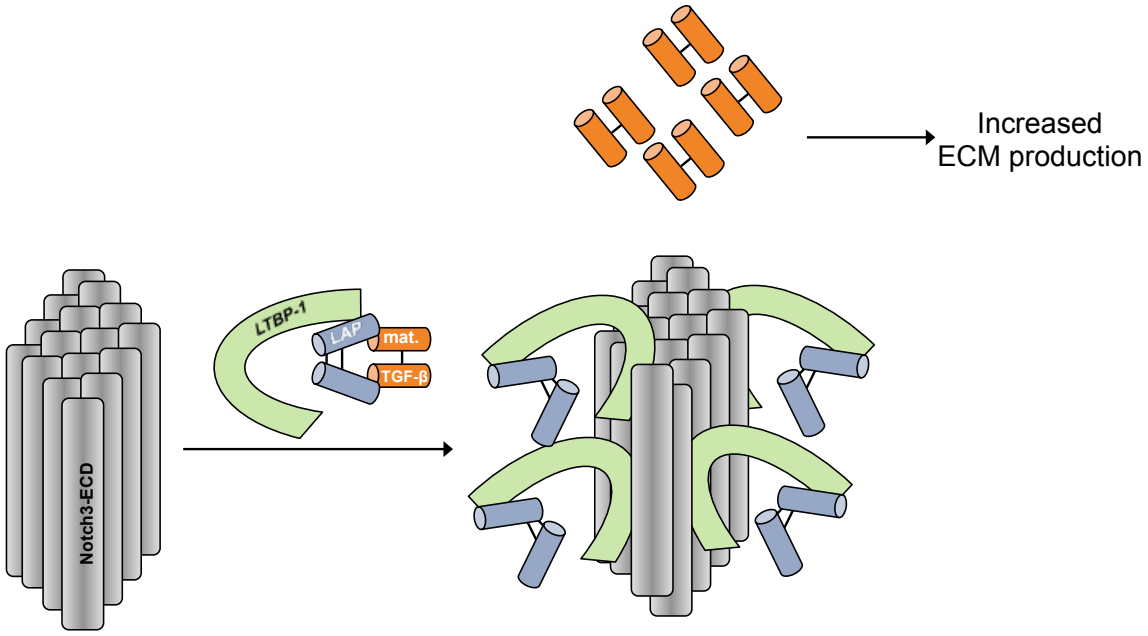

Figure 32: Potential pathomechanism in CADASIL. Notch3-ECD deposits (grey bars) recruit LTBP-1 (green hemicycle) into deposits by a co-aggregation mechanism requiring a direct interaction. LTBP-1 mediates the co-sequestration of covalently bound LAP (orange dimer) into the deposits. Possibly, a conformational change of LAP could release mature TGF-β (blue dimer), which could induce the induction of ECM production.

4.4 Is the TGF-β pathway dysregulated in CADASIL?

LTBP-1 controls the extracellular storage of TGF-β by covalent association with its pro-domain LAP. Thus, LTBP-1 recruitment into Notch3-ECD deposits might have an impact on TGF-β activity. The essential step in the TGF-β signaling cascade is the release of the mature ligand from its association with LAP by protease-dependent or -independent mechanisms prior to the activation of its transmembrane receptors and the subsequent intracellular signaling cascade (Robertson and Rifkin, 2013). Therefore, the expression pattern of LAP was studied and increased levels in the tunica media of CADASIL-affected vessels were detected. This finding strongly suggests LTBP-1-mediated sequestration of LAP into Notch3-ECD deposits and indicates an involvement of the TGF-β pathway in CADASIL pathogenesis.

It remains to be established whether this results in an alteration of TGF-β bioavailability and if so, in which way. TGF-β signaling influences a number of physiological processes including proliferation, differentiation, migration and apoptosis and is also a crucial mediator of fibrotic processes (Ruiz-Ortega et al., 2007). On vascular cells, the TGF-β has a

wide range of diverse effects and its function is cell-dependent. VSMCs are dose-dependently influenced by TGF-β: At low concentrations their migration and proliferation is induced by increased contractile protein expression (Rudijanto, 2007). Contractile vSMCs counteract daily fluctuations in arterial blood pressure to avoid potentially deleterious increases or decreases in cerebral blood flow. To maintain a roughly stable cerebral perfusion, vSMCs mediate dilation and constriction of cerebral arteries when blood pressure decreases and increases, respectively (Iadecola and Davisson, 2008). High TGF-β levels, however, inhibit the expression of contractile proteins in vSMCs causing cytostasis and the so-called non-contractile or synthetic phenotype (Rudijanto, 2007). Thus, synthetic vSMCs loose their ability to contract and relax in response to blood pressure changes in the brain. Interestingly, the CADASIL mouse model TgNotch3^{R169C} displays reduced functional reactivity of vSMCs (Joutel et al., 2010). Assumingly, elevated TGF-β levels in CADASIL-affected arterioles could induce the synthetic phenotype of vSMCs impairing their functionality and contributing to the reduced myogenic responses.

In addition, elevated TGF-β also elicits pro-fibrotic effects on vSMCs by stimulating the production of ECM proteins and suppressing proteases, which degrade ECM (Massague, 1990). The cytokine connective tissue growth factor (CTGF), secreted by endothelial cells and fibroblasts, is a prominent TGF-β target gene promoting fibroblast proliferation and matrix production of fibronectin, proteoglycans and various types of collagens (Leask and Abraham, 2004). Additionally, TGF-β also promotes the increased incorporation of fibrillin-1 into the ECM without stimulating its transcription (Kissin et al., 2002). Consequently, the accumulation of fibronectin, fibrillin-1 and collagens (type I, III and VI) (Miao et al., 2004, Miao et al., 2006, Oide et al., 2008, Dong et al., 2012) contributing to the prominent fibrotic thickening of CADASIL vessels could be attributed to increased TGF-β bioavailability.

Dysregulated TGF-β signaling has been demonstrated in a variety of inherited vascular diseases including Marfan syndrome, a systemic connective tissue disorder (Doyle et al., 2012). The disease is caused by autosomal dominant mutations in fibrillin-1 leading to defective microfibril formation, vessel fibrosis and vascular defects such as aortic aneurysms (Judge and Dietz, 2005). It is now established that increased TGF-β bioavailability and signaling activity is responsible for the deleterious fibrotic responses (Neptune et al., 2003) possibly due to ineffective incorporation of LTBP-1 into altered microfibrils of the vascular ECM (Gomez et al., 2009). Notch3-ECD aggregates might have a similar effect by sequestering LTBP-1 and preventing its incorporation into ECM. Thus, CADASIL and Marfan Syndrome might share a similar mechanism contributing to individual pathomechanisms in differently affected tissues. In Marfan syndrome, mainly

larger vessels such as the aorta are affected while the brain vasculature is not involved (Judge and Dietz, 2005).

However, alterations in TGF-β signaling have also been reported in the cerebral microvasculature (Hara et al., 2009, Shiga et al., 2011). Cerebral autosomal recessive arteriopathy with subcortical infarcts and leukoencephalopathy (CARASIL) is a rare recessively inherited form of SVD sharing the main clinical manifestation with CADASIL, although additional symptoms such as alopecia (premature baldness) and vertebral disc herniation are also observed (Fukutake, 2011). Disease-causing recessive mutations in the gene encoding high temperature requirement protein A1 (HtrA1), a conserved serine protease, invariably result in a loss of HtrA1 activity. Consequently, a lack of substrate processing is considered the underlying pathomechanism (Hara et al., 2009). Studies in our group have shown that HtrA1 cleaves LTBP-1 in its N-terminal hinge region reducing LTBP-1's ability to bind fibronectin and resulting in dysregulated TGF-β signaling (Beaufort et al., PNAS in press).

Remarkably, HtrA1 was also identified in the proteomic analysis of Notch3-ECD enriched murine and human brain fractions (Monet-Lepretre et al., 2013). Moreover, further proteins with a role in TGF-β biology were found to be increased in diseased vessels. These included Emilin, an inhibitor of proteolytic conversion of pro-TGF-β into LAP and mature ligand (Hynes, 2009) and Nidogen, βig-h3/TGFBI (transforming growth factor, β induced) and Perlecan, all of which are TGF-β inducible ECM components (Iozzo, 1998, Melrose et al., 2008, Zakin and De Robertis, 2010, Monet-Lepretre et al., 2013). This lends further support to the hypothesis that the TGF-β pathway plays a role in CADASIL disease development. Surprisingly, LTBP-1 was not amongst the identified factors, which could be due to the use of whole brain tissue instead of isolated vessels possibly containing only minute amounts of LTBP-1. Alternatively, it might be difficult to detect LTBPs using mass spectrometry, a possibility supported by the low number of specific peptides assigned to LTBP-2 and LTBP-4 (Monet-Lepretre et al., 2013).

It is tempting to speculate that a dysregulation of TGF-β activity might represent a common feature of both CADASIL and CARASIL. Thompson and Hakim postulated already in 2009 that increased TGF-β signaling might be responsible for fibrotic vessel alterations in sporadic SVD patients (Thompson and Hakim, 2009). Thus, a more detailed analysis of the different aspects of the TGF-β pathway in both diseases are required to substantiate its role in SVD pathogenesis. This should include a comprehensive examination of TGF-β signaling in TgNotch3^{R169C} mice, which represent an established CADASIL model (Joutel et al., 2010). Since Notch3-ECD accumulation has been shown to represent one of the earliest pathological events in this model, studying its effects on TGF-β

pathway could deepen our understanding of disease pathomechanisms and help in addressing the question whether LTBP-1 co-aggregation occurs prior to vessel fibrosis. Additional insights might be gained by mating this strain with LTBP-1 knockout animals (Drews et al., 2008).

Treatment options aiming at the restoration of normal TGF-β activity levels have already been proposed in Marfan syndrome. The blood pressure lowering agent losartan, which blocks the angiotensin II type 1 receptor and antagonizes TGF-β signaling, can prevent and even reverse symptoms, especially the aortic wall thickness, in a Marfan syndrome mouse model (Habashi et al., 2006). TGF-β acts downstream of angiotensin II, which is a potent vasoconstrictor inducing TGF-β1 mRNA and protein expression and subsequently vascular fibrosis (Ruiz-Ortega et al., 2007). In case of an increase in bioactive TGF-β in CADASIL, losartan might potentially have a beneficial effect on CADASIL patients as well.

4.5 Conclusion

Complex pathophysiological processes altering vessel morphology in CADASIL likely involve several interacting pathways. Recent evidence implicated a role of the TGF-β pathway in sporadic and familial SVD (Thompson and Hakim, 2009, Hara et al., 2009, Monet-Lepretre et al., 2013) and the role of TGF-β regulators fibronectin, fibrillin-1 and members of the LTBP family in CADASIL-related Notch3-ECD aggregation was investigated. LTBP-1 was identified as a Notch3-ECD interacting protein, which co-aggregates into CADASIL-specific deposits. Likely, LTBP-1 mediates the recruitment of its covalent interaction partner LAP with the possible consequence of uncontrolled release of mature TGF-β from its extracellular storage (see Figure 32). This could evoke fibrotic processes such as excess deposition of collagens, fibrillin-1 and fibronectin. Especially in small arterioles, the massively increased vessel wall thickness is responsible for the narrowing of the vascular lumen. Vessel wall modifications promote decreased cerebral blood flow, reduced vasoreactivity and chronic subcortical ischemia all of which are critical for the development of stroke and vascular dementia (Brulin et al., 2002, Miao et al., 2004).

5 List of references

AMBERLA, K., WALJAS, M., TUOMINEN, S., ALMKVIST, O., POYHONEN, M., TUISKU, S., KALIMO, H. & VIITANEN, M. 2004. Insidious cognitive decline in CADASIL. *Stroke,* 35**,** 1598-602.

ARBOLEDA-VELASQUEZ, J. F., MANENT, J., LEE, J. H., TIKKA, S., OSPINA, C., VANDERBURG, C. R., FROSCH, M. P., RODRIGUEZ-FALCON, M., VILLEN, J., GYGI, S., LOPERA, F., KALIMO, H., MOSKOWITZ, M. A., AYATA, C., LOUVI, A. & ARTAVANIS-TSAKONAS, S. 2011. Hypomorphic Notch 3 alleles link Notch signaling to ischemic cerebral small-vessel disease. *Proc Natl Acad Sci U S A,* 108**,** E128-35.

ARTAVANIS-TSAKONAS, S., RAND, M. D. & LAKE, R. J. 1999. Notch signaling: cell fate control and signal integration in development. *Science,* 284**,** 770-6.

BELIN DE CHANTEMELE, E. J., RETAILLEAU, K., PINAUD, F., VESSIERES, E., BOCQUET, A., GUIHOT, A. L., LEMAIRE, B., DOMENGA, V., BAUFRETON, C., LOUFRANI, L., JOUTEL, A. & HENRION, D. 2008. Notch3 is a major regulator of vascular tone in cerebral and tail resistance arteries. *Arterioscler Thromb Vasc Biol,* 28**,** 2216-24.

BLAUMUELLER, C. M., QI, H., ZAGOURAS, P. & ARTAVANIS-TSAKONAS, S. 1997. Intracellular cleavage of Notch leads to a heterodimeric receptor on the plasma membrane. *Cell,* 90**,** 281-91.

BROU, C., LOGEAT, F., GUPTA, N., BESSIA, C., LEBAIL, O., DOEDENS, J. R., CUMANO, A., ROUX, P., BLACK, R. A. & ISRAEL, A. 2000. A novel proteolytic cleavage involved in Notch signaling: the role of the disintegrin-metalloprotease TACE. *Mol Cell,* 5**,** 207-16.

BRULIN, P., GODFRAIND, C., LETEURTRE, E. & RUCHOUX, M. M. 2002. Morphometric analysis of ultrastructural vascular changes in CADASIL: analysis of 50 skin biopsy specimens and pathogenic implications. *Acta Neuropathol,* 104**,** 241-8.

CALABRO, N. E., KRISTOFIK, N. J. & KYRIAKIDES, T. R. 2014. Thrombospondin-2 and extracellular matrix assembly. *Biochim Biophys Acta,* 1840**,** 2396-2402.

CARONTI, B., CALANDRIELLO, L., FRANCIA, A., SCORRETTI, L., MANFREDI, M., SANSOLINI, T., PENNISI, E. M., CALDERARO, C. & PALLADINI, G. 1998. Cerebral autosomal dominant arteriopathy with subcortical infarcts and leucoencephalopathy (CADASIL). Neuropathological and in vitro studies of abnormal elastogenesis. *Acta Neurol Scand,* 98**,** 259-67.

CERONI, M., POLONI, T. E., TONIETTI, S., FABOZZI, D., UGGETTI, C., FREDIANI, F., SIMONETTI, F., MALASPINA, A., ALIMONTI, D., CELANO, M., FERRARI, M. & CARRERA, P. 2000. Migraine with aura and white matter abnormalities: Notch3 mutation. *Neurology,* 54**,** 1869-71.

CHABRIAT, H., JOUTEL, A., DICHGANS, M., TOURNIER-LASSERVE, E. & BOUSSER, M. G. 2009. Cadasil. *Lancet Neurol,* 8**,** 643-53.

CHABRIAT, H., LEVY, C., TAILLIA, H., IBA-ZIZEN, M. T., VAHEDI, K., JOUTEL, A., TOURNIER-LASSERVE, E. & BOUSSER, M. G. 1998. Patterns of MRI lesions in CADASIL. *Neurology,* 51**,** 452-7.

DALLAS, S. L., SIVAKUMAR, P., JONES, C. J., CHEN, Q., PETERS, D. M., MOSHER, D. F., HUMPHRIES, M. J. & KIELTY, C. M. 2005. Fibronectin regulates latent transforming growth factor-beta (TGF beta) by controlling matrix assembly of latent TGF beta-binding protein-1. *J Biol Chem,* 280**,** 18871-80.

DAVOUS, P., KHOUBESSERIAN, P., TRIC, P. & TELERMAN-TOPPET, N. 1991. [Mitochondrial encephalopathy affecting only the central nervous system]. *Rev Neurol (Paris),* 147**,** 538-41.

DICHGANS, M. 2007. Genetics of ischaemic stroke. *Lancet Neurol,* 6**,** 149-61.

DICHGANS, M. 2009. Cognition in CADASIL. *Stroke,* 40**,** S45-7.

DICHGANS, M., FILIPPI, M., BRUNING, R., IANNUCCI, G., BERCHTENBREITER, C., MINICUCCI, L., UTTNER, I., CRISPIN, A., LUDWIG, H., GASSER, T. & YOUSRY, T. A. 1999. Quantitative MRI in CADASIL: correlation with disability and cognitive performance. *Neurology,* 52**,** 1361-7.

DICHGANS, M., HERZOG, J. & GASSER, T. 2001. NOTCH3 mutation involving three cysteine residues in a family with typical CADASIL. *Neurology,* 57**,** 1714-7.

DICHGANS, M., LUDWIG, H., MULLER-HOCKER, J., MESSERSCHMIDT, A. & GASSER, T. 2000. Small in-frame deletions and missense mutations in CADASIL: 3D models predict misfolding of Notch3 EGF-like repeat domains. *Eur J Hum Genet,* 8**,** 280-5.

DICHGANS, M., MAYER, M., UTTNER, I., BRUNING, R., MULLER-HOCKER, J., RUNGGER, G., EBKE, M., KLOCKGETHER, T. & GASSER, T. 1998. The phenotypic spectrum of CADASIL: clinical findings in 102 cases. *Ann Neurol,* 44**,** 731-9.

DOMENGA, V., FARDOUX, P., LACOMBE, P., MONET, M., MACIAZEK, J., KREBS, L. T., KLONJKOWSKI, B., BERROU, E., MERICSKAY, M., LI, Z., TOURNIER-LASSERVE, E., GRIDLEY, T. & JOUTEL, A. 2004. Notch3 is required for arterial identity and maturation of vascular smooth muscle cells. *Genes Dev,* 18**,** 2730-5.

DONG, H., BLAIVAS, M. & WANG, M. M. 2012. Bidirectional encroachment of collagen into the tunica media in cerebral autosomal dominant arteriopathy with subcortical infarcts and leukoencephalopathy. *Brain Res,* 1456**,** 64-71.

DOYLE, J. J., GERBER, E. E. & DIETZ, H. C. 2012. Matrix-dependent perturbation of TGFbeta signaling and disease. *FEBS Lett,* 586**,** 2003-15.

DREWS, F., KNOBEL, S., MOSER, M., MUHLACK, K. G., MOHREN, S., STOLL, C., BOSIO, A., GRESSNER, A. M. & WEISKIRCHEN, R. 2008. Disruption of the latent transforming growth factor-beta binding protein-1 gene causes alteration in facial structure and influences TGF-beta bioavailability. *Biochim Biophys Acta,* 1783**,** 34-48.

DUBOIS, C. M., LAPRISE, M. H., BLANCHETTE, F., GENTRY, L. E. & LEDUC, R. 1995. Processing of transforming growth factor beta 1 precursor by human furin convertase. *J Biol Chem,* 270**,** 10618-24.

DUBROCA, C., LACOMBE, P., DOMENGA, V., MACIAZEK, J., LEVY, B., TOURNIER-LASSERVE, E., JOUTEL, A. & HENRION, D. 2005. Impaired vascular mechanotransduction in a transgenic mouse model of CADASIL arteriopathy. *Stroke,* 36**,** 113-7.

DUCROS, A., NAGY, T., ALAMOWITCH, S., NIBBIO, A., JOUTEL, A., VAHEDI, K., CHABRIAT, H., IBA-ZIZEN, M. T., JULIEN, J., DAVOUS, P., GOAS, J. Y., LYON-CAEN, O., DUBOIS, B., DUCROCQ, X., SALSA, F., RAGNO, M., BURKHARD, P., BASSETTI, C., HUTCHINSON, M., VERIN, M., VIADER, F., CHAPON, F., LEVASSEUR, M., MAS, J. L., DELRIEU, O. & ET AL. 1996. Cerebral autosomal dominant arteriopathy with subcortical infarcts and leukoencephalopathy, genetic homogeneity, and mapping of the locus within a 2-cM interval. *Am J Hum Genet,* 58**,** 171-81.

DUERING, M., CSANADI, E., GESIERICH, B., JOUVENT, E., HERVE, D., SEILER, S., BELAROUSSI, B., ROPELE, S., SCHMIDT, R., CHABRIAT, H. & DICHGANS, M. 2013. Incident lacunes preferentially localize to the edge of white matter hyperintensities: insights into the pathophysiology of cerebral small vessel disease. *Brain,* 136**,** 2717-26.

DUERING, M., KARPINSKA, A., ROSNER, S., HOPFNER, F., ZECHMEISTER, M., PETERS, N., KREMMER, E., HAFFNER, C., GIESE, A., DICHGANS, M. & OPHERK, C. 2011. Co-aggregate formation of CADASIL-mutant NOTCH3: a single-particle analysis. *Hum Mol Genet,* 20**,** 3256-65.

DUERING, M., RIGHART, R., CSANADI, E., JOUVENT, E., HERVE, D., CHABRIAT, H. & DICHGANS, M. 2012. Incident subcortical infarcts induce focal thinning in connected cortical regions. *Neurology,* 79**,** 2025-8.

FORTEZA, A. M., BROZMAN, B., RABINSTEIN, A. A., ROMANO, J. G. & BRADLEY, W. G. 2001. Acetazolamide for the treatment of migraine with aura in CADASIL. *Neurology,* 57**,** 2144-5.

FOUILLADE, C., BARON-MENGUY, C., DOMENGA-DENIER, V., THIBAULT, C., TAKAMIYA, K., HUGANIR, R. & JOUTEL, A. 2013. Transcriptome analysis

for Notch3 target genes identifies Grip2 as a novel regulator of myogenic response in the cerebrovasculature. *Arterioscler Thromb Vasc Biol,* 33**,** 76-86.

FUKUTAKE, T. 2011. Cerebral autosomal recessive arteriopathy with subcortical infarcts and leukoencephalopathy (CARASIL): from discovery to gene identification. *J Stroke Cerebrovasc Dis,* 20**,** 85-93.

GAYRAUD, B., KEENE, D. R., SAKAI, L. Y. & RAMIREZ, F. 2000. New insights into the assembly of extracellular microfibrils from the analysis of the fibrillin 1 mutation in the tight skin mouse. *J Cell Biol,* 150**,** 667-80.

GIESE, A., BADER, B., BIESCHKE, J., SCHAFFAR, G., ODOY, S., KAHLE, P. J., HAASS, C. & KRETZSCHMAR, H. 2005. Single particle detection and characterization of synuclein co-aggregation. *Biochem Biophys Res Commun,* 333**,** 1202-10.

GOMEZ, D., AL HAJ ZEN, A., BORGES, L. F., PHILIPPE, M., GUTIERREZ, P. S., JONDEAU, G., MICHEL, J.-B. & VRANCKX, R. 2009. Syndromic and non-syndromic aneurysms of the human ascending aorta share activation of the Smad2 pathway. *The Journal of Pathology,* 218**,** 131-142.

GOUMANS, M. J., LIU, Z. & TEN DIJKE, P. 2009. TGF-beta signaling in vascular biology and dysfunction. *Cell Res,* 19**,** 116-27.

HABASHI, J. P., JUDGE, D. P., HOLM, T. M., COHN, R. D., LOEYS, B. L., COOPER, T. K., MYERS, L., KLEIN, E. C., LIU, G., CALVI, C., PODOWSKI, M., NEPTUNE, E. R., HALUSHKA, M. K., BEDJA, D., GABRIELSON, K., RIFKIN, D. B., CARTA, L., RAMIREZ, F., HUSO, D. L. & DIETZ, H. C. 2006. Losartan, an AT1 antagonist, prevents aortic aneurysm in a mouse model of Marfan syndrome. *Science,* 312**,** 117-21.

HARA, K., SHIGA, A., FUKUTAKE, T., NOZAKI, H., MIYASHITA, A., YOKOSEKI, A., KAWATA, H., KOYAMA, A., ARIMA, K., TAKAHASHI, T., IKEDA, M., SHIOTA, H., TAMURA, M., SHIMOE, Y., HIRAYAMA, M., ARISATO, T., YANAGAWA, S., TANAKA, A., NAKANO, I., IKEDA, S., YOSHIDA, Y., YAMAMOTO, T., IKEUCHI, T., KUWANO, R., NISHIZAWA, M., TSUJI, S. & ONODERA, O. 2009. Association of HTRA1 mutations and familial ischemic cerebral small-vessel disease. *N Engl J Med,* 360**,** 1729-39.

HARITUNIANS, T., BOULTER, J., HICKS, C., BUHRMAN, J., DISIBIO, G., SHAWBER, C., WEINMASTER, G., NOFZIGER, D. & SCHANEN, C. 2002. CADASIL Notch3 mutant proteins localize to the cell surface and bind ligand. *Circ Res,* 90**,** 506-8.

HYNES, R. O. 2009. The extracellular matrix: not just pretty fibrils. *Science,* 326**,** 1216-9.

IADECOLA, C. 2013. The pathobiology of vascular dementia. *Neuron,* 80**,** 844-66.

IADECOLA, C. & DAVISSON, R. L. 2008. Hypertension and cerebrovascular dysfunction. *Cell Metab,* 7**,** 476-84.

IOZZO, R. V. 1998. Matrix proteoglycans: from molecular design to cellular function. *Annu Rev Biochem,* 67**,** 609-52.

ISHIKO, A., SHIMIZU, A., NAGATA, E., TAKAHASHI, K., TABIRA, T. & SUZUKI, N. 2006. Notch3 ectodomain is a major component of granular osmiophilic material (GOM) in CADASIL. *Acta Neuropathol,* 112**,** 333-9.

ISOGAI, Z., ONO, R. N., USHIRO, S., KEENE, D. R., CHEN, Y., MAZZIERI, R., CHARBONNEAU, N. L., REINHARDT, D. P., RIFKIN, D. B. & SAKAI, L. Y. 2003. Latent transforming growth factor beta-binding protein 1 interacts with fibrillin and is a microfibril-associated protein. *J Biol Chem,* 278**,** 2750-7.

JOUTEL, A. 2011. Pathogenesis of CADASIL: transgenic and knock-out mice to probe function and dysfunction of the mutated gene, Notch3, in the cerebrovasculature. *Bioessays,* 33**,** 73-80.

JOUTEL, A., ANDREUX, F., GAULIS, S., DOMENGA, V., CECILLON, M., BATTAIL, N., PIGA, N., CHAPON, F., GODFRAIN, C. & TOURNIER-LASSERVE, E. 2000. The ectodomain of the Notch3 receptor accumulates within the cerebrovasculature of CADASIL patients. *J Clin Invest,* 105**,** 597-605.

JOUTEL, A., CORPECHOT, C., DUCROS, A., VAHEDI, K., CHABRIAT, H., MOUTON, P., ALAMOWITCH, S., DOMENGA, V., CECILLION, M., MARECHAL, E., MACIAZEK, J., VAYSSIERE, C., CRUAUD, C., CABANIS, E. A., RUCHOUX, M. M., WEISSENBACH, J., BACH, J. F., BOUSSER, M. G. & TOURNIER-LASSERVE, E. 1996. Notch3 mutations in CADASIL, a hereditary adult-onset condition causing stroke and dementia. *Nature,* 383**,** 707-10.

JOUTEL, A., CORPECHOT, C., DUCROS, A., VAHEDI, K., CHABRIAT, H., MOUTON, P., ALAMOWITCH, S., DOMENGA, V., CECILLION, M., MARECHAL, E., MACIAZEK, J., VAYSSIERE, C., CRUAUD, C., CABANIS, E. A., RUCHOUX, M. M., WEISSENBACH, J., BACH, J. F., BOUSSER, M. G. & TOURNIER-LASSERVE, E. 1997. Notch3 mutations in cerebral autosomal dominant arteriopathy with subcortical infarcts and leukoencephalopathy (CADASIL), a mendelian condition causing stroke and vascular dementia. *Ann N Y Acad Sci,* 826**,** 213-7.

JOUTEL, A., MONET, M., DOMENGA, V., RIANT, F. & TOURNIER-LASSERVE, E. 2004. Pathogenic mutations associated with cerebral autosomal dominant arteriopathy with subcortical infarcts and leukoencephalopathy differently affect Jagged1 binding and Notch3 activity via the RBP/JK signaling Pathway. *Am J Hum Genet,* 74**,** 338-47.

JOUTEL, A., MONET-LEPRETRE, M., GOSELE, C., BARON-MENGUY, C., HAMMES, A., SCHMIDT, S., LEMAIRE-CARRETTE, B., DOMENGA, V., SCHEDL, A., LACOMBE, P. & HUBNER, N. 2010. Cerebrovascular dysfunction and microcirculation rarefaction precede white matter lesions in a mouse genetic model of cerebral ischemic small vessel disease. *J Clin Invest,* 120**,** 433-45.

JUDGE, D. P. & DIETZ, H. C. 2005. Marfan's syndrome. *Lancet,* 366**,** 1965-76.

KALARIA, R. N. 1996. Cerebral vessels in ageing and Alzheimer's disease. *Pharmacol Ther,* 72**,** 193-214.

KALIMO, H., RUCHOUX, M. M., VIITANEN, M. & KALARIA, R. N. 2002. CADASIL: a common form of hereditary arteriopathy causing brain infarcts and dementia. *Brain Pathol,* 12**,** 371-84.

KARLSTROM, H., BEATUS, P., DANNAEUS, K., CHAPMAN, G., LENDAHL, U. & LUNDKVIST, J. 2002. A CADASIL-mutated Notch 3 receptor exhibits impaired intracellular trafficking and maturation but normal ligand-induced signaling. *Proc Natl Acad Sci U S A,* 99**,** 17119-24.

KISSIN, E. Y., LEMAIRE, R., KORN, J. H. & LAFYATIS, R. 2002. Transforming growth factor beta induces fibroblast fibrillin-1 matrix formation. *Arthritis Rheum,* 46**,** 3000-9.

KOSKI, C., SAHARINEN, J. & KESKI-OJA, J. 1999. Independent promoters regulate the expression of two amino terminally distinct forms of latent transforming growth factor-beta binding protein-1 (LTBP-1) in a cell type-specific manner. *J Biol Chem,* 274**,** 32619-30.

KUO, D. S., LABELLE-DUMAIS, C. & GOULD, D. B. 2012. COL4A1 and COL4A2 mutations and disease: insights into pathogenic mechanisms and potential therapeutic targets. *Hum Mol Genet,* 21**,** R97-110.

LEASK, A. & ABRAHAM, D. J. 2004. TGF-beta signaling and the fibrotic response. *Faseb j,* 18**,** 816-27.

LESNIK OBERSTEIN, S. A., VAN DUINEN, S. G., VAN DEN BOOM, R., MAAT-SCHIEMAN, M. L., VAN BUCHEM, M. A., VAN HOUWELINGEN, H. C., HEGEMAN-KLEINN, I. M., FERRARI, M. D., BREUNING, M. H. & HAAN, J. 2003. Evaluation of diagnostic NOTCH3 immunostaining in CADASIL. *Acta Neuropathol,* 106**,** 107-11.

LOW, W. C., SANTA, Y., TAKAHASHI, K., TABIRA, T. & KALARIA, R. N. 2006. CADASIL-causing mutations do not alter Notch3 receptor processing and activation. *Neuroreport,* 17**,** 945-9.

MANDELKOW, E. M. & MANDELKOW, E. 1992. Microtubule oscillations. *Cell Motil Cytoskeleton,* 22**,** 235-44.

MAS, J. L., DILOUYA, A. & DE RECONDO, J. 1992. A familial disorder with subcortical ischemic strokes, dementia, and leukoencephalopathy. *Neurology,* 42**,** 1015-9.

MASSAGUE, J. 1990. The transforming growth factor-beta family. *Annu Rev Cell Biol,* 6**,** 597-641.

MASSAM-WU, T., CHIU, M., CHOUDHURY, R., CHAUDHRY, S. S., BALDWIN, A. K., MCGOVERN, A., BALDOCK, C., SHUTTLEWORTH, C. A. & KIELTY, C. M. 2010. Assembly of fibrillin microfibrils governs extracellular deposition of latent TGF beta. *J Cell Sci,* 123**,** 3006-18.

MAYER, M., STRAUBE, A., BRUENING, R., UTTNER, I., PONGRATZ, D., GASSER, T., DICHGANS, M. & MULLER-HOCKER, J. 1999. Muscle and skin biopsies are a sensitive diagnostic tool in the diagnosis of CADASIL. *J Neurol,* 246**,** 526-32.

MELROSE, J., HAYES, A. J., WHITELOCK, J. M. & LITTLE, C. B. 2008. Perlecan, the "jack of all trades" proteoglycan of cartilaginous weight-bearing connective tissues. *Bioessays,* 30**,** 457-69.

MENG, H., ZHANG, X., HANKENSON, K. D. & WANG, M. M. 2009. Thrombospondin 2 potentiates notch3/jagged1 signaling. *J Biol Chem,* 284**,** 7866-74.

MENG, H., ZHANG, X., LEE, S. J., STRICKLAND, D. K., LAWRENCE, D. A. & WANG, M. M. 2010. Low density lipoprotein receptor-related protein-1 (LRP1) regulates thrombospondin-2 (TSP2) enhancement of Notch3 signaling. *J Biol Chem,* 285**,** 23047-55.

MIAO, Q., PALONEVA, T., TUISKU, S., ROINE, S., POYHONEN, M., VIITANEN, M. & KALIMO, H. 2006. Arterioles of the lenticular nucleus in CADASIL. *Stroke,* 37**,** 2242-7.

MIAO, Q., PALONEVA, T., TUOMINEN, S., POYHONEN, M., TUISKU, S., VIITANEN, M. & KALIMO, H. 2004. Fibrosis and stenosis of the long penetrating cerebral arteries: the cause of the white matter pathology in cerebral autosomal dominant arteriopathy with subcortical infarcts and leukoencephalopathy. *Brain Pathol,* 14**,** 358-64.

MONET-LEPRETRE, M., BARDOT, B., LEMAIRE, B., DOMENGA, V., GODIN, O., DICHGANS, M., TOURNIER-LASSERVE, E., COHEN-TANNOUDJI, M., CHABRIAT, H. & JOUTEL, A. 2009. Distinct phenotypic and functional features of CADASIL mutations in the Notch3 ligand binding domain. *Brain,* 132**,** 1601-12.

MONET-LEPRETRE, M., HADDAD, I., BARON-MENGUY, C., FOUILLOT-PANCHAL, M., RIANI, M., DOMENGA-DENIER, V., DUSSAULE, C., COGNAT, E., VINH, J. & JOUTEL, A. 2013. Abnormal recruitment of extracellular matrix proteins by excess Notch3 ECD: a new pathomechanism in CADASIL. *Brain,* 136**,** 1830-45.

MUMM, J. S., SCHROETER, E. H., SAXENA, M. T., GRIESEMER, A., TIAN, X., PAN, D. J., RAY, W. J. & KOPAN, R. 2000. A ligand-induced extracellular cleavage regulates gamma-secretase-like proteolytic activation of Notch1. *Mol Cell,* 5**,** 197-206.

NEPTUNE, E. R., FRISCHMEYER, P. A., ARKING, D. E., MYERS, L., BUNTON, T. E., GAYRAUD, B., RAMIREZ, F., SAKAI, L. Y. & DIETZ, H. C. 2003. Dysregulation of TGF-beta activation contributes to pathogenesis in Marfan syndrome. *Nat Genet,* 33**,** 407-11.

OIDE, T., NAKAYAMA, H., YANAGAWA, S., ITO, N., IKEDA, S. & ARIMA, K. 2008. Extensive loss of arterial medial smooth muscle cells and mural extracellular matrix in cerebral autosomal recessive arteriopathy with subcortical infarcts and leukoencephalopathy (CARASIL). *Neuropathology,* 28**,** 132-42.

OKEDA, R., ARIMA, K. & KAWAI, M. 2002. Arterial changes in cerebral autosomal dominant arteriopathy with subcortical infarcts and leukoencephalopathy (CADASIL) in relation to pathogenesis of diffuse myelin loss of cerebral white matter: examination of cerebral medullary arteries by reconstruction of serial sections of an autopsy case. *Stroke,* 33**,** 2565-9.

OLESEN, J., GUSTAVSSON, A., SVENSSON, M., WITTCHEN, H. U. & JONSSON, B. 2012. The economic cost of brain disorders in Europe. *Eur J Neurol,* 19**,** 155-62.

OLOFSSON, A., ICHIJO, H., MOREN, A., TEN DIJKE, P., MIYAZONO, K. & HELDIN, C. H. 1995. Efficient association of an amino-terminally extended form of human latent transforming growth factor-beta binding protein with the extracellular matrix. *J Biol Chem,* 270**,** 31294-7.

ONO, R. N., SENGLE, G., CHARBONNEAU, N. L., CARLBERG, V., BACHINGER, H. P., SASAKI, T., LEE-ARTEAGA, S., ZILBERBERG, L., RIFKIN, D. B., RAMIREZ, F., CHU, M. L. & SAKAI, L. Y. 2009. Latent transforming growth factor beta-binding proteins and fibulins compete for fibrillin-1 and exhibit exquisite specificities in binding sites. *J Biol Chem,* 284**,** 16872-81.

OPHERK, C., DUERING, M., PETERS, N., KARPINSKA, A., ROSNER, S., SCHNEIDER, E., BADER, B., GIESE, A. & DICHGANS, M. 2009a. CADASIL mutations enhance spontaneous multimerization of NOTCH3. *Hum Mol Genet,* 18**,** 2761-7.

OPHERK, C., PETERS, N. & DICHGANS, M. 2009b. [Vasculitis and hereditary small vessel diseases]. *Internist (Berl),* 50**,** 1200-9.

OPHERK, C., PETERS, N., HERZOG, J., LUEDTKE, R. & DICHGANS, M. 2004. Long-term prognosis and causes of death in CADASIL: a retrospective study in 411 patients. *Brain,* 127**,** 2533-9.

PANTONI, L. 2010. Cerebral small vessel disease: from pathogenesis and clinical characteristics to therapeutic challenges. *Lancet Neurol,* 9**,** 689-701.

PANTONI, L. & GARCIA, J. H. 1997. Pathogenesis of leukoaraiosis: a review. *Stroke,* 28**,** 652-9.

PAQUET, C., JOUVENT, E., MINE, M., VITAL, A., HUGON, J., CHABRIAT, H. & GRAY, F. 2010. A cortical form of CADASIL with cerebral Abeta amyloidosis. *Acta Neuropathol,* 120**,** 813-20.

PARDALI, E. & TEN DIJKE, P. 2012. TGFbeta signaling and cardiovascular diseases. *Int J Biol Sci,* 8**,** 195-213.

PENTON, A. L., LEONARD, L. D. & SPINNER, N. B. 2012. Notch signaling in human development and disease. *Semin Cell Dev Biol,* 23**,** 450-7.

PETERS, N., HOLTMANNSPOTTER, M., OPHERK, C., GSCHWENDTNER, A., HERZOG, J., SAMANN, P. & DICHGANS, M. 2006. Brain volume changes in CADASIL: a serial MRI study in pure subcortical ischemic vascular disease. *Neurology,* 66**,** 1517-22.

PETERS, N., OPHERK, C., BERGMANN, T., CASTRO, M., HERZOG, J. & DICHGANS, M. 2005a. Spectrum of mutations in biopsy-proven CADASIL: implications for diagnostic strategies. *Arch Neurol,* 62**,** 1091-4.

PETERS, N., OPHERK, C., DANEK, A., BALLARD, C., HERZOG, J. & DICHGANS, M. 2005b. The pattern of cognitive performance in CADASIL: a monogenic condition leading to subcortical ischemic vascular dementia. *Am J Psychiatry,* 162**,** 2078-85.

PETERS, N., OPHERK, C., ZACHERLE, S., CAPELL, A., GEMPEL, P. & DICHGANS, M. 2004. CADASIL-associated Notch3 mutations have differential effects both on ligand binding and ligand-induced Notch3 receptor signaling through RBP-Jk. *Exp Cell Res,* 299**,** 454-64.

PRAKASH, N., HANSSON, E., BETSHOLTZ, C., MITSIADIS, T. & LENDAHL, U. 2002. Mouse Notch 3 expression in the pre- and postnatal brain: relationship to the stroke and dementia syndrome CADASIL. *Exp Cell Res,* 278**,** 31-44.

RAINES, E. W. 2000. The extracellular matrix can regulate vascular cell migration, proliferation, and survival: relationships to vascular disease. *Int J Exp Pathol,* 81**,** 173-82.

RAMIREZ, F., SAKAI, L. Y., RIFKIN, D. B. & DIETZ, H. C. 2007. Extracellular microfibrils in development and disease. *Cell Mol Life Sci,* 64**,** 2437-46.

RAZVI, S. S., DAVIDSON, R., BONE, I. & MUIR, K. W. 2005. The prevalence of cerebral autosomal dominant arteriopathy with subcortical infarcts and leucoencephalopathy (CADASIL) in the west of Scotland. *J Neurol Neurosurg Psychiatry,* 76**,** 739-41.

RICHARDS, A., VAN DEN MAAGDENBERG, A. M., JEN, J. C., KAVANAGH, D., BERTRAM, P., SPITZER, D., LISZEWSKI, M. K., BARILLA-LABARCA, M. L., TERWINDT, G. M., KASAI, Y., MCLELLAN, M., GRAND, M. G., VANMOLKOT, K. R., DE VRIES, B., WAN, J., KANE, M. J., MAMSA, H.,

SCHAFER, R., STAM, A. H., HAAN, J., DE JONG, P. T., STORIMANS, C. W., VAN SCHOONEVELD, M. J., OOSTERHUIS, J. A., GSCHWENDTER, A., DICHGANS, M., KOTSCHET, K. E., HODGKINSON, S., HARDY, T. A., DELATYCKI, M. B., HAJJ-ALI, R. A., KOTHARI, P. H., NELSON, S. F., FRANTS, R. R., BALOH, R. W., FERRARI, M. D. & ATKINSON, J. P. 2007. C-terminal truncations in human 3'-5' DNA exonuclease TREX1 cause autosomal dominant retinal vasculopathy with cerebral leukodystrophy. *Nat Genet,* 39**,** 1068-70.

ROBERTSON, I. B. & RIFKIN, D. B. 2013. Unchaining the beast; insights from structural and evolutionary studies on TGFbeta secretion, sequestration, and activation. *Cytokine Growth Factor Rev,* 24**,** 355-72.

RUDIJANTO, A. 2007. The role of vascular smooth muscle cells on the pathogenesis of atherosclerosis. *Acta Med Indones,* 39**,** 86-93.

RUIZ-ORTEGA, M., RODRÍGUEZ-VITA, J., SANCHEZ-LOPEZ, E., CARVAJAL, G. & EGIDO, J. 2007. TGF-β signaling in vascular fibrosis. *Cardiovascular Research,* 74**,** 196-206.

RUTTEN, J. W., BOON, E. M., LIEM, M. K., DAUWERSE, J. G., PONT, M. J., VOLLEBREGT, E., MAAT-KIEVIT, A. J., GINJAAR, H. B., LAKEMAN, P., VAN DUINEN, S. G., TERWINDT, G. M. & LESNIK OBERSTEIN, S. A. 2013. Hypomorphic NOTCH3 alleles do not cause CADASIL in humans. *Hum Mutat,* 34**,** 1486-9.

SAHARINEN, J. & KESKI-OJA, J. 2000. Specific sequence motif of 8-Cys repeats of TGF-beta binding proteins, LTBPs, creates a hydrophobic interaction surface for binding of small latent TGF-beta. *Mol Biol Cell,* 11**,** 2691-704.

SAHARINEN, J., TAIPALE, J. & KESKI-OJA, J. 1996. Association of the small latent transforming growth factor-beta with an eight cysteine repeat of its binding protein LTBP-1. *EMBO J,* 15**,** 245-53.

SHI, M., ZHU, J., WANG, R., CHEN, X., MI, L., WALZ, T. & SPRINGER, T. A. 2011. Latent TGF-beta structure and activation. *Nature,* 474**,** 343-9.

SHIGA, A., NOZAKI, H., YOKOSEKI, A., NIHONMATSU, M., KAWATA, H., KATO, T., KOYAMA, A., ARIMA, K., IKEDA, M., KATADA, S., TOYOSHIMA, Y., TAKAHASHI, H., TANAKA, A., NAKANO, I., IKEUCHI, T., NISHIZAWA, M. & ONODERA, O. 2011. Cerebral small-vessel disease protein HTRA1 controls the amount of TGF-beta1 via cleavage of proTGF-beta1. *Hum Mol Genet,* 20**,** 1800-10.

SIMPSON, P. 1997. Notch signalling in development: on equivalence groups and asymmetric developmental potential. *Curr Opin Genet Dev,* 7**,** 537-42.

SONNINEN, V. & SAVONTAUS, M. L. 1987. Hereditary multi-infarct dementia. *Eur Neurol,* 27**,** 209-15.

SOURANDER, P. & WALINDER, J. 1977. Hereditary multi-infarct dementia. Morphological and clinical studies of a new disease. *Acta Neuropathol,* 39**,** 247-54.

STEVENS, D. L., HEWLETT, R. H. & BROWNELL, B. 1977. Chronic familial vascular encephalopathy. *Lancet,* 1**,** 1364-5.

TEN DIJKE, P. & ARTHUR, H. M. 2007. Extracellular control of TGFbeta signalling in vascular development and disease. *Nat Rev Mol Cell Biol,* 8**,** 857-69.

THOMPSON, C. S. & HAKIM, A. M. 2009. Living beyond our physiological means: small vessel disease of the brain is an expression of a systemic failure in arteriolar function: a unifying hypothesis. *Stroke,* 40**,** e322-30.

TIKKA, S., MYKKANEN, K., RUCHOUX, M. M., BERGHOLM, R., JUNNA, M., POYHONEN, M., YKI-JARVINEN, H., JOUTEL, A., VIITANEN, M., BAUMANN, M. & KALIMO, H. 2009. Congruence between NOTCH3 mutations and GOM in 131 CADASIL patients. *Brain,* 132**,** 933-9.

TODOROVIC, V. & RIFKIN, D. B. 2012. LTBPs, more than just an escort service. *J Cell Biochem,* 113**,** 410-8.

TOURNIER-LASSERVE, E., IBA-ZIZEN, M. T., ROMERO, N. & BOUSSER, M. G. 1991. Autosomal dominant syndrome with strokelike episodes and leukoencephalopathy. *Stroke,* 22**,** 1297-302.

TOURNIER-LASSERVE, E., JOUTEL, A., MELKI, J., WEISSENBACH, J., LATHROP, G. M., CHABRIAT, H., MAS, J. L., CABANIS, E. A., BAUDRIMONT, M., MACIAZEK, J. & ET AL. 1993. Cerebral autosomal dominant arteriopathy with subcortical infarcts and leukoencephalopathy maps to chromosome 19q12. *Nat Genet,* 3**,** 256-9.

VISWANATHAN, A., GRAY, F., BOUSSER, M. G., BAUDRIMONT, M. & CHABRIAT, H. 2006. Cortical neuronal apoptosis in CADASIL. *Stroke,* 37**,** 2690-5.

WAGENSEIL, J. E. & MECHAM, R. P. 2009. Vascular extracellular matrix and arterial mechanics. *Physiol Rev,* 89**,** 957-89.

WALLAYS, G., NUYENS, D., SILASI-MANSAT, R., SOUFFREAU, J., CALLAERTS-VEGH, Z., VAN NUFFELEN, A., MOONS, L., D'HOOGE, R., LUPU, F., CARMELIET, P., COLLEN, D. & DEWERCHIN, M. 2011. Notch3 Arg170Cys knock-in mice display pathologic and clinical features of the neurovascular disorder cerebral autosomal dominant arteriopathy with subcortical infarcts and leukoencephalopathy. *Arterioscler Thromb Vasc Biol,* 31**,** 2881-8.

WARDLAW, J. M., DENNIS, M. S., WARLOW, C. P. & SANDERCOCK, P. A. 2001. Imaging appearance of the symptomatic perforating artery in patients with lacunar infarction: occlusion or other vascular pathology? *Ann Neurol,* 50**,** 208-15.

WARDLAW, J. M., SMITH, C. & DICHGANS, M. 2013a. Mechanisms of sporadic cerebral small vessel disease: insights from neuroimaging. *Lancet Neurol,* 12**,** 483-97.

WARDLAW, J. M., SMITH, E. E., BIESSELS, G. J., CORDONNIER, C., FAZEKAS, F., FRAYNE, R., LINDLEY, R. I., O'BRIEN, J. T., BARKHOF, F., BENAVENTE, O. R., BLACK, S. E., BRAYNE, C., BRETELER, M., CHABRIAT, H., DECARLI, C., DE LEEUW, F. E., DOUBAL, F., DUERING, M., FOX, N. C., GREENBERG, S., HACHINSKI, V., KILIMANN, I., MOK, V., OOSTENBRUGGE, R., PANTONI, L., SPECK, O., STEPHAN, B. C., TEIPEL, S., VISWANATHAN, A., WERRING, D., CHEN, C., SMITH, C., VAN BUCHEM, M., NORRVING, B., GORELICK, P. B. & DICHGANS, M. 2013b. Neuroimaging standards for research into small vessel disease and its contribution to ageing and neurodegeneration. *Lancet Neurol,* 12**,** 822-38.

WARLOW, C., SUDLOW, C., DENNIS, M., WARDLAW, J. & SANDERCOCK, P. 2003. Stroke. *Lancet,* 362**,** 1211-24.

WHITE, E. S. & MURO, A. F. 2011. Fibronectin splice variants: Understanding their multiple roles in health and disease using engineered mouse models. *IUBMB Life,* 63**,** 538-546.

ZAKIN, L. & DE ROBERTIS, E. M. 2010. Extracellular regulation of BMP signaling. *Curr Biol,* 20**,** R89-92.

6 List of figures

7 List of tables

8 Abbreviations

α-SMA	Alpha smooth muscle actin
β-ME	2-Mercaptoethanol
2-D	Two dimensional
AA	Acryl–bisacrylamide
AEC	3-amino-9-ethylcarbazole
APP	Amyloid precursor protein
APS	Ammoniumpersulfate
BSA	Bovine serum albumin
CADASIL	Cerebral autosomal dominant arteriopathy with subcortical infarcts and leukoencephalopathy
CAD	CADASIL
CARASIL	Cerebral autosomal recessive arteriopathy with subcortical infarcts and leukoencephalopathy
CBF	Cerebral blood flow
CNS	Central nervous system
COL4A1	Collagen type IVα1
Ctrl	Control
Cys	Cysteine
DMEM	Dulbecco's modified eagle medium
DMSO	Dimethyl sulfoxide
DNA	Deoxyribonucleic acid
EBVNA 1	Epstein barr virus nuclear antigen 1
ECD	Extracellular domain
ECM	Extracellular matrix
EDTA	Ethylenediaminetetraacetic acid disodium
EGF	Epidermal growth factor
ELISA	Enzyme linked immunosorbent assay
FBS	Fetal Bovine Serum
GOM	Granular osmiophilic material

HA	Hemagglutinin
HEK	Human embryonic kidney
HRP	Horse reddish peroxidase
HtrA1	High temperature requirement A1
IDC	Intracellular domain
ICH	Immunohistochemistry
IF	Immunofluorescence
ISD	Institute for Stroke and Dementia Research
LAP	Latency associated peptide
LLC	Large latency complex
LRS	Ligand recognition site
LTBP	Latent transforming growth factor binding protein
MEM	Minimum essential media
MRI	Magnetic resonance imaging
PAC	P1-derived artificial chromosome
PBS	Phosphate buffered saline
PCR	Polymerase chain reaction assays
PFA	Paraformaldehyde
RNA	Ribonucleic acid
RVCL	Retinal vasculopathy with cerebral leukodystrophy
SDS	Sodium dodecyl sulfate
SDS-PAGE	Sodium dodecyl sulfate polyacrylamide gel electrophoresis
SEM	Standard error of the mean
SIFT	Scanning for intensely fluorescent targets
SPBA	Solid phase binding assay
SVD	Small vessel disease
TACE	TNFα-converting enzyme
TEMED	Tetramethylethylenediamine
TGF-β	Transforming growth factor-beta
TGFBI	Transforming growth factor, beta-induced, 68kDa
TIMP3	Tissue inhibitor of metalloprotease 3

TM	Transmembrane domain
TNF-α	Tumor necrosis factor-α
Tris	Tris(hydroxymethyl)-Aminomethane
TSP-2	Thrombospondin-2
vSMC	Vascular smooth muscle cell
WB	Western blot
WT	Wild-type

All indications of quantity were termed according to the international system of units.

9 Acknowledgements

During my PhD studies I had the privilege to be surrounded by many inspiring and encouraging people who have directly or indirectly supported me and allowed me to complete my thesis. I would like to acknowledge all of these people.

Frist, I would like to thank Prof. Dr. Martin Dichgans for giving me the opportunity to join his laboratory. Moreover, I am extremely thankful that PD Dr. Christian Opherk recruited me to the ISD and guided me during the first three years of my thesis. Your enthusiasm and knowledge were great inspiration and it has been a pleasure to work with you. I express my deepest gratitude to PD Dr. Christof Haffner, who took me under his wings and supervised me during the most critical phase of my PhD. You always had an open door for me and without your guidance and support, this thesis would not have been possible. I also really appreciate it that Prof Dr. Martin Biel supervised this thesis and that Prof. Dr. Nikolaus Plesnila, Prof. Dr. Christian Wahl-Schott, Prof. Dr. Stefan Zahler and Prof. Dr. Angelika Vollmar evaluated my work and participated in my PhD examination.

Furthermore, I am grateful to my collaborators Dr. Thomas Arzberger, Dr. Anne Joutel and Dr. Saskia Lesnik-Oberstein for kindly providing the human brain samples. I also appreciate Dr. Elisabeth Kremmer and Dr. Lynn Sakai for valuable antibodies and Prof. Dr. Jorma Keski-Oja for providing LTBP-1 plasmids.

I further want to acknowledge Dr. Nathalie Beaufort and Dr. Marco Duering for scientific input throughout the years and Barbara Linder and Melanie Schneider for helping out with experiments.

I am deeply grateful to have spent four years with the best colleagues ever. We have been there for each other in joy and frustration. We cared for each other and shared numerous awful jokes. Eva Scharrer, Patrizia Hanecker and Caroline Prell, I don't think I would have survived without you! The most joyful thanks I dedicate to all the other fellow lab members. You guys made my working days brighter and many times absolutely hilarious!

Especially I wish to thank my beloved friends. Your support during my lab-free time kept me safe and sane. Thank you Sandra, Dani, Steffi and Isabella for numerous lunch and dinner sessions; Johanna, Flori, Fabi, Philipp and Michi for distracting me during weekends; Betti for morning running sessions; and Nadine, Lea and Dana for always being there for me.

Last but not least, I want to thank my family for unfailing support and love during my whole life and finally, heartfelt thanks to Markus, who has supported me unconditionally and helped me through all difficulties even when I was totally obnoxious.

11 Publications and meetings

Publications

KAST, J., HANECKER, P., BEAUFORT, N., GIESE, A., JOUTEL, A., DICHGANS, M., OPHERK, C. & HAFFNER, C. 2014. Sequestration of latent TGF-beta binding protein 1 into CADASIL-related Notch3-ECD deposits. *Acta Neuropathol Commun,* 2**,** 96.

BOUMAN, L., SCHLIERF, A., LUTZ, A. K., SHAN, J., DEINLEIN, A., **KAST, J.**, GALEHDAR, Z., PALMISANO, V., PATENGE, N., BERG, D., GASSER, T., AUGUSTIN, R., TRUMBACH, D., IRRCHER, I., PARK, D. S., WURST, W., KILBERG, M. S., TATZELT, J. & WINKLHOFER, K. F. 2011. Parkin is transcriptionally regulated by ATF4: evidence for an interconnection between mitochondrial stress and ER stress. *Cell Death Differ,* 18**,** 769-82.

Meetings

October 2013	The Notch Meeting, Athens, Greece; Oral presentation
March 2013	<interact> 2014, Munich; Poster presentation
January 2013	ANIM, Mannheim; Poster presentation